Technische Universität München
Lehrstuhl für Nachrichtentechnik
Prof. Dr.sc.tech. Gerhard Kramer

Master's Thesis

Intelligent Reflecting Surface-aided Beam Alignment for mmWave Communications

Vorgelegt von:
Florian Muhr

München, September 2022

Betreut von:
Mari Kobayashi, Lorenzo Zaniboni

Master's Thesis am
Lehrstuhl für Nachrichtentechnik (LNT)
der Technischen Universität München (TUM)
Titel : Intelligent Reflecting Surface-aided Beam Alignment for mmWave Communications
Autor : Florian Muhr

Ich versichere hiermit wahrheitsgemäß, die Arbeit bis auf die dem Aufgabensteller bereits bekannte Hilfe selbständig angefertigt, alle benutzten Hilfsmittel vollständig und genau angegeben und alles kenntlich gemacht zu haben, was aus Arbeiten anderer unverändert oder mit Abänderung entnommen wurde.

München, 09.09.2022

Ort, Datum (Florian Muhr)

Contents

List of Figures

List of Tables

List of Abbreviations

3GPP	3rd Generation Partnership Project
AoA	angle-of-arrival
AoD	angle-of-departure
AWGN	additive white gaussian noise
BA	beam alignment
BF	beamforming
BS	base station
CP	cyclic prefix
CRLB	Cramér-Rao lower bound
CSI-RS	channel state information reference signal
DFT	discrete Fourier transform
DL	Downlink
FIM	Fisher information matrix
FoV	field of view
HPBW	half power beam width
IRS	intelligent reflecting surface
LoS	line-of-sight
ML	maximum likelihood
mmWave	millimeter wave
NN	neural network

OFDM	orthogonal frequency division multiplexing
PCB	printed circuit board
RCS	radar cross-section
RF	radio frequency
RMSE	root-mean-square error
SNR	signal-to-noise ratio
UE	user equipment
UL	Uplink
ULA	uniform linear array

Abstract

As millimeter wave (mmWave) systems experience severe propagation and penetration losses, establishing a reliable communication link is quite challenging. To address this problem, directional beamforming (BF) utilizing electrically large antenna arrays is required both at the base station (BS) and at the user equipment (UE) to overcome the high losses. The process of determining these BF directions is referred to as beam alignment (BA). Owing to the sparsity of mmWave channels, BA can usually be performed if the BS and the UE know their respective angle-of-arrival (AoA) that corresponds to the most dominant scatterer in the channel. However, due to the very low initial signal-to-noise ratio (SNR) before any BF, this AoA information is difficult to obtain.

In this thesis, to enhance the UE's sensing and processing capabilities, the UE is assumed to be equipped with a hybrid intelligent reflecting surface (IRS), which enables the UE to simultaneously sense and reflect a portion of an incoming signal. By exploiting this capability, a complete BA scheme is proposed for a communications scenario in which only the BS is transmitting pilot symbols. In the resulting scheme, the BS and the UE both probe a random subset of the angular range in every slot of BA with high gain and vary the probed direction such that the entire angular range is explored after as few slots as possible. Then, the UE first estimates its AoA in each slot based on all so far received signals using a multi-slot maximum likelihood (ML) estimation method. Once this AoA estimate converges to a stable value, the UE activates the IRS and configures it for reflection towards its estimated AoA. Afterwards, the BS finds its AoA by employing a similar estimation method as the UE. The BA scheme is terminated after a predefined maximum number of slots is exceeded. Extensive simulations demonstrate that the proposed scheme is suitable for BA if the SNR at the UE is higher than $-15\,\mathrm{dB}$. Otherwise, AoA estimation at the BS becomes infeasible due to the very high path loss of the two-way channel. For SNRs higher than $-15\,\mathrm{dB}$, the performance of the proposed scheme is found to improve significantly with increasing SNR as well as with an increased number of slots. Compared to other approaches established in the literature, the proposed scheme is inferior for very low SNRs of less than $-10\,\mathrm{dB}$ and superior for higher SNRs. Moreover, by increasing the number of antennas at both the BS and the UE, the performance of the proposed scheme improves significantly compared to other approaches.

1. Introduction

To meet the continuously increasing demand for higher data rates in the near future, millimeter wave (mmWave) systems are often considered a promising candidate. Reason for this is that the mmWave frequency band, defined in this thesis as the spectrum from 30 GHz to 300 GHz, enables the use of larger spectral channels compared to current systems operating in the traditional sub-6 GHz spectrum [2]. However, due to their high operating frequencies, mmWave systems are subject to severe propagation and penetration losses [3], which makes establishing a reliable communication link more challenging. Contrary to that, a high operating frequency, or similarly a small wavelength, allows to increase the number of antenna elements for a given physical size, resulting in electrically large antenna arrays. To then overcome the high losses, such antenna arrays must be utilized to perform directional beamforming (BF) both at the base station (BS) and at the user equipment (UE) to find a path conveying enough signal power [4]. The process of determining these BF directions is referred to as beam alignment (BA).
For any currently existing BA scheme, a reliable and precise channel estimate is required. Owing to the sparsity of mmWave channels, such estimate is often given as the angle-of-arrivals (AoAs) of one or few dominant scatterers in the channel connecting the BS and the UE [5]. However, due to the very low initial signal-to-noise ratio (SNR) before any BF is performed, this AoA estimate is difficult to obtain. Existing BA schemes often aim to make the AoA acquistion problem more tractable by introducing a predefined set of BF vectors, called BF codebook. The AoA estimate is then found as the angle corresponding to the vector in the codebook that performs best with respect to a certain metric [6]. Since these codebooks contain only a limited number of BF vectors to keep the introduced overhead low, these codebook-based solutions come at the cost of being limited by the accuracy of their respective codebook. For this reason, codebook-free approaches to BA have the potential to achieve more accurate results than codebook-based approaches [6], yet, they are also more difficult to formulate.
To enhance the sensing and processing capabilities at the UE, within the scope of this thesis an intelligent reflecting surface (IRS) is assumed to be attached to the UE. IRSs are passive planar arrays consisting of a large number of sub-wavelength sized elements that allow to control the reflection of incident signals by tuning the phase shifts at the

individual elements accordingly. Most of the time, these surfaces are thought to be placed in between the BS and the UE where they serve as configurable reflectors to shape the propagation environment. The main objective is then to use the IRS to extend the range for reliable communication or to increase the rank of the channel matrix [7]. Contrary to that, the IRS considered in this thesis is attached to the UE and is thought to be a hybrid IRS, that is, besides acting as a configurable reflector, the IRS has additionally the ability to sense a portion of an incident signal [8]. Within the scope of this work, the main objective of using the IRS is then to maximize the SNR for the data transmission phase that directly follows after BA. This is done while saving power at the UE as no pilot transmission is required and without the need of a dedicated feedback channel between the BS and the UE to share side information. In addition, equipping a UE with a hybrid IRS allows the UE during Downlink (DL) transmission to reflect a portion of the received signal back to the BS, and hence enables the of use beam tracking techniques.
Summarizing, the present thesis studies a complete BA scheme between a single BS and a single UE that is equipped with a hybrid IRS. The main objective is to maximize the SNR for the data transmission phase while exploiting the capabilities of the hybrid IRS.

1.1. Literature Survey

Different strategies to BA in mmWave systems have been proposed in the literature, such as codebook-based approaches which are implemented in various standards such as IEEE 802.11ad or IEEE 802.15.3c [2]. These approaches utilize a set of predefined beam patterns, i.e. the BF codebook, and aim to find the beam pattern that leads to the strongest signal between the BS and the UE.
To exploit the poor scattering nature of mmWave channels, the authors in [9] introduced the concept of hierarchical multi-resolution codebooks. The idea is to start the BA process with wide, i.e. almost isotropic, beams and then reduce the beam width in subsequent iterations to end up with a narrow, i.e. directional, beam pointing to the unknown AoA. More precisely, the authors use a bisection search algorithm and initialize the BA scheme with two wide beams covering the whole angular range of interest in the first stage of the codebook. Then, the beam that maximizes the received power is determined and the angular range corresponding to this beam is probed by two narrower beams. This process is repeated until the final stage of the codebook is reached, and hence a narrow beam corresponding to a certain AoA is determined.
Based on the concept of hierarchical multi-resolution codebooks, in [10], an adaptive BF strategy, called hierarchical posterior matching, is developed for a single-path channel model. This strategy yields a noisy generalization of the bisection search approach, in-

troduced in [9], by using the posterior to obtain almost equally-probable subsets in the hierarchical codebook. Additionally, the authors formulate upper bounds for the expected search time to reach a certain target resolution as well as for the error probability in the AoA estimate.

For a single-carrier multi-user scenario where the devices implement a hybrid digital analog structure, a time-domain BA scheme is examined in [1]. In this paper, the authors utilize pseudo-noise sequences due to their good autocorrelation properties to find an estimate of the power spread function in the AoA-angle-of-departure (AoD) domain. Then, by reformulating the power spread function estimation as a least-squares problem, each UE finds its strongest AoA-AoD pair via non-negative least squares. For the case that any side information is available at the BS and potentially also at the UE, [11] shows that the performance of the time-domain BA scheme from [1] can be further improved in terms of beam training overhead.

Besides codebook-based strategies, also codebook-free approaches have been studied in the literature. For example, in [6], a deep neural network (NN) is proposed to solve the adaptive BA problem at the BS for a single-user scenario with a single-path channel. As input to the network, the authors consider the approximated posterior distribution of the AoA that is computed using the minimum mean squared error of the fading coefficient. The deep NN then designs the sensing vector for the next measurement based on this approximated distribution, and hence the network designs overall a sequence of adaptive sensing vectors to optimize the final AoA detection performance.

The research on IRSs from a communications perspective is, compared to the research on BA, a rather new field that has only begun in recent years. For this reason, the authors in [12] provide a fundamental explanation on IRSs by deriving a far-field path loss model based on physical optics. Further, they interpret an IRS as an array of diffuse scatterers and demonstrate how the overall IRS acts as a directional beamformer when the phase shifts at the individual elements are tuned accordingly. Combining the found results, a physically correct system model is derived for a communications scenario over a two-way channel where one path is given by the line-of-sight (LoS) path and the other by the reflection from the IRS. Using the derived path loss and system model, the same authors study in [7] how IRSs can be used to increase the rank of the channel matrix. They demonstrate that substantial multiplexing gains are possible when the IRS phases are tuned to achieve constructive interference at the UE.

Another work covering IRSs from a rather general point of view is provided in [13]. In this paper, the authors start with the fundamentals of IRSs by describing channel and signal models as well as practical and hardware constraints. Afterwards, the optimization of IRS parameters is considered for various scenarios such as single-user or multi-user,

single-antenna or multi-antenna as well as for different modulation schemes. For the respective scenarios, different optimization problems are considered and in particular, for IRS-aided orthogonal frequency division multiplexing (OFDM) systems, the maximization of the achievable rate is used. A different approach to optimizing the parameters at the IRS is described in [14], where the phase configuration at the IRS is determined by using a deep NN. This network is trained using the received pilot signals and the optimal IRS parameters as input-output pair with the aim to minimize the mean squared error between the predicted and optimal IRS parameters.
For an adaptive sensing scenario, the design of the IRS parameters is studied in [15], where the authors propose a deep learning architecture that is composed of two separate NNs. The first is a combination of a long-short term memory network and a conventional feed-forward NN and is used in each step to update a hidden state vector based on the most recent observation. This observation is obtained by an agent that actively interacts with the environment. After that, the proposed architecture designs in each step the new adaptive sensing strategy based on the updated hidden state vector. Then, after a specified number of time frames, the second network, which is a feed-forward NN, maps the hidden and cell state of the long-short term memory network to the final IRS parameters. By changing the cost function of the architecture, the authors also propose to use the same deep-learning based architecture for the adaptive BA problem at the BS. However, they make the unrealistic assumption that the SNR is known to the BS and can hence be given as an input to the architecture.
In [16], a practical model for an IRS-aided wideband OFDM system is investigated to illustrate the inaccuracy of the commonly used IRS model that is based on idealized reflection coefficients. Simulation results show that the complex reflection coefficient varies strongly with the operating frequency and based on this result, an algorithm for joint power allocation and reflection optimization is proposed.
Another work on IRSs is provided in [8], where the concept of hybrid reflecting and sensing IRSs is introduced. A hybrid IRS is characterized by the ability to sense a portion of an incident signal, while reflecting the remaining part of it in a controlled direction. To achieve this goal, the authors consider a hybrid meta-atom that is on the one hand loaded by a varactor diode to control the reflected signal and on the other hand modified to couple to a waveguide in order to process a portion of the incident signal. Using a simplified model that assumes no coupling between the parameters of each meta-atom as well as ideal reflection coefficients, a full-wave electromagnetic simulation is conducted to discuss the capabilities and arising challenges of hybrid IRSs. This simplified model for a hybrid IRS is also considered for the IRS in this thesis and is described in more detail in Sec. 2.1. A more detailed model of a hybrid IRSs that uses less simplifications and

additionally considers arising practical challenges is derived in [17].
A different potential application of IRSs is in enhancing security and privacy aspects of wireless communications. For example, in [18], an IRS is employed to minimize the signal-to-interference-plus-noise-ratio at an eavesdropper in a satellite-terrestrial integrated network, while other approaches consider an IRS to increase the secrecy rate of a legitimate communication for a single- or multi-user scenario [19, 20].

1.2. Contributions

The present thesis studies a complete BA protocol in a mmWave system between a single BS and a single UE that is equipped with a hybrid IRS. By referring to the considered UE as an IRS-integrated device, the main contributions can be summarized as follows:

1) Consideration of a communications scenario including an IRS-integrated device

2) Derivation of a multi-slot maximum likelihood (ML) estimation scheme for AoA estimation with constant or slot-varying channel coefficient

3) Derivation of the exact and approximated Cramér-Rao lower bound (CRLB) for the AoA estimation at an IRS-integrated device

4) Derivation of a complete BA scheme between a BS and an IRS-integrated device

1.3. Outline

The remainder of the present thesis is organized as follows. Chapter 2 first introduces the considered system model from a physical as well as from a communications point of view before deriving the signal and communications model for the BA phase as well as for the subsequent communications phase.
Next, Ch. 3 starts by providing a high-level overview of the general BA problem. Afterwards, the current standard as well as the approach taken in this thesis to solve the problem are briefly introduced. At the end of the chapter, a mathematical formulation of the general BA problem is derived and discussed in detail.
Chapter 4 then presents the proposed BA scheme. The individual components of this scheme, namely the employed estimation methods, the design strategy for the combining matrices and the design strategy for the IRS parameters are each highlighted individually and discussed in detail. Afterwards, a performance analysis of the overall scheme is conducted on the basis of the CRLB. The chapter concludes by providing an overview of the proposed BA scheme in the form of an algorithm.

After describing the proposed scheme from a theoretical perspective, simulation results are presented and discussed in Ch. 5.
Finally, Ch. 6 draws a conclusion and gives an outlook for potential future research.

1.4. Notation

This thesis denotes scalars as lower-case non-boldface letters (e.g., a), vectors as lower-case boldface letters (e.g., $\mathbf{a}$), matrices as upper-case boldface letters (e.g. $\mathbf{A}$) and sets as upper-case calligraphic letters (e.g., $\mathcal{A}$). Furthermore, the cardinality of set $\mathcal{A}$ is denoted by $|\mathcal{A}|$. The real and imaginary part of a complex scalar x are respectively given by $\mathrm{Re}\{x\}$ and $\mathrm{Im}\{x\}$, while the absolute value and phase of x are respectively denoted by $|x|$ and $\angle x$. Further, for a matrix $\mathbf{A}$, $\mathbf{A}^{\mathsf{T}}$, $\mathbf{A}^{*}$ and $\mathbf{A}^{\mathsf{H}}$ refer to its transpose, complex conjugate and hermitian (conjugate transpose). For a vector $\mathbf{a}$, $\|\mathbf{a}\|_2$ is its euclidean norm and $\mathrm{diag}(\mathbf{a})$ a diagonal matrix with $\mathbf{a}$ on its main diagonal. The identity matrix of dimension $\mathrm{M} \times \mathrm{M}$ is given by $\mathbf{I}_{\mathrm{M}}$ and the all-one vector as well as the zero vector of dimension $\mathrm{M} \times 1$ are respectively denoted by $\mathbf{1}_{\mathrm{M}}$ and $\mathbf{0}_{\mathrm{M}}$. $\otimes$ is the Kronecker product, $\mathrm{vec}(\cdot)$ the vectorization operator and $*$ the convolution operator. Further, $\delta(\cdot)$ represents the Dirac delta function and $\mathbb{E}[\cdot]$ the expectation operator. The natural logarithm is denoted by $\log(\cdot)$ and the logarithm to the base n by $\log_{\mathrm{n}}(\cdot)$, where $n \in \mathbb{N}$. The estimate of a variable ϕ is denoted by $\hat{\phi}$. $\mathcal{N}_{\mathcal{C}}(\boldsymbol{\mu}, \boldsymbol{\Sigma})$ denotes the complex multivariate normal distribution with mean vector $\boldsymbol{\mu}$ and covariance matrix $\boldsymbol{\Sigma}$. The short notation $[m]$ defines the set of non-negative integers $\{1, \ldots, m\}$, for every $m \in \mathbb{N}$.

2. System Model

A mmWave system consisting of a single BS and a single UE that is equipped with a hybrid IRS is considered. The BS is equipped with N_{a} antennas and N_{rf} radio frequency (RF) chains, while the UE is equipped with L_{a} antennas, given by the L_{a} surface elements of the IRS, and L_{rf} RF chains. Further, the UE is connected to the IRS controller such that the setting at the IRS is fully determined by the UE at any time during BA. An overview of the considered system is shown in Fig. 2.1. Although a detailed description of the depicted system is provided within this chapter, the main aspects are briefly outlined in the following.

Looking at Fig. 2.1, the BS is assumed to transmit pilot signals to which an initial BF is applied. The transmitted signal then passes through the DL channel which, similarly to the Uplink (UL) channel, is assumed to be a linear-time varying LoS channel. Next, at the UE, a portion of the transmitted signal is sensed, while the rest of the signal is reflected, with the amount that is sensed or reflected being determined by the configured magnitudes of the reflection coefficients at the IRS elements, denoted by β_l, for $l = 1, \ldots, L_{\mathrm{a}}$. Note that this requires all IRS elements to be mutually independent. Both the sensed and the reflected signal are also potentially phase shifted at the IRS. Further, as the number of RF chains is typically much smaller than the number of antennas in mmWave systems, both the UE and the BS implement a combining stage and obtain a low-dimensional observation of the received signal.

At the beginning of this chapter, in Sec. 2.1, an introduction to IRSs as well as their physical principles is provided and the IRS model considered in this thesis is explained. Next, Sec. 2.2 discusses the considered channel model as well as the physical model. Afterwards, Sec. 2.3 first introduces the signal model used during BA, before deriving expressions for the received signal at the UE and at the BS, respectively. At the end of the section, the SNRs at the UE and the BS before BA are discussed briefly. Similar to Sec. 2.3, Sec. 2.4 first introduces the signal and communications model for the communications phase, i.e. the data transmission phase, that directly follows after BA and concludes by shortly discussing the resulting SNR.

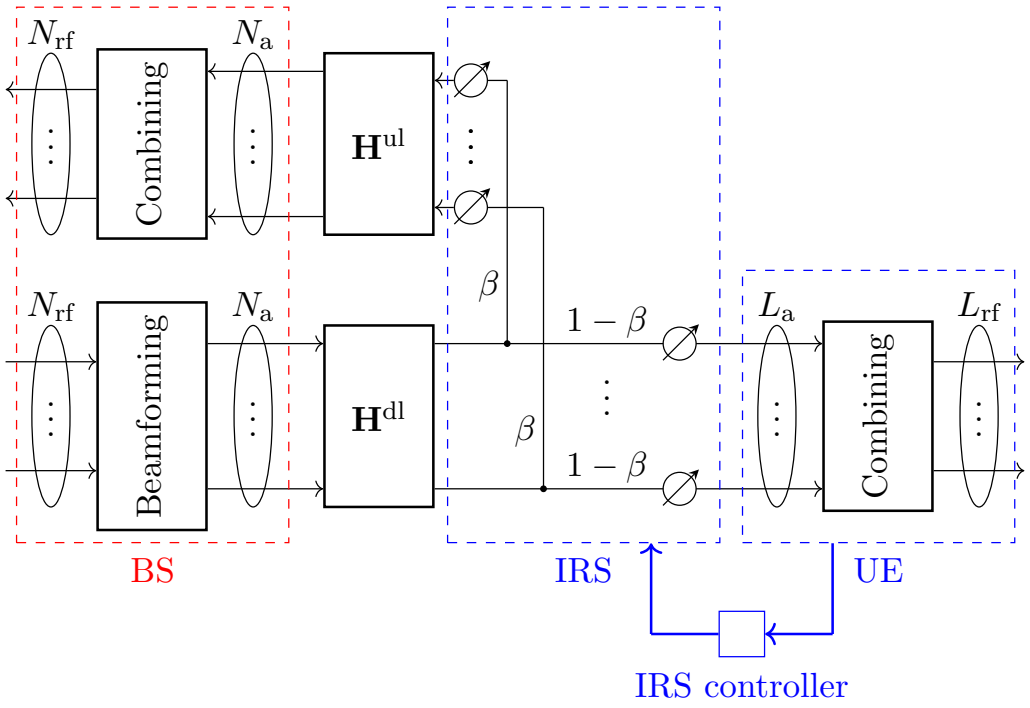

Figure 2.1.: Overview of considered system model.

2.1. Intelligent Reflecting Surface

Intelligent reflecting surfaces (IRSs) are a novel technology often introduced as a method to enable a real-time configuration of the radio environment. These surfaces are typically composed of a large number of small reflecting elements which, when tuned accordingly, allow the reflection of an incoming wave in any particular direction. Contrary to the typically considered setup where the IRS is placed in between the BS and the UE, the IRS considered in this thesis is assumed to be attached directly to the UE. Furthermore, instead of using the IRS only as a configurable reflector, the considered IRS is assumed to be able to sense a portion of the incoming signal, while the remaining part of the signal is reflected in a controllable direction, as introduced in [8] and further developed in [17]. An IRS that enables this capability of simultaneous sensing and reflection is sometimes referred to as hybrid IRS within this thesis. The main objective of using the hybrid IRS is then to exploit this ability of simultaneously sensing and reflecting an incoming signal in order to maximize the SNR after BA.

The considered IRS can be thought of as a planar surface that is comprised of L_{a} small surface elements, where each of these elements is assumed to have dimensions $a \times b$. Further, each element is assumed to be sub-wavelength sized and the individual elements

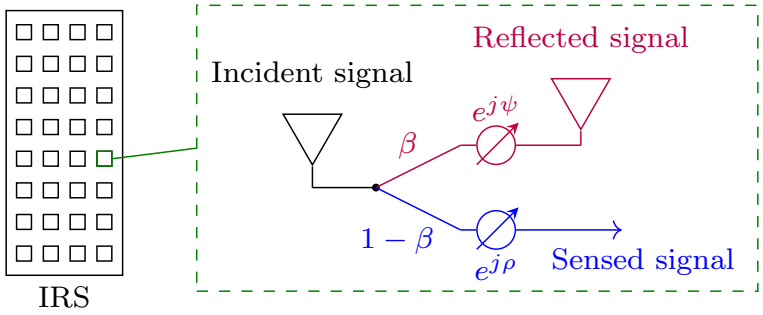

Figure 2.2.: Model of a single surface element of the considered hybrid IRS.

are assumed to be sub-wavelength spaced. Typically, as described in [16], an individual surface element of an IRS is constructed as a printed circuit board (PCB) with a metal patch on the top layer of the PCB as well as a metal sheet on the bottom layer. The top and bottom layer are additionally connected via a varactor diode that based on the applied bias voltage yields a different equivalent capacitance. The equivalent circuit of such IRS surface element is given by a resonant circuit whose overall impedance can be controlled by the equivalent capacitance of the varactor diode. Then, as explained in [12], at each element of the IRS, an incoming electromagnetic wave induces an electric surface current whose surface phase profile can be adjusted by configuring the impedance at each surface element. If the resulting surface phase profile approximates the phase profile given by the generalized Snell's Law for reflection in a certain direction, the overall IRS acts as a directional beamformer towards this direction. This briefly discussed model for the individual IRS surface elements holds for the case that the IRS is used as a configurable reflector only. To additionally account for the sensing capabilities of each element, the design of the hybrid meta-atom from [8] is considered, where the surface elements, that are similarly modeled as resonant circuits, are modified in order to couple to a waveguide. The sensed signal is then contained within the waveguide where it is potentially phase shifted before it reaches the UE, while the signal to be reflected remains at the respective IRS surface element. Therefore, using this design, the incident signal is first split into a reflected and a sensed signal, before a tunable phase shift is applied to each of the resulting signals. A model of a single surface element of the considered hybrid IRS is sketched in Fig. 2.2.

Formally, for an incident signal x at the l-th element of the IRS, the reflected and sensed signal are respectively given by $\beta_l e^{-j\psi_l} x$ and $(1-\beta_l)e^{-j\rho_l} x$, where $\beta_l \in [0,1]$ denotes the amplitude of the reflection coefficient, $\psi_l \in [-\pi, \pi]$ the tunable phase shift for the reflected signal and $\rho_l \in [-\pi, \pi]$ the tunable phase shift for the sensed signal. Further, for an incident signal $\mathbf{x} \in \mathbb{C}^{L_\mathrm{a} \times 1}$, the overall reflected and sensed signal at the IRS are

respectively given by $\mathbf{\Phi}^{\mathsf{H}}\mathbf{x}$ and $\mathbf{D}^{\mathsf{H}}\mathbf{x}$, where

$$\mathbf{\Phi} = \operatorname{diag}\left(\beta_1 e^{j\psi_1}, \ldots, \beta_{L_\mathrm{a}} e^{j\psi_{L_\mathrm{a}}}\right) \tag{2.1}$$

$$\mathbf{D} = \operatorname{diag}\left((1-\beta_1) e^{j\rho_1}, \ldots, (1-\beta_{L_\mathrm{a}}) e^{j\rho_{L_\mathrm{a}}}\right) \tag{2.2}$$

denote the reflection and sensing matrix of the IRS, respectively. Looking at Fig. 2.1, observe that any phase shifts applied at the hybrid IRS to the sensed signal can easily be compensated at the combining stage of the UE. Hence, without loss of generality, it can be assumed that all phase shifts that are applied to the received signal at the UE are applied at the combining stage such that the phase shifts $\rho_l \; \forall \; l$ can be omitted from the model of the sensing matrix in Eq. (2.2). To further simplify the expressions for the reflection and the sensing matrix of the IRS as well as their design process, it is assumed that $\beta_1 = \beta_2 = \cdots = \beta_{L_\mathrm{a}}$ holds. This means that at every IRS element the same magnitude of the reflection coefficient is applied. To shorten the notation, the magnitude of the reflection coefficient is denoted by β in the following for all IRS elements and for simplicity, is referred to as reflection coefficient for the remaining part of the thesis. Using these simplifications, the expressions for the reflection and sensing matrix of the IRS reduce to

$$\mathbf{\Phi}(\beta, \boldsymbol{\psi}) = \beta \operatorname{diag}\left(e^{j\psi_1}, \ldots, e^{j\psi_{L_\mathrm{a}}}\right) \tag{2.3}$$

$$\mathbf{D}(\beta) = (1-\beta)\, \mathbf{I}_{L_\mathrm{a}} \tag{2.4}$$

,

where the dependency on the remaining IRS parameters is made explicit once for illustration purposes and $\boldsymbol{\psi} \coloneqq [\psi_1, \ldots, \psi_{L_\mathrm{a}}]$ contains all phase shifts applied to the reflected signal.

Note that the definition of the reflection and sensing matrix are based on a simplified model that does not hold in practice but is used due to its mathematical simplicity. First, in compliance with [8], it is assumed that there is no coupling between the individual parameters of a single IRS element, i.e. there is no coupling between the reflection coefficient and the corresponding phase shifts nor between the phase shifts themselves. In practice, these parameters are certainly coupled and not every combination of parameters is possible, as discussed in more detail in [17]. Note, however, that the considered hybrid IRS model would allow for a deterministic coupling between the phase shifts of an IRS element. The reason for is that any resulting phase shifts applied to the sensed signal can still be compensated at the combining stage if the coupling is deterministic and known. Since this generalization does, however, not change the overall hybrid IRS model, the simplifying assumption of no coupling is used. Second, the resulting reflection

coefficient and phase shifts at each element are assumed to be ideal, meaning that they are independent of parameters such as the operating frequency or the quality factor of the resonant circuit. However, this independence does not hold in practice, as shown in [16]. Finally, for simplicity, both the sensing and the reflection matrix are assumed to be of size $L_\mathrm{a} \times L_\mathrm{a}$. Yet, in practice, the number of elements used for sensing would be much smaller than the number of elements used for reflection due to power constraints.
For the subsequent sections and chapters, only the expressions for the reflection and sensing matrix, see Eq. (2.3) and (2.4), respectively, are of interest. However, it should be kept in mind that these are based on assumptions and idealizations that do not hold in practice.

2.2. Channel Model

A system operating in the mmWave frequency band, i.e. between 30 GHz and 300 GHz, and consisting of a single BS and a single UE is considered. The carrier frequency of the system is denoted by f_c and the channel bandwidth by B. The BS is equipped with N_rf RF chains that are connected to an antenna array of N_a antennas as well as with a radar receiver that is co-located with the BS. The UE is equipped with a hybrid IRS that consists of L_rf RF chains and L_a surface elements, where each of the surface elements is assumed to be able to simultaneously reflect and sense an incoming signal, as discussed in Sec. 2.1. For simplicity, it is assumed that the transmit and receive array of the BS coincide and that the transmit and receive signal are separated by full-duplex processing, similar to [21].
Both the BS and the UE are considered to be equipped with a uniform linear array (ULA). Assuming a spacing of $\lambda/2$ between the individual elements at both arrays, where $\lambda = c/f_\mathrm{c}$ is the wavelength corresponding to the carrier frequency f_c and c is the speed of light, the array response vectors for the BS and the UE are respectively given by

$$\begin{aligned} [\mathbf{a}(\theta)]_m &= e^{j\pi\,(m-1)\sin(\theta)} \quad m \in [N_\mathrm{a}] \\ [\mathbf{b}(\phi)]_l &= e^{j\pi\,(l-1)\sin(\phi)} \quad l \in [L_\mathrm{a}] \end{aligned}, \tag{2.5}$$

where $\theta \in \left[-\frac{\pi}{2}, \frac{\pi}{2}\right]$ is the AoA or AoD at the BS, $\phi \in \left[-\frac{\pi}{2}, \frac{\pi}{2}\right]$ is the AoA or AoD at the UE and $[N_\mathrm{a}]$ and $[L_\mathrm{a}]$ refer to the index sets $\{1, \ldots, N_\mathrm{a}\}$ and $\{1, \ldots, L_\mathrm{a}\}$, respectively. Note that, although an IRS is typically a planar array which could be modeled more accurately by a uniform planar array, a ULA is used in this thesis to simplify subsequent derivations.
Between the BS and the UE, a linear time-varying LoS channel is considered for both

the DL and UL transmission. In delay-Doppler domain, the DL and UL channel are respectively given by

$$\mathbf{H}^{\mathrm{dl}}(\tau,\nu) = h^{\mathrm{dl}}\mathbf{b}(\phi)\mathbf{a}^{\mathsf{T}}(\theta)\delta(\tau-\tau_0/2)\delta(\nu-\nu_0/2) \in \mathbb{C}^{L_{\mathrm{a}}\times N_{\mathrm{a}}}, \tag{2.6}$$

$$\mathbf{H}^{\mathrm{ul}}(\tau,\nu) = h^{\mathrm{ul}}\mathbf{a}(\theta)\mathbf{b}^{\mathsf{T}}(\phi)\delta(\tau-\tau_0/2)\delta(\nu-\nu_0/2) \in \mathbb{C}^{N_{\mathrm{a}}\times L_{\mathrm{a}}}, \tag{2.7}$$

where h^{dl} and h^{ul} are the attenuation coefficients of the respective channel, τ_0 is the two-way delay, ν_0 the two-way Doppler shift and $\mathbf{a}(\theta)$ and $\mathbf{b}(\phi)$ are the ULA response vectors of the BS and UE depending on their respective AoA, as defined in Eq. (2.5). It is assumed that all channel coefficients defined in Eqs. (2.6) and (2.7) remain constant over N_{slot} slots, where N_{slot} defines the number of slots used for BA. Note that this assumption is justified when the rate at which parameters are measured is high, e.g. every microsecond. As then, a fast moving UE can not cover enough distance between two consecutive measurements that a noticeable change in the AoA or delay is achieved, and hence the variation in AoA and delay is negligible. However, since the UE is moving with a certain velocity that is assumed to be constant, a nonzero Doppler shift is measured.
Further, the overall two-way channel $\mathbf{H}_i(\tau,\nu) \in \mathbb{C}^{N_{\mathrm{a}}\times N_{\mathrm{a}}}$ in the i-th slot of BA is found in delay-Doppler domain from the Eqs. (2.6) and (2.7) by a two-dimensional convolution as

$$\begin{aligned}\mathbf{H}_i(\tau,\nu) &= \mathbf{H}^{\mathrm{ul}}(\tau,\nu) * \mathbf{\Phi}_i^{\mathsf{H}}\mathbf{H}^{\mathrm{dl}}(\tau,\nu)\\ &\overset{(a)}{=} h^{\mathrm{dl}}h^{\mathrm{ul}}\mathbf{a}(\theta)\mathbf{b}^{\mathsf{T}}(\phi)\mathbf{\Phi}_i^{\mathsf{H}}\mathbf{b}(\phi)\mathbf{a}^{\mathsf{T}}(\theta)\delta(\tau-\tau_0)\delta(\nu-\nu_0)\\ &\overset{(b)}{=} h(\mathbf{\Phi}_i)\mathbf{a}(\theta)\mathbf{a}^{\mathsf{T}}(\theta)\delta(\tau-\tau_0)\delta(\nu-\nu_0),\end{aligned} \tag{2.8}$$

where $\mathbf{\Phi}_i$ is the reflection matrix of the IRS configured by the UE in the i-th slot, see Eq. (2.3), (a) follows since for the convolution of two delta functions $\delta(\tau-\tau_a)*\delta(\tau-\tau_b) = \delta(\tau-\tau_a-\tau_b)$[1] holds and (b) follows from the definition of the two-way channel coefficient $h(\mathbf{\Phi}_i)$ as

$$h(\mathbf{\Phi}_i) \coloneqq h^{\mathrm{dl}}h^{\mathrm{ul}}\mathbf{b}^{\mathsf{T}}(\phi)\mathbf{\Phi}_i^{\mathsf{H}}\mathbf{b}(\phi). \tag{2.9}$$

Note that in Eq. (2.9), the expression $\mathbf{b}^{\mathsf{T}}(\phi)\mathbf{\Phi}_i^{\mathsf{H}}\mathbf{b}(\phi)$ defines the gain provided by the IRS in the i-th slot of BA, when the IRS is tuned according to the reflection matrix $\mathbf{\Phi}_i$. Generally, this gain is complex valued, where its magnitude $|\mathbf{b}^{\mathsf{T}}(\phi)\mathbf{\Phi}_i^{\mathsf{H}}\mathbf{b}(\phi)|$ refers to the actual gain provided by the IRS and its phase $\angle(\mathbf{b}^{\mathsf{T}}(\phi)\mathbf{\Phi}_i^{\mathsf{H}}\mathbf{b}(\phi))$ to the phase shift that is introduced by the reflection at the IRS. Without loss of generality, assuming that this phase shift is included in the phase of the complex valued UL attenuation coefficient h^{dl},

[1] Using the Laplace transformation, this identity is proven by
$\mathcal{L}(\delta(\tau-\tau_a)*\delta(\tau-\tau_b)) = \mathcal{L}(\delta(\tau-\tau_a))\mathcal{L}(\delta(\tau-\tau_b)) = e^{-s\tau_a}e^{-s\tau_b} = e^{-s(\tau_a+\tau_b)} = \mathcal{L}(\delta(\tau-\tau_a-\tau_b))$.

the IRS gain $G_{\text{irs}}(\mathbf{\Phi}_i)$ can be defined as

$$G_{\text{irs}}(\mathbf{\Phi}_i) \coloneqq \left|\mathbf{b}^{\mathsf{T}}(\phi)\mathbf{\Phi}_i^{\mathsf{H}}\mathbf{b}(\phi)\right|. \tag{2.10}$$

Furthermore, instead of the delay-Doppler domain, the channels can similarly be defined in the time-delay domain by applying the inverse Fourier transform with respect to ν to the respective delay-Doppler representation of a channel [22]. The DL, UL and overall two-way channel in time-delay domain are then respectively denoted by

$$\begin{aligned}\mathbf{H}^{\text{dl}}(\tau,t) &= \mathcal{F}_{\nu}^{-1}\{\mathbf{H}^{\text{dl}}(\tau,\nu)\} = \int_{-\infty}^{\infty}\mathbf{H}^{\text{dl}}(\tau,\nu)e^{j2\pi\nu t}\,d\nu \\ &= h^{\text{dl}}\mathbf{b}(\phi)\mathbf{a}^{\mathsf{T}}(\theta)\delta(\tau-\tau_0/2)e^{j\pi\nu_0 t},\end{aligned} \tag{2.11}$$

$$\begin{aligned}\mathbf{H}^{\text{ul}}(\tau,t) &= \mathcal{F}_{\nu}^{-1}\{\mathbf{H}^{\text{ul}}(\tau,\nu)\} = \int_{-\infty}^{\infty}\mathbf{H}^{\text{ul}}(\tau,\nu)e^{j2\pi\nu t}\,d\nu \\ &= h^{\text{ul}}\mathbf{a}(\theta)\mathbf{b}^{\mathsf{T}}(\phi)\delta(\tau-\tau_0/2)e^{j\pi\nu_0 t},\end{aligned} \tag{2.12}$$

$$\begin{aligned}\mathbf{H}_i(\tau,t) &= \mathcal{F}_{\nu}^{-1}\{\mathbf{H}_i(\tau,\nu)\} = \int_{-\infty}^{\infty}\mathbf{H}_i(\tau,\nu)e^{j2\pi\nu t}\,d\nu \\ &= h(\mathbf{\Phi}_i)\mathbf{a}(\theta)\mathbf{a}^{\mathsf{T}}(\theta)\delta(\tau-\tau_0)e^{j2\pi\nu_0 t},\end{aligned} \tag{2.13}$$

where $\mathcal{F}_{\nu}^{-1}\{\cdot\}$ denotes the inverse Fourier transform with respect to ν.

2.3. Signal and Communications Model for Beam Alignment Phase

As mentioned in Sec. 2.2, the overall BA scheme is divided in N_{slot} slots of equal length. For each signal that is sent in one of these N_{slot} slots, an orthogonal frequency division multiplexing (OFDM) modulated signal is considered, as OFDM is the most used modulation format for multicarrier scenarios. Therefore, the overall bandwidth B is divided into M subcarriers with Δf denoting the subcarrier spacing between two adjacent subcarriers and the time duration of one slot T_{slot} is divided into N symbols, each of duration T_{o}. With this division of the time-frequency resources, the OFDM signal defines an $N \times M$ grid in each slot i, for $i = 1, \ldots, N_{\text{slot}}$. Typically, the subcarrier spacing is chosen to satisfy

$$\nu_{\max} \ll \Delta f, \tag{2.14}$$

where $\nu_{\max}$ is the maximum possible Doppler shift within the system. This also defines the duration of a single OFDM symbol as $T = 1/\Delta f$. Further, to avoid inter-symbol

interference between adjacent OFDM symbols, each symbol is preceded by a cyclic prefix (CP) of duration T_{cp}, resulting in an overall symbol duration of $T_{\mathrm{o}} = T + T_{\mathrm{cp}}$ and an overall slot duration of $T_{\mathrm{slot}} = NT_{\mathrm{o}}$.
Mathematically, the OFDM modulated signal with CP is expressed in the i-th slot by

$$s_i(t) = \sum_{n=0}^{N-1} \sum_{m=0}^{M-1} x_i[n,m]\, \mathsf{rect}\left(\frac{t - nT_{\mathrm{o}}}{T_{\mathrm{o}}}\right) e^{j2\pi m\Delta f(t - T_{\mathrm{cp}} - nT_{\mathrm{o}})}, \tag{2.15}$$

where $x_i[n,m]$ denotes the complex pilot symbol at the m-th subcarrier and the n-th OFDM symbol and $\mathsf{rect}(\cdot)$ is the rectangular function defined by

$$\mathsf{rect}(t) = \begin{cases} 1, & t \in [0,1] \\ 0, & \text{else} \end{cases}.$$

Note that during all N_{slot} slots of BA the pilots are assumed to be transmitted by the BS. Further, the magnitude of the transmitted pilot symbols is chosen to fulfill the average power constraint given by

$$\mathbb{E}\left[|x_i[n,m]|^2\right] = P_{\mathrm{t}}, \quad \forall (i,n,m). \tag{2.16}$$

For simplicity, it is assumed that the signal in Eq. (2.15) is repeated over all RF chains at the BS, such that the signal transmitted by the BS in the i-th slot is given by

$$\mathbf{s}_i(t) = \mathbf{f}_i \sum_{n=0}^{N-1} \sum_{m=0}^{M-1} x_i[n,m]\, \mathsf{rect}\left(\frac{t - nT_{\mathrm{o}}}{T_{\mathrm{o}}}\right) e^{j2\pi m\Delta f(t - T_{\mathrm{cp}} - nT_{\mathrm{o}})}, \tag{2.17}$$

where $\mathbf{f}_i \in \mathbb{C}^{N_{\mathrm{a}}}$ denotes a generic BF vector of unit norm.

Design of Transmit Beamforming Vector

For the present thesis, it is assumed that during the whole BA protocol, the BS always transmits a fixed wide beam, i.e. a low-directional beam that yields a similar gain over the whole angular range of interest. Thus, since the BF vector $\mathbf{f}_i$ in Eq. (2.17) is the same in every slot i, the subscript i can be omitted and the BF vector is denoted by $\mathbf{f}$ in the following. For the design of this vector $\mathbf{f}$, the strategy chosen in [23] is adopted. Therefore, the field of view (FoV) $\Omega = [-\frac{\pi}{2}, \frac{\pi}{2}]$ is divided into G equidistant angles $\tilde{\theta}_i$ and the matrix $\mathbf{A} = [\mathbf{a}(\tilde{\theta}_1), \ldots, \mathbf{a}(\tilde{\theta}_G)] \in \mathbb{C}^{N_{\mathrm{a}} \times G}$ is defined, where $\mathbf{a}(\cdot)$ is the ULA response vector at the BS defined in Eq. (2.5). Further, the desired radiation pattern is defined by $\bar{\mathbf{b}} = [\bar{b}_1, \ldots, \bar{b}_G]^{\intercal} \in \mathbb{R}^G$, where $\bar{b}_i$ corresponds to the magnitude of the desired radiation

pattern at angle $\tilde{\theta}_i$. Since the transmit BF vector $\mathbf{f}$ should cover the whole angular range with a similar gain of approximately 0 dB, the individual $\bar{b}_i$ should be set to this value for all $i = 1, \ldots, G$. The transmit BF vector $\mathbf{f} \in \mathbb{C}^{N_\mathrm{a}}$ of unit norm is then found as the solution to the magnitude least-squares problem denoted by

$$\begin{aligned} \min_{\mathbf{f}} \quad & \left\| \mathbf{A}^{\mathsf{H}} \mathbf{f} - \bar{\mathbf{b}} \right\|_2^2 \\ \text{s.t.} \quad & \|\mathbf{f}\|_2 = 1 \end{aligned} \quad . \tag{2.18}$$

Hybrid Beamforming Architecture

As described in [2], due to hardware constraints, it is impractical for mmWave systems to equip each antenna element with a separate RF chain. A common approach to tackle this problem is to use hybrid architectures which employ a much smaller number of RF chains than antenna elements. These architectures then implement an additional combining stage which connects the high-dimensional analog domain, given by the number of antenna elements, to the low-dimensional digital domain, given by the number of RF chains. Within this combining stage, each RF chain can be either connected to each antenna element or only to a subset of antenna elements.
To include this hardware constraint in the present system model, both the BS and the UE are assumed to implement a hybrid BF architecture meaning that for both, the number of RF chains is much smaller than the number of antenna elements. Additionally, it is assumed for both that in the implemented hybrid architecture, each RF chain is connected to each antenna element. Therefore, to model the combining stage, both the BS and the UE apply a combining matrix to the signal received at their ULA such that they only have access to a low-dimensional observation of the channel. This combining stage is also illustrated in Fig. 2.1. The combining matrix is denoted by $\mathbf{U}_\mathrm{BS} \in \mathbb{C}^{N_\mathrm{a} \times N_\mathrm{rf}}$ for the BS and by $\mathbf{U}_\mathrm{UE} \in \mathbb{C}^{L_\mathrm{a} \times L_\mathrm{rf}}$ for the UE. In addition, since these combining matrices can be reconfigured in each slot, $\mathbf{U}_{\mathrm{BS},i}$ and $\mathbf{U}_{\mathrm{UE},i}$ refer to the respective combining matrix in the i-th slot of BA at the BS and at the UE.

Received Signal at UE

Note that before transmitting the signals for BA, the UE first needs to synchronize and obtain a meaningful signal model. However, as synchronization is not the main focus of this work and numerous literature exists on the subject, see for example [1, 24], synchronization is not considered and it is assumed that this step has already been performed and that the output of this step, that is the discrete delay estimate, is known and correct.

Under the presence of additive white gaussian noise (AWGN) $\tilde{\mathbf{w}}_i(t) \sim \mathcal{N}(\mathbf{0}, \sigma^2 \mathbf{I}_{L_\mathrm{a}})$, where $\sigma^2 = N_0 B$ is the noise power at bandwidth B and $N_0 = -4 \times 10^{21}\,\mathrm{W/Hz}$ is the noise power density, the received signal at the UE in the i-th slot is given by

$$\tilde{\mathbf{y}}_i(t) = \mathbf{D}_i^{\mathsf{H}} \int \mathbf{H}^{\mathrm{dl}}(t,\tau)\mathbf{s}_i(t-\tau)d\tau + \tilde{\mathbf{w}}_i(t), \tag{2.19}$$

with $\mathbf{D}_i$ denoting the sensing matrix of the IRS configured by the UE in the i-th slot, see Eq. (2.4). Using the expression for the DL channel and for the transmitted signal, see Eqs. (2.11) and (2.17), respectively, Eq. (2.19) can be rewritten as

$$\begin{aligned}\tilde{\mathbf{y}}_i(t) = {} & h^{\mathrm{dl}} \mathbf{D}_i^{\mathsf{H}} \mathbf{b}(\phi)\mathbf{a}^{\mathsf{T}}(\theta) e^{j\pi\nu_0 t}\mathbf{f} \\ & \sum_{n=0}^{N-1}\sum_{m=0}^{M-1} x_i[n,m]\mathsf{rect}\left(\frac{t-\tau_0/2-nT_\mathrm{o}}{T_\mathrm{o}}\right) e^{j2\pi m\Delta f(t-\tau_0/2-T_\mathrm{cp}-nT_\mathrm{o})} + \tilde{\mathbf{w}}_i(t).\end{aligned}$$

Due to the hybrid BF architecture, the UE applies its combining matrix to $\tilde{\mathbf{y}}_i(t)$ to obtain

$$\begin{aligned}\mathbf{y}_i(t) &= \mathbf{U}_{\mathrm{UE},i}^{\mathsf{H}}\, \tilde{\mathbf{y}}_i(t) \\ &= h^{\mathrm{dl}} \mathbf{U}_{\mathrm{UE},i}^{\mathsf{H}}\, \mathbf{D}_i^{\mathsf{H}} \mathbf{b}(\phi)\mathbf{a}^{\mathsf{T}}(\theta) e^{j\pi\nu_0 t}\mathbf{f} \\ &\quad \sum_{n=0}^{N-1}\sum_{m=0}^{M-1} x_i[n,m]\mathsf{rect}\left(\frac{t-\tau_0/2-nT_\mathrm{o}}{T_\mathrm{o}}\right) e^{j2\pi m\Delta f(t-\tau_0/2-T_\mathrm{cp}-nT_\mathrm{o})} + \mathbf{w}_i(t),\end{aligned}$$

with $\mathbf{w}_i(t) = \mathbf{U}_{\mathrm{UE},i}^{\mathsf{H}} \tilde{\mathbf{w}}_i(t) \sim \mathcal{N}(\mathbf{0}, \mathbf{U}_{\mathrm{UE},i}^{\mathsf{H}} \mathbf{U}_{\mathrm{UE},i})$ denoting the noise after the combining matrix. Note that, depending on the structure of the combining matrix, $\mathbf{w}_i(t)$ does not necessarily represent white noise. However, as the combining matrix is designed by the UE in every slot i, it is assumed that the UE always aims to choose the combining matrix as a semi-unitary matrix such that $\mathbf{U}_{\mathrm{UE},i}^{\mathsf{H}} \mathbf{U}_{\mathrm{UE},i} \approx \mathbf{I}_{L_\mathrm{rf}}$, and hence $\mathbf{w}_i(t) \sim \mathcal{N}(\mathbf{0}, \sigma^2 \mathbf{I}_{L_\mathrm{rf}})$ holds in good approximation.

Next, by sampling the observed signal with the sampling interval $\frac{T}{M}$ and taking into account the estimated discrete delay $\hat{l}_0 \frac{T}{M}$ from the synchronization, the received signal $\mathbf{y}_i(t)$ is sampled at $t = nT_\mathrm{o} + (\hat{l}_0 + m)T/M$, where $n = 0, \ldots, N-1$ and $m = 0, \ldots, M-1$.

The sampled signal at the UE yields NM discrete observations given by

$$\begin{aligned}\bar{\mathbf{y}}_i[n,m] &= \mathbf{y}_i(t)|_{t=nT_\mathrm{o}+(\hat{l}_0+m)T/M} \\ &= h^{\mathrm{dl}}\mathbf{U}_{\mathrm{UE},i}^{\mathsf{H}}\,\mathbf{D}_i^{\mathsf{H}}\mathbf{b}(\phi)\mathbf{a}^{\mathsf{T}}(\theta)e^{j\pi\nu_0(nT_\mathrm{o}+(\hat{l}_0+m)T/M)}\mathbf{f} \\ &\quad \sum_{n'=0}^{N-1}\sum_{m'=0}^{M-1} x_i[n',m']\mathsf{rect}\left(\frac{(n-n')T_\mathrm{o}+(\hat{l}_0+m)T/M-\frac{\tau_0}{2}}{T_\mathrm{o}}\right) \\ &\quad e^{j2\pi m'\Delta f((n-n')T_\mathrm{o}+(\hat{l}_0+m)T/M-\frac{\tau_0}{2}-T_\mathrm{cp})}+\bar{\mathbf{w}}_i[n,m],\end{aligned} \tag{2.20}$$

where $\bar{\mathbf{w}}_i[n,m]$ has the same statistics as $\mathbf{w}_i(t)$.
Under the assumption that $\hat{l}_0$ is chosen s.t. $\hat{l}_0\frac{T}{M} > \frac{\tau_0}{2}$ during synchronization, it follows that $(\hat{l}_0+m)\frac{T}{M}-\frac{\tau_0}{2}\in(0,T)$, for $m=0,\dots,M-1$. Then, since $T<T_\mathrm{o}$, the argument of the $\mathsf{rect}(\cdot)$-function in Eq. (2.20) is in the range $[0,1]$ if and only if $n'=n$. Hence, the sum over n' collapses and the $\mathsf{rect}(\cdot)$-function can be omitted by setting $n'=n$ as this yields the only nonzero term.
Denoting $\mathbf{V}_i=\mathbf{D}_i\mathbf{U}_{\mathrm{UE},i}$ as the overall combining matrix at the UE in the i-th slot and setting $n'=n$, Eq. (2.20) simplifies to

$$\begin{aligned}\bar{\mathbf{y}}_i[n,m] &= h^{\mathrm{dl}}\mathbf{V}_i^{\mathsf{H}}\mathbf{b}(\phi)\mathbf{a}^{\mathsf{T}}(\theta)e^{j\pi\nu_0(nT_\mathrm{o}+(\hat{l}_0+m)T/M)}\mathbf{f} \\ &\quad \sum_{m'=0}^{M-1} x_i[n,m']e^{j2\pi m'\Delta f((\hat{l}_0+m)T/M-\frac{\tau_0}{2}-T_\mathrm{cp})}+\bar{\mathbf{w}}_i[n,m] \\ &= h^{\mathrm{dl}}e^{j\pi\nu_0\hat{l}_0T/M}\mathbf{V}_i^{\mathsf{H}}\mathbf{b}(\phi)\mathbf{a}^{\mathsf{T}}(\theta)e^{j\pi\nu_0nT_\mathrm{o}}\mathbf{f} \\ &\quad \sum_{m'=0}^{M-1} x_i[n,m']e^{j2\pi\frac{m}{M}(m'+\frac{\nu_0}{2}T)}e^{j2\pi m'\Delta f(\hat{l}_0T/M-\tau_0/2-T_\mathrm{cp})}+\bar{\mathbf{w}}_i[n,m] \\ &= \tilde{h}^{\mathrm{dl}}\mathbf{V}_i^{\mathsf{H}}\mathbf{b}(\phi)\mathbf{a}^{\mathsf{T}}(\theta)e^{j\pi\nu_0nT_\mathrm{o}}\mathbf{f} \\ &\quad \sum_{m'=0}^{M-1} x_i[n,m']e^{j2\pi\frac{m}{M}(m'+\frac{\nu_0}{2}T)}e^{-j2\pi m'\Delta f(\tau_0/2+\gamma)}+\bar{\mathbf{w}}_i[n,m],\end{aligned} \tag{2.21}$$

where $\tilde{h}^{\mathrm{dl}}=h^{\mathrm{dl}}e^{j\pi\nu_0\hat{l}_0\frac{T}{M}}$ and $\gamma=-\frac{\hat{l}_0}{\Delta fM}+T_\mathrm{cp}$.
Note that since the received symbol $\bar{\mathbf{y}}_i[n,m]$ only depends on pilot symbols sent at time n, i.e. $x_i[n,m']$, there is no inter-symbol interference present in the system. Also, rewriting the expression $e^{j2\pi\frac{m}{M}(m'+\frac{\nu_0}{2}T)}$ as

$$e^{j2\pi\frac{m}{M}(m'+\frac{\nu_0}{2}T)}=e^{j2\pi\frac{mm'}{M}(1+\frac{\nu_0}{2m'\Delta f})} \tag{2.22}$$

shows that due to the term $1 + \frac{\nu_0}{2m'\Delta f}$ the subcarriers are no longer orthogonal to each other, and hence there is inter-carrier interference present in the system. However, due to the assumption in (2.14), the term $\frac{\nu_0}{2m'\Delta f}$ is negligible and the expression (2.22) simplifies to $e^{j2\pi\frac{mm'}{M}}$ such that the subcarriers are approximately orthogonal. Equation (2.21) then reads

$$\bar{\mathbf{y}}_i[n,m] = \tilde{h}^{\mathrm{dl}}\mathbf{V}_i^{\mathsf{H}}\mathbf{b}(\phi)\mathbf{a}^{\mathsf{T}}(\theta)e^{j\pi\nu_0 nT_{\mathrm{o}}}\mathbf{f}\sum_{m'=0}^{M-1} x_i[n,m']e^{j2\pi\frac{mm'}{M}}e^{-j2\pi m'\Delta f(\frac{\tau_0}{2}+\gamma)} + \bar{\mathbf{w}}_i[n,m]. \tag{2.23}$$

Finally, applying the discrete Fourier transform (DFT) with respect to m to (2.23) yields the observed signal at the UE as

$$\begin{aligned}
\boldsymbol{y}_i[n,m] &= \frac{1}{M}\sum_{k=0}^{M-1}\bar{\mathbf{y}}_i[n,k]e^{-j2\pi\frac{mk}{M}} \\
&= \frac{1}{M}\tilde{h}^{\mathrm{dl}}\mathbf{V}_i^{\mathsf{H}}\mathbf{b}(\phi)\mathbf{a}^{\mathsf{T}}(\theta)e^{j\pi\nu_0 nT_{\mathrm{o}}}\mathbf{f} \\
&\quad \sum_{m'=0}^{M-1} x_i[n,m']e^{-j2\pi m'\Delta f(\frac{\tau_0}{2}+\gamma)}\sum_{k=0}^{M-1}e^{j2\pi\frac{k}{M}(m'-m)} + \boldsymbol{w}_i[n,m] \\
&= g^{\mathrm{dl}}\mathbf{V}_i^{\mathsf{H}}\mathbf{b}(\phi)x_i[n,m]e^{-j2\pi m\Delta f(\frac{\tau_0}{2}+\gamma)}e^{j\pi\nu_0 nT_{\mathrm{o}}} + \boldsymbol{w}_i[n,m],
\end{aligned} \tag{2.24}$$

where $\boldsymbol{w}_i[n,m] = \frac{1}{M}\sum_{k=0}^{M-1}\bar{\mathbf{w}}_i[n,k]e^{-j2\pi\frac{mk}{M}} \sim \mathcal{N}_{\mathcal{C}}(\mathbf{0},\sigma^2\mathbf{I}_{L_{\mathrm{rf}}})$ is the noise after the DFT that has the same statistics as $\bar{\mathbf{w}}_i[n,m]$, $g^{\mathrm{dl}} = \tilde{h}^{\mathrm{dl}}\mathbf{a}^{\mathsf{T}}(\theta)\mathbf{f}$ is the overall complex DL channel coefficient, and the last equality follows from the orthogonal property of the DFT of which the proof can be found in [25]. Based on the expression for the observed signal at the UE in Eq. (2.24), the notation

$$\boldsymbol{y}_i = [\boldsymbol{y}_i^{\mathsf{T}}[0,0],\boldsymbol{y}_i^{\mathsf{T}}[0,1],\ldots,\boldsymbol{y}_i^{\mathsf{T}}[N-1,M-1]]^{\mathsf{T}} \in \mathbb{C}^{NML_{\mathrm{rf}}\times 1}$$

is introduced for subsequent chapters to denote the overall received signal at the UE in the i-th slot over all subcarriers and OFDM symbols.

Received Signal at BS

Similar to the received signal at the UE, AWGN $\tilde{\mathbf{n}}_i(t) \sim \mathcal{N}(\mathbf{0},\sigma^2\mathbf{I}_{N_{\mathrm{a}}})$ of power $\sigma^2 = N_0 B$ is assumed at the BS such that the received signal in the i-th slot after the combining

matrix is

$$\begin{aligned}\mathbf{r}_i(t) &= \mathbf{U}_{\mathrm{BS},i}^{\mathsf{H}} \int \mathbf{H}_i(t,\tau)\mathbf{s}_i(t-\tau)d\tau + \mathbf{U}_{\mathrm{BS},i}^{\mathsf{H}}\tilde{\mathbf{n}}_i(t) \\ &= h(\mathbf{\Phi}_i)\mathbf{U}_{\mathrm{BS},i}^{\mathsf{H}}\mathbf{a}(\theta)\mathbf{a}^{\mathsf{T}}(\theta)\mathbf{s}_i(t-\tau_0)e^{j2\pi\nu_0 t} + \mathbf{n}_i(t) \\ &= h(\mathbf{\Phi}_i)\mathbf{U}_{\mathrm{BS},i}^{\mathsf{H}}\mathbf{a}(\theta)\mathbf{a}^{\mathsf{T}}(\theta)e^{j2\pi\nu_0 t}\mathbf{f} \\ &\quad \sum_{n=0}^{N-1}\sum_{m=0}^{M-1} x_i[n,m]\mathsf{rect}\left(\frac{t-\tau_0-nT_{\mathrm{o}}}{T_{\mathrm{o}}}\right)e^{j2\pi m\Delta f(t-\tau_0-T_{\mathrm{cp}}-nT_{\mathrm{o}})} + \mathbf{n}_i(t),\end{aligned}$$

where $\mathbf{n}_i(t) = \mathbf{U}_{\mathrm{BS},i}^{\mathsf{H}}\tilde{\mathbf{n}}_i(t) \sim \mathcal{N}(\mathbf{0}, \mathbf{U}_{\mathrm{BS},i}^{\mathsf{H}}\mathbf{U}_{\mathrm{BS},i})$ is the noise after the combining matrix and $h(\mathbf{\Phi}_i)$ is the overall channel coefficient defined in Eq. (2.9). Note that similar to the combining matrix at the UE, it is assumed that the combining matrix at the BS is designed in every slot i with the aim to obtain a semi-unitary matrix such that $\mathbf{n}_i(t) \sim \mathcal{N}(\mathbf{0}, \sigma^2\mathbf{I}_{N_{\mathrm{rf}}})$ holds in good approximation.
By using a sampling interval of $\frac{T}{M}$ and removing the CP in each OFDM symbol, the received signal $\mathbf{r}_i(t)$ is sampled at $t = nT_{\mathrm{o}} + T_{\mathrm{cp}} + mT/M$, for $n = 0,\ldots,N-1$ and $m = 0,\ldots,M-1$. The sampled signal at the BS reads

$$\begin{aligned}\bar{\mathbf{r}}_i[n,m] &= \mathbf{r}_i(t)|_{t=nT_{\mathrm{o}}+T_{\mathrm{cp}}+mT/M} \\ &= h(\mathbf{\Phi}_i)\mathbf{U}_{\mathrm{BS},i}^{\mathsf{H}}\mathbf{a}(\theta)\mathbf{a}^{\mathsf{T}}(\theta)e^{j2\pi\nu_0(nT_{\mathrm{o}}+T_{\mathrm{cp}}+mT/M)}\,\mathbf{f} \\ &\quad \sum_{n'=0}^{N-1}\sum_{m'=0}^{M-1} x_i[n',m']\mathsf{rect}\left(\frac{(n'-n)T_{\mathrm{o}}+T_{\mathrm{cp}}+mT/M-\tau_0}{T_{\mathrm{o}}}\right) \\ &\quad e^{j2\pi m'\Delta f((n-n')T_{\mathrm{o}}+mT/M-\tau_0)} + \bar{\mathbf{n}}_i[n,m],\end{aligned} \tag{2.25}$$

where $\bar{\mathbf{n}}_i[n,m] = \mathbf{n}_i(nT_{\mathrm{o}} + T_{\mathrm{cp}} + mT/M) \sim \mathcal{N}_{\mathcal{C}}(\mathbf{0}, \sigma^2\mathbf{I}_{N_{\mathrm{rf}}})$. Similar to the derivation for the received signal at the UE, the argument of the $\mathsf{rect}(\cdot)$-function in Eq. (2.25) is in the range $[0,1]$ if and only if $n' = n$, and thus the sum over n' as well as the $\mathsf{rect}(\cdot)$-function can be omitted by setting $n' = n$. Equation (2.25) becomes

$$\begin{aligned}\bar{\mathbf{r}}_i[n,m] = h(\mathbf{\Phi}_i)\mathbf{U}_{\mathrm{BS},i}^{\mathsf{H}}\mathbf{a}(\theta)\mathbf{a}^{\mathsf{T}}(\theta)e^{j2\pi\nu_0(nT_{\mathrm{o}}+T_{\mathrm{cp}}+mT/M)}\,\mathbf{f} \\ \sum_{m'=0}^{M-1} x_i[n,m']e^{j2\pi\frac{m}{M}m'}e^{-j2\pi m'\Delta f\tau_0} + \bar{\mathbf{n}}_i[n,m],\end{aligned}$$

which can be further simplified by recalling assumption (2.14) and the fact that $T_{\text{cp}} < T$ to

$$\begin{aligned}\bar{\mathbf{r}}_i[n,m] = h(\boldsymbol{\Phi}_i)\mathbf{U}_{\text{BS},i}^{\mathsf{H}}\mathbf{a}(\theta)\mathbf{a}^{\mathsf{T}}(\theta)e^{j2\pi\nu_0 nT_{\text{o}}}\,\mathbf{f} \\ \sum_{m'=0}^{M-1} x_i[n,m']e^{j2\pi\frac{m}{M}m'}e^{-j2\pi m'\Delta f\tau_0} + \bar{\mathbf{n}}_i[n,m].\end{aligned} \tag{2.26}$$

By applying the DFT with respect to m to Eq. (2.26), the observed signal at the BS in the i-th slot and at the m-th subcarrier and n-th OFDM symbol is

$$\begin{aligned}\boldsymbol{r}_i[n,m] &= \frac{1}{M}\sum_{k=0}^{M-1}\bar{\mathbf{r}}_i[n,k]e^{-j2\pi\frac{mk}{M}} \\ &= \frac{1}{M}h(\boldsymbol{\Phi}_i)\mathbf{U}_{\text{BS},i}^{\mathsf{H}}\mathbf{a}(\theta)\mathbf{a}^{\mathsf{T}}(\theta)e^{j2\pi\nu_0 nT_{\text{o}}}\mathbf{f} \\ &\quad \sum_{m'=0}^{M-1} x_i[n,m']e^{-j2\pi m'\Delta f\tau_0}\sum_{k=0}^{M-1}e^{j2\pi\frac{k}{M}(m'-m)} + \boldsymbol{n}_i[n,m] \\ &= g_i^{\text{ul}}\mathbf{U}_{\text{BS},i}^{\mathsf{H}}\mathbf{a}(\theta)x_i[n,m]e^{j2\pi nT_{\text{o}}\nu_0}e^{-j2\pi m\Delta f\tau_0} + \boldsymbol{n}_i[n,m],\end{aligned} \tag{2.27}$$

where $\boldsymbol{n}_i[n,m] = \frac{1}{M}\sum_{k=0}^{M-1}\bar{\mathbf{n}}_i[n,k]e^{-j2\pi\frac{mk}{M}} \sim \mathcal{N}_{\mathcal{C}}(\mathbf{0},\sigma^2\mathbf{I}_{N_{\text{rf}}})$ is the noise after the DFT that has the same statistics as $\bar{\mathbf{n}}_i[n,m]$, $g_i^{\text{ul}} = h(\boldsymbol{\Phi}_i)\mathbf{a}^{\mathsf{T}}(\theta)\mathbf{f}$ is the overall complex UL channel coefficient and the last equality follows from the orthogonal property of the DFT, as derived in [25]. Based on the expression for the observed signal at the BS in Eq. (2.27), the notation

$$\boldsymbol{r}_i = [\boldsymbol{r}_i^{\mathsf{T}}[0,0],\boldsymbol{r}_i^{\mathsf{T}}[0,1],\ldots,\boldsymbol{r}_i^{\mathsf{T}}[N-1,M-1]]^{\mathsf{T}} \in \mathbb{C}^{NMN_{\text{rf}}\times 1}$$

is introduced for subsequent chapters to denote the overall received signal at the BS in the i-th slot over all subcarriers and OFDM symbols.

SNR before beamforming

Recalling Eq. (2.24), the SNR at the UE before BF is given by

$$\text{SNR}_{\text{UE,BBF}} = \frac{\lambda^2}{(4\pi d)^2}\frac{P_{\text{t}}}{\sigma^2}, \tag{2.28}$$

where $\lambda^2/(4\pi d)^2 = \left|h^{\text{dl}}\right|^2$ is the attenuation for a given distance d between the BS and the UE, P_{t} is the transmit power of the BS defined in Eq. (2.16) and σ^2 is the noise power introduced in Eq. (2.19). For the definition of the SNR as in Eq. (2.28), the IRS

is assumed to be deactivated, i.e. $\beta = 0$, as otherwise an additional factor of $(1-\beta)^2$ is required. Similarly, by considering Eq. (2.27), the SNR at the BS before BF reads

$$\mathrm{SNR}_{\mathrm{BS,BBF}} = \frac{\lambda^2 \sigma_{\mathrm{rcs,bbf}}}{(4\pi)^3 d^4} \frac{P_\mathrm{t}}{\sigma^2}, \tag{2.29}$$

where $\frac{\lambda^2 \sigma_{\mathrm{rcs,bbf}}}{(4\pi)^3 d^4}$ is the attenuation coefficient for the radar reflected signal after the two-way channel [26], $\sigma_{\mathrm{rcs,bbf}}$ denotes the radar cross-section (RCS) of the IRS before BF and d, P_t and σ^2 are defined as in Eq. (2.28). For more information on the RCS of the IRS, refer to Sec. 5.1. To define the SNR at the BS before BF as in Eq. (2.29), the UE is assumed to not apply any BF to its reflected signal. For this reason, the reflection matrix at the IRS is set to $\mathbf{\Phi} = \mathrm{diag}\left(\sqrt{L_\mathrm{a}}, 0, \ldots, 0\right)$. Note that, although this reflection matrix is not possible from the definition in Eq. (2.3), it is used for Eq. (2.29) to obtain a meaningful definition of the SNR at the BS before BF.
Observe that these SNRs before BF illustrate the fundamental challenge that communication at mmWave brings along and the main reason BA is required. On the one hand, due to the high operating frequency at mmWave bands, or equivalently the small wavelength λ, a severe path loss occurs. On the other hand, utilizing the large bandwidth available at mmWave frequencies increases the noise power σ^2 noticeably compared to conventional sub-6 GHz systems. Both these aspects have a negative impact on the SNR and combined with the fact that the transmit power P_t is limited, the resulting SNRs before BF are very low, especially at the BS due to the two-way channel. These low initial SNRs motivate the need for BA which establishes a directional BF between the BS and the UE to overcome the high path loss and ensures a reliable communication.

2.4. Signal and Communications Model for Communications Phase

The communications phase, used for the DL transmission of payload data, follows directly after BA and is the main reason BA is performed in the first place. At the beginning of the communications phase, the AoAs estimated during BA are used to construct the BF vectors at the BS and the UE respectively as

$$\begin{aligned} \mathbf{f}_{\mathrm{comm}} &= \frac{1}{\sqrt{N_\mathrm{a}}} \mathbf{a}^*(\hat{\theta}_{N_{\mathrm{slot}}}) \\ \mathbf{u}_{\mathrm{comm}} &= \frac{1}{\sqrt{L_\mathrm{a}}} \mathbf{b}(\hat{\phi}_{N_{\mathrm{slot}}}) \end{aligned}, \tag{2.30}$$

where $\hat{\theta}_{N_{\text{slot}}}$ and $\hat{\phi}_{N_{\text{slot}}}$ denote the final estimate of the AoA at the BS and the UE, respectively, after performing BA for N_{slot} slots and the subscript here and in the following refers to the communications phase. Note that in Eq. (2.30), for simplicity, both the BS and the UE are assumed to only use a single RF chain during the communications phase, i.e. $L_{\text{rf}} = N_{\text{rf}} = 1$, and hence $\|\mathbf{f}_{\text{comm}}\|_2^2 = \|\mathbf{u}_{\text{comm}}\|_2^2 = 1$ holds.
For the signal model, similar to the BA phase, see Sec. 2.3, an OFDM modulated signal over M subcarriers with subcarrier spacing Δf and over N symbols with CP duration T_{cp} is considered for the communications phase. Further, the IRS is switched off after BA, meaning $\mathbf{D}_{\text{comm}} = \mathbf{I}_{L_{\text{a}}}$ holds for the sensing matrix and no signal is reflected back to the BS, i.e. there is no two-way channel during the communications phase. Then, assuming the same DL channel as during BA and denoting the sent data symbols by $x_{\text{comm}}[n,m]\ \forall\, n,m$, the received signal at the UE is found similar to Eq. (2.24) as

$$\begin{aligned} y_{\text{comm}}[n,m] &= \tilde{h}^{\text{dl}} \mathbf{a}^{\mathsf{T}}(\theta) \mathbf{f}_{\text{comm}}\, \mathbf{u}_{\text{comm}}^{\mathsf{H}} \mathbf{b}(\phi)\, x_{\text{comm}}[n,m] e^{-j2\pi\Delta f(\frac{\tau_0}{2}+\gamma)} e^{j\pi\nu_0 n T_{\text{o}}} + w_{\text{comm}}[n,m] \\ &= \mathbf{a}^{\mathsf{T}}(\theta) \mathbf{f}_{\text{comm}}\, \mathbf{u}_{\text{comm}}^{\mathsf{H}} \mathbf{b}(\phi)\, \tilde{x}[n,m] + w_{\text{comm}}[n,m], \end{aligned} \tag{2.31}$$

where $w_{\text{comm}}[n,m] \sim \mathcal{NC}(0,\sigma^2)$ is AWGN with the same noise power $\sigma^2 = BN_0$ as during BA and $\tilde{x}[n,m] \coloneqq \tilde{h}^{\text{dl}} x_{\text{comm}}[n,m] e^{-j2\pi\Delta f(\frac{\tau_0}{2}+\gamma)} e^{j\pi\nu_0 n T_{\text{o}}}$. From Eq. (2.31), the SNR for DL transmission in the communications phase, i.e. after BF, can be calculated as

$$\begin{aligned} \text{SNR}_{\text{ABF}} &= \frac{|\tilde{x}|^2 \left|\mathbf{a}^{\mathsf{T}}(\theta) \mathbf{f}_{\text{comm}}\, \mathbf{u}_{\text{comm}}^{\mathsf{H}} \mathbf{b}(\phi)\right|^2}{\sigma^2} \\ &= \frac{\lambda^2}{(4\pi d)^2} \frac{P_{\text{t}}}{\sigma^2} \left|\mathbf{a}^{\mathsf{T}}(\theta) \mathbf{f}_{\text{comm}}\, \mathbf{u}_{\text{comm}}^{\mathsf{H}} \mathbf{b}(\phi)\right|^2 . \end{aligned} \tag{2.32}$$

This expression justifies the design of the BF vectors for the communications phase in Eq. (2.30), since then, the SNR after BF is maximized if the estimated AoAs equal the true AoAs. Denoting the transmit gain by $g_{\text{tx}} = \mathbf{a}^{\mathsf{T}}(\theta)\mathbf{f}_{\text{comm}}$, the receive gain by $g_{\text{rx}} = \mathbf{u}_{\text{comm}}^{\mathsf{H}}\mathbf{b}(\phi)$ and recalling Eq. (2.28), the SNR after BF for the DL transmission can be rewritten as

$$\text{SNR}_{\text{ABF}} = \frac{\lambda^2}{(4\pi d)^2} \frac{P_{\text{t}}}{\sigma^2} \left|g_{\text{tx}} g_{\text{rx}}\right|^2 = \text{SNR}_{\text{UE,BBF}} \left|g_{\text{tx}} g_{\text{rx}}\right|^2 . \tag{2.33}$$

where the expression $|g_{\text{tx}} g_{\text{rx}}|^2 \coloneqq |\mathbf{a}^{\mathsf{T}}(\theta)\mathbf{f}_{\text{comm}}\, \mathbf{u}_{\text{comm}}^{\mathsf{H}} \mathbf{b}(\phi)|^2$ defines the overall BF gain. Equation (2.33) illustrates the general aim of BA, namely maximizing the SNR after BF by maximizing the overall BF gain $|g_{\text{tx}} g_{\text{rx}}|^2 = |\mathbf{a}^{\mathsf{T}}(\theta)\mathbf{f}_{\text{comm}}\, \mathbf{u}_{\text{comm}}^{\mathsf{H}} \mathbf{b}(\phi)|^2$.

3. General Problem Formulation

After describing the system model in Ch. 2, the overall problem considered in the present work is introduced in this chapter. In general, the main objective of any BA scheme is to find the best beam pair between the BS and the UE to ensure a reliable communication in a timely manner. To accomplish this in the present system model, it is sufficient that both the BS and the UE estimate their respective AoA within a predefined target accuracy and afterwards, perform a handshake to indicate the end of the BA protocol.
In this chapter, Sec. 3.1 first provides a high-level description of the general BA problem in mmWave systems and afterwards, introduces the current standard as well as the approach that is taken in this thesis to solve the BA problem. At the end, Sec. 3.2 derives a mathematical formulation for the general BA problem and discusses the found results.

3.1. High-Level Formulation

As briefly explained in Sec. 2.3, the SNR before suitable BF is very low in mmWave systems, especially when compared to systems operating in the traditional sub-6 GHz spectrum. The main reason for this is that due to the high operating frequency, mmWave systems are subject to severe propagation and penetration losses. Yet, since for these systems electrically large antenna arrays can be constructed on a small physical size, highly directional BF gains can and have to be utilized to significantly increase the operating SNR, and thus to overcome the high losses. To utilize these BF gains in the system introduced in Ch. 2, both the UE and the BS must determine their respective AoA since the spatial characteristics of the communication channels, see Eqs. (2.6) – (2.8), are fully determined by these AoAs. Then, by tuning their respective antenna aperture for BF towards their respective AoA, a reliable communication can be established. The task of finding these AoAs and aligning the highly directional beams of the UE and the BS is referred to as the BA problem or as the overall objective of BA.
Since the BA problem in general is very difficult to solve, the standard defined by the 3$^{\text{rd}}$ Generation Partnership Project (3GPP) for 5G resorts to a three-phase heuristic approach to tackle the problem [27]. In the first phase, called beam sweep and measurement, an exhaustive search over all beam pairs that are based on a predefined codebook

is conducted. For each beam pair, the quality of the received signal is measured with respect to a certain metric at the UE or at the BS. Then, in the second phase, called beam determination, either the UE or the BS identifies the best beam pair if a predefined threshold is exceeded, for example by choosing the pair that maximizes the SNR. Finally, the heuristic approach concludes with the beam reporting phase in which the entity which determined the best beam pair informs the other entity about the final beam pair for the subsequent communication. Note that for this reporting only a one-sided BF gain can be utilized. Similar to this approach defined by 3GPP, the heuristic approach proposed in this thesis can also be partitioned into three phases. For this, first recall from Sec. 2.3 that during the entire time of BA, the BS is assumed to transmit a fixed wide beam that yields a similar gain over the whole angular range of interest. Then, the three phases of the proposed BA scheme can be categorized as follows:

1) *UE measurement + AoA estimation*
   In the first phase, the UE keeps the IRS deactivated by setting $\beta = 0$, meaning that no signal is reflected back to the BS. With this setting, the SNR before BF at the UE, see Eq. (2.28), is maximized, and thus the highest estimation accuracy can be achieved. Then, during every slot within this phase, the UE chooses its combining matrix with respect to its design strategy and ultimately obtains an observation of the transmitted signal. After that, using all observations up to the present slot, the UE estimates its AoA according to its employed estimation method. This process is repeated until in a certain slot, a target estimation accuracy is obtained or, since this accuracy can not be directly measured, until the UE is confident in its estimate. To capture this confidence, the fluctuation of the AoA estimate across multiple slots is considered and it is assumed that the estimation is successful if the estimate stays within a certain interval for a predefined number of slots.

2) *IRS activation, BS measurement + AoA estimation*
   At the beginning of this phase, the UE configures the IRS for reflection towards its estimated AoA. While this configuration determines the applied phase shifts ψ_l, for $l = 1, \ldots, L_\mathrm{a}$, as shown later in Sec. 4.3, different values for β are possible. The UE can either set β to one to maximize the SNR before BF at the BS, see Eq. (2.29), or to any value in the open interval $(0, 1)$ if the UE wants to further receive a signal and refine its estimate by continuing the strategy described in 1). Regardless of the ultimately chosen value of β, this illustrates that first the UE needs to estimate its AoA up to a certain accuracy in order to be able to reflect the signal back to the BS with a large BF gain. Then, similar to the first phase, during every slot within this phase, the BS chooses its combining matrix, obtains a new observation

and finds its AoA estimate from its employed estimation method by considering all past and present observations. The second phase is concluded once the predefined maximum number of slots is exceeded or, alternatively, once the BS is confident in its estimate, with the confidence being defined exactly as in 1).

3) *BA completion*
The BS informs the UE about the end of the BA scheme by sending a predefined signal that terminates the BA protocol. Contrary to the approach defined by 3GPP, a two-sided BF gain can be utilized for this reporting since both the BS and the UE have already estimated their respective AoA. Note that this reporting is in theory only possible if, in the second phase, the UE chooses a value for β that allows itself to still be able to understand the termination request of the BS, i.e. $\beta < 1$. However, as this detail has only a very minor impact on the final performance, it is mentioned here for completeness but discarded for the simulations in Ch. 5.

Observe that the achieved accuracy of the considered BA scheme heavily depends on the employed estimation methods and the strategies for the design of the combining matrices as well as the value of β across all slots of BA. For this reason, these components are considered individually in Ch. 4 in detail to optimize the performance of the BA scheme.

3.2. Mathematical Formulation

After explaining the general BA problem as well as the considered approach from a high-level perspective in Sec. 3.1, these aspects are now discussed from a more technical point of view in the following. To find a formulation for the general BA problem, recall from Sec. 2.4 that the overall objective to be solved during BA is to maximize the SNR after BF, see Eq. (2.33), by maximizing the BF gain given by

$$|g_{\mathrm{tx}} g_{\mathrm{rx}}|^2 = |\mathbf{a}^{\mathsf{T}}(\theta)\mathbf{f}_{\mathrm{comm}}\,\mathbf{u}_{\mathrm{comm}}^{\mathsf{H}}\mathbf{b}(\phi)|^2 = \left|\mathbf{a}^{\mathsf{T}}(\theta)\frac{\mathbf{a}^*(\hat{\theta}_{N_{\mathrm{slot}}})}{\sqrt{N_{\mathrm{a}}}}\,\frac{\mathbf{b}^{\mathsf{H}}(\hat{\phi}_{N_{\mathrm{slot}}})}{\sqrt{L_{\mathrm{a}}}}\mathbf{b}(\phi)\right|^2 ,$$

where $\hat{\theta}_{N_{\mathrm{slot}}}$ and $\hat{\phi}_{N_{\mathrm{slot}}}$ refer to the final AoA estimate at the BS and the UE, respectively. To find these estimates in any slot i of BA, both the BS and the UE employ an estimation method denoted by

$$\hat{\phi}_i = \mathcal{E}_{\mathrm{UE}}\left(\boldsymbol{y}^{(i)}, \left(\mathbf{U}_{\mathrm{UE}}^{(i)}, \beta^{(i)}, \boldsymbol{\psi}^{(i)}, \mathbf{f}^{(i)}\right)\right) , \tag{3.1}$$

$$\hat{\theta}_i = \mathcal{E}_{\mathrm{BS}}\left(\boldsymbol{r}^{(i)}, \left(\mathbf{U}_{\mathrm{BS}}^{(i)}, \beta^{(i)}, \boldsymbol{\psi}^{(i)}, \mathbf{f}^{(i)}\right)\right) \tag{3.2}$$

where the superscript $(i) = \{1, \ldots, i\}$ indicates that all observations and used parameters up to the i-th slot are relevant to the estimation methods, e.g. $\boldsymbol{y}^{(i)} = \{\boldsymbol{y}_1, \ldots, \boldsymbol{y}_i\}$ with $\boldsymbol{y}_i$ referring to the signal received at the UE over all subcarriers and all time symbols in the i-th slot. Note that, although the transmit BF vector $\mathbf{f}$, see Eq. (2.18), is assumed to be constant during BA within the scope of this thesis, the dependency on $\mathbf{f}^{(i)} = \{\mathbf{f}_1, \ldots, \mathbf{f}_i\}$ in Eqs. (3.1) and (3.2) is made explicit for the case of slot-varying transmit BF vectors to obtain a more general formulation.
Then, the general BA problem can be stated as the maximization of the (unnormalized) BF gain as

$$
\begin{aligned}
\max_{s \in \mathcal{S}, \mathcal{E}_{UE}(\cdot,\cdot), \mathcal{E}_{BS}(\cdot,\cdot)} \quad & \mathbb{E}\left[\left|\mathbf{a}^{\mathsf{T}}(\theta)\, \mathbf{a}^{*}(\hat{\theta}_{N_{\text{slot}}})\, \mathbf{b}^{\mathsf{H}}(\hat{\phi}_{N_{\text{slot}}}) \mathbf{b}(\phi)\right|^2\right] \\
\text{s.t.} \quad & \forall i = 1, \ldots, N_{\text{slot}} \\
& s_i = \{\mathbf{U}_{\text{UE},i}, \mathbf{U}_{\text{BS},i}, \beta_i, \boldsymbol{\psi}_i, \mathbf{f}_i\} \\
& \hat{\phi}_i = \mathcal{E}_{\text{UE}}\left(\boldsymbol{y}^{(i)}, s^{(i)}\right) \\
& \hat{\theta}_i = \mathcal{E}_{\text{BS}}\left(\boldsymbol{r}^{(i)}, s^{(i)}\right) \\
& \|\mathbf{f}_i\|_2^2 = 1 \\
& \left\|[\mathbf{U}_{\text{UE},i}]_m\right\|_2^2 = \frac{1}{L_{\text{rf}}} \quad \forall \quad m = 1, \ldots, L_{\text{rf}} \\
& \left\|[\mathbf{U}_{\text{BS},i}]_n\right\|_2^2 = \frac{1}{N_{\text{rf}}} \quad \forall \quad n = 1, \ldots, N_{\text{rf}} \\
& \beta_i \in [0, 1] \\
& [\boldsymbol{\psi}_i]_l \in [-\pi, \pi] \quad \forall \quad l = 1, \ldots, L_{\text{a}} \\
& \left(\beta_{j+1}, \boldsymbol{\psi}_{j+1}\right) = \mathcal{G}_j\left(\boldsymbol{y}^{(j)}, s^{(j)}\right) \quad \forall \quad j = 1, \ldots, N_{\text{slot}} - 1
\end{aligned}
\qquad , \qquad (3.3)
$$

where the expectation is taken over all stochastic parameters,

$$
\mathcal{S} = \left\{\mathbf{U}_{\text{UE}}^{(N_{\text{slot}})}, \mathbf{U}_{\text{BS}}^{(N_{\text{slot}})}, \beta^{(N_{\text{slot}})}, \boldsymbol{\psi}^{(N_{\text{slot}})}, \mathbf{f}^{(N_{\text{slot}})}\right\}
$$

denotes the set of all strategies for the design of the sequence of combining matrices, the sequence of IRS parameters and the sequence of transmit BF vectors across all N_{slot} slots of BA, s is the strategy ultimately chosen across all N_{slot} slots, s_i the strategy chosen in the i-th slot and $s^{(i)}$ denotes all strategies chosen up to the i-th slot. Further, $\mathcal{E}_{\text{UE}}(\cdot,\cdot)$ and $\mathcal{E}_{\text{BS}}(\cdot,\cdot)$ are the employed estimation methods of the BS and the UE introduced in Eqs. (3.1) and (3.2), respectively, and $\mathcal{G}_j(\cdot,\cdot)$ is the strategy chosen in the j-th slot to determine the IRS parameters of the subsequent slot $j+1$. Finally, the notation $\boldsymbol{y}_i$ and $\boldsymbol{r}_i$

respectively refers to the received signal at the UE and the BS in the i-th slot over all M subcarriers and N time symbols, as introduced in Sec. 2.3. Note that Eq. (3.3) describes the general BA problem between a BS and a UE that is equipped with a hybrid IRS. To obtain the corresponding formulation for BA without an IRS, the IRS parameters β and $\boldsymbol{\psi}$ as well as the design strategy $\mathcal{G}_j(\cdot,\cdot)$ can be simply omitted from the optimization problem and from the set $\mathcal{S}$.

Since the objective in Eq. (3.3) is infeasible to be solved analytically, common approaches to BA, such as standard defined by 3GPP for 5G, resort to a heuristic approach to solve the general BA problem [27], as explained in Sec. 3.1. Such heuristic approach is usually only used to find the best design strategy $s \in \mathcal{S}$ rather than to optimize the estimation methods $\mathcal{E}_{\mathrm{UE}}(\cdot,\cdot)$ and $\mathcal{E}_{\mathrm{BS}}(\cdot,\cdot)$, respectively, since these estimation methods can be optimized separately from the design strategy s and are often decided on before the actual BA. Then, to determine the best design strategy $s \in \mathcal{S}$ for the case that no IRS is used, most heuristic approaches restrict the space from which the transmit BF vectors and combining matrices can be chosen to a so called beamforming codebook $\bar{\mathcal{V}} = \{\bar{\mathbf{v}}_1, \ldots, \bar{\mathbf{v}}_K\}$, i.e. a set of predefined BF vectors $\bar{\mathbf{v}}_1, \ldots, \bar{\mathbf{v}}_K$, where $K = |\bar{\mathcal{V}}|$ denotes the size of the codebook. Usually, such codebook is constructed before the start of the BA protocol by first discretizing the angular range into K equally spaced angles and afterwards, computing a BF vector for each obtained angle. For these codebook-based approaches, the individual BF vectors are computed in a way that each of them yields a certain gain towards their corresponding angle as well as small region around it and almost no gain over the remaining angular space. The idea of such approach is then to sample a subset $\bar{\mathcal{V}}_i$ from $\bar{\mathcal{V}}$ in every slot i of BA and use this subset as combining matrix in the current slot. More precisely, by denoting the beamforming codebook of the BS and the UE by $\mathcal{U}_{\mathrm{BS}}$ and $\mathcal{U}_{\mathrm{UE}}$, respectively, a codebook-based approach to BA proceeds as follows. In every slot i, the BS randomly chooses one vector from $\mathcal{U}_{\mathrm{BS}}$ as its transmit BF vector $\mathbf{f}_i$ and N_{rf} vectors from $\mathcal{U}_{\mathrm{BS}}$ as its combining matrix $\mathbf{U}_{\mathrm{BS},i}$, while the UE randomly chooses L_{rf} vectors from $\mathcal{U}_{\mathrm{UE}}$ as its combining matrix $\mathbf{U}_{\mathrm{UE},i}$. Using this method, the whole angular range of interest is explored after a certain number of slots and the AoA can be estimated at the BS and the UE, respectively.

While the design strategy for the combining matrices in this thesis can be derived similar to the just discussed conventional approach for finding the best strategy $s \in \mathcal{S}$ when no IRS is used, the employed estimation methods as well as the IRS parameters must be designed as well. For this reason, Ch. 4 discusses each of these components individually in detail to optimize the performance of the proposed BA scheme.

4. Proposed Scheme

While discussing the general BA problem in Ch. 3, it has been shown that the approach taken in this thesis heavily depends on the employed estimation methods as well as on the strategies for designing the combining matrices and the IRS parameters. For this reason, this chapter introduces the proposed scheme to design each of these components. First, in Sec. 4.1, the employed methods for the AoA estimation at the UE and at the BS, respectively, are derived. Next, Sec. 4.2 discusses the used strategy for designing the combining matrices both at the BS as well as the UE, before Sec. 4.3 introduces the design strategy for the IRS parameters. Afterwards, a performance analysis of the overall system is conducted by deriving the CRLB of the AoA estimation at the UE in Sec. 4.4. The chapter concludes by summarizing the proposed BA scheme in the form of an algorithm in Sec. 4.5.

4.1. Multi-slot Maximum Likelihood Estimation

As discussed in Sec. 3.1, in order to solve the BA problem for the considered system and to establish a reliable communication, the BS as well as the UE are required to estimate their respective AoA. For this reason, a maximum likelihood (ML) scheme is derived for the AoA estimation at the BS and the UE. To further increase the accuracy of the ultimately implemented estimation methods, in a certain slot of BA, all observations up to the current slot are taken into account for the AoA estimation such that the accuracy of the estimate improves over time. Then, in every slot of BA, the employed multi-slot ML estimation methods find the AoA at the BS and at the UE as the angles that make the set of all observations made up to the current slot most probable.
Since the expressions for the received signal at the UE and the BS differ by the fact that at the BS the overall complex channel coefficient is varying in each slot, compare Eq. (2.24) and Eq. (2.27), the ML estimate is derived for each entity separately. Nevertheless, as this coefficient is the only difference in the respective expressions for the received signals, part of the derivation is similar for both the UE and the BS, and thus results are reused whenever possible. Note that part of the derivation is moved to Appendix A for the sake of clarity.

4.1.1. ML estimation at UE

To derive the multi-slot ML estimate at the UE, the expression for the observed signal at the UE in Eq. (2.24) is rewritten as

$$\begin{aligned}\boldsymbol{y}_i[n,m] &= g^{\mathrm{dl}}\mathbf{V}_i^{\mathsf{H}}\mathbf{b}(\phi)x_i[n,m]\underbrace{e^{-j2\pi m\Delta f\left(\frac{\tau_0}{2}+\psi\right)}e^{j\pi\nu_0 nT_o}}_{:=t_{n,m}(\tau_0,\nu_0)}+\boldsymbol{w}_i[n,m]\\ &= g^{\mathrm{dl}}\mathbf{V}_i^{\mathsf{H}}\mathbf{b}(\phi)x_i[n,m]t_{n,m}(\tau_0,\nu_0)+\boldsymbol{w}_i[n,m]. \end{aligned} \tag{4.1}$$

Based on Eq. (4.1), the expression for the signal received in the i-th slot over all M subcarriers and N OFDM symbols can then be formulated by stacking all NM observations $\boldsymbol{y}_i[n,m]$, for $n=0,\dots,N-1$ and $m=0,\dots,M-1$, into a column vector $\boldsymbol{y}_i\in\mathbb{C}^{NML_{\mathrm{rf}}\times 1}$ which yields

$$\begin{aligned}\boldsymbol{y}_i &= \begin{bmatrix}\boldsymbol{y}_i[0,0]\\ \boldsymbol{y}_i[0,1]\\ \vdots\\ \boldsymbol{y}_i[N-1,M-1]\end{bmatrix}\\ &= \begin{bmatrix}x_i[0,0]\ t_{0,0}(\tau_0,\nu_0)\\ x_i[0,1]\ t_{0,1}(\tau_0,\nu_0)\\ \vdots\\ x_i[N-1,M-1]\ t_{N-1,M-1}(\tau_0,\nu_0)\end{bmatrix}\otimes\left(g^{\mathrm{dl}}\mathbf{V}_i^{\mathsf{H}}\mathbf{b}(\phi)\right)+\begin{bmatrix}\boldsymbol{w}_i[0,0]\\ \boldsymbol{w}_i[0,1]\\ \vdots\\ \boldsymbol{w}_i[N-1,M-1]\end{bmatrix}\\ &= \left(\mathbf{T}(\tau_0,\nu_0)\otimes g^{\mathrm{dl}}\mathbf{V}_i^{\mathsf{H}}\mathbf{b}(\phi)\right)\boldsymbol{x}_i+\boldsymbol{w}_i\\ &= g^{\mathrm{dl}}\mathbf{G}_i(\tau_0,\nu_0,\phi)\boldsymbol{x}_i+\boldsymbol{w}_i, \end{aligned} \tag{4.2}$$

where

$$\begin{aligned}\boldsymbol{x}_i &\coloneqq [x_i[0,0],x_i[0,1],\dots,x_i[N-1,M-1]]^{\mathsf{T}} &&\in\mathbb{C}^{NM\times 1},\\ \boldsymbol{w}_i &\coloneqq [\boldsymbol{w}_i^{\mathsf{T}}[0,0],\boldsymbol{w}_i^{\mathsf{T}}[0,1],\dots,\boldsymbol{w}_i^{\mathsf{T}}[N-1,M-1]]^{\mathsf{T}} &&\in\mathbb{C}^{NML_{\mathrm{rf}}\times 1},\\ \mathbf{T}(\tau_0,\nu_0) &\coloneqq \mathrm{diag}\left(t_{0,0}(\tau_0,\nu_0),\ \dots,t_{N-1,M-1}(\tau_0,\nu_0)\right) &&\in\mathbb{C}^{NM\times NM},\\ \mathbf{G}_i(\tau_0,\nu_0,\phi) &\coloneqq \mathbf{T}(\tau_0,\nu_0)\otimes\mathbf{V}_i^{\mathsf{H}}\mathbf{b}(\phi) &&\in\mathbb{C}^{NML_{\mathrm{rf}}\times NM}. \end{aligned}$$

Recall from Sec. 2.3 that the UE aims to design its combining matrix in every slot i of BA as a semi-unitary matrix such that the AWGN assumption for the observed signal in Eq. (4.1) holds in good approximation. For this reason, $\boldsymbol{w}_i\sim\mathcal{N}_{\mathcal{C}}(\mathbf{0},\sigma^2\mathbf{I}_{NML_{\mathrm{rf}}})$ also

holds, and hence $\boldsymbol{y}_i \sim \mathcal{N}_{\mathbb{C}}\left(g^{\mathrm{dl}}\mathbf{G}_i(\tau_0,\nu_0,\phi)\boldsymbol{x}_i,\, \sigma^2\mathbf{I}_{NML_{\mathrm{rf}}}\right)$. Thus, the likelihood-function of $\boldsymbol{y}_i$ is given by

$$L(\boldsymbol{y}_i;(g^{\mathrm{dl}},\tau_0,\nu_0,\phi)) = \frac{1}{\det(2\pi\sigma^2\mathbf{I}_{NML_{\mathrm{rf}}})^{1/2}}\ \exp\left(-\frac{1}{2\sigma^2}\left((\boldsymbol{y}_i - g^{\mathrm{dl}}\mathbf{G}_i\boldsymbol{x}_i)^{\mathsf{H}}(\mathbf{y}_i - g^{\mathrm{dl}}\mathbf{G}_i\boldsymbol{x}_i)\right)\right), \tag{4.3}$$

where the dependency of $\mathbf{G}_i$ on τ_0, ν_0 and ϕ is omitted here and in the following for the sake of clarity. Collecting all observations made up to the i-th slot, denoted by $\boldsymbol{y}^{(i)} = \{\boldsymbol{y}_1,\ldots,\boldsymbol{y}_i\}$, the log-likelihood function of $\boldsymbol{y}^{(i)}$ is defined by

$$\begin{aligned}\ell(\boldsymbol{y}^{(i)};(g^{\mathrm{dl}},\tau_0,\nu_0,\phi)) &= \log\left(L(\boldsymbol{y}^{(i)};(g^{\mathrm{dl}},\tau_0,\nu_0,\phi))\right)\\ &= \log\Big(\prod_{s=1}^{i} L(\boldsymbol{y}_i;(g^{\mathrm{dl}},\tau_0,\nu_0,\phi))\Big)\\ &= \sum_{s=1}^{i}\log\left(L(\boldsymbol{y}_i;(g^{\mathrm{dl}},\tau_0,\nu_0,\phi))\right).\end{aligned} \tag{4.4}$$

Using Eq. (4.4), the ML estimate of the unknown parameters is given in the i-th slot according to [28] by

$$\begin{aligned}(\hat{g}_i^{\mathrm{dl}},\hat{\tau}_i,\hat{\nu}_i,\hat{\phi}_i) &= \underset{g^{\mathrm{dl}},\tau_0,\nu_0,\phi}{\arg\max}\ \ell(\boldsymbol{y}^{(i)};(g^{\mathrm{dl}},\tau_0,\nu_0,\phi))\\ &= \underset{g^{\mathrm{dl}},\tau_0,\nu_0,\phi}{\arg\min}\ \sum_{s=1}^{i}\left\|\boldsymbol{y}_s - g^{\mathrm{dl}}\mathbf{G}_s\boldsymbol{x}_s\right\|_2^2\\ &= \underset{g^{\mathrm{dl}},\tau_0,\nu_0,\phi}{\arg\min}\ \sum_{s=1}^{i}\boldsymbol{y}_s^{\mathsf{H}}\boldsymbol{y}_s + \left|g^{\mathrm{dl}}\right|^2(\mathbf{G}_s\boldsymbol{x}_s)^{\mathsf{H}}\mathbf{G}_s\boldsymbol{x}_s - 2\mathrm{Re}\left\{(g^{\mathrm{dl}})^{\mathsf{H}}\boldsymbol{x}_s^{\mathsf{H}}\mathbf{G}_s^{\mathsf{H}}\boldsymbol{y}_s\right\}\\ &= \underset{g^{\mathrm{dl}},\tau_0,\nu_0,\phi}{\arg\min}\ \sum_{s=1}^{i}\left|g^{\mathrm{dl}}\right|^2\boldsymbol{x}_s^{\mathsf{H}}\mathbf{G}_s^{\mathsf{H}}\mathbf{G}_s\boldsymbol{x}_s - 2\mathrm{Re}\left\{(g^{\mathrm{dl}})^{*}\boldsymbol{x}_s^{\mathsf{H}}\mathbf{G}_s^{\mathsf{H}}\boldsymbol{y}_s\right\}.\end{aligned} \tag{4.5}$$

Denoting $\mathbf{Y}_s = [\boldsymbol{y}_s[0,0],\ldots,\boldsymbol{y}_s[N-1,M-1]] \in \mathbb{C}^{L_{\mathrm{rf}}\times NM}$ as the matrix containing all observations of the UE in the s-th slot as its columns and defining

$$\begin{aligned}\mathbf{V}_{(i)} &\coloneqq \sum_{s=1}^{i}\|\boldsymbol{x}_s\|_2^2\mathbf{V}_s\mathbf{V}_s^{\mathsf{H}},\\ \mathbf{c}_{(i)}(\tau_0,\nu_0) &\coloneqq \left[\sum_{s=1}^{i}\boldsymbol{x}_s^{\mathsf{T}}\mathbf{T}(\tau_0,\nu_0)\mathbf{Y}_s^{\mathsf{H}}\mathbf{V}_s^{\mathsf{H}}\right]^{\mathsf{H}},\end{aligned} \tag{4.6}$$

the ML estimate in Eq. (4.5) simplifies to

$$(\hat{g}_i^{\mathrm{dl}}, \hat{\tau}_i, \hat{\nu}_i, \hat{\phi}_i) = \underset{g^{\mathrm{dl}},\tau_0,\nu_0,\phi}{\arg\max}\ \mathrm{Re}\left\{2g^{\mathrm{dl}}\mathbf{c}_{(i)}^{\mathsf{H}}(\tau_0,\nu_0)\mathbf{b}(\phi) - \left|g^{\mathrm{dl}}\right|^2\mathbf{b}^{\mathsf{H}}(\phi)\mathbf{V}_{(i)}\mathbf{b}(\phi)\right\}, \tag{4.7}$$

where the derivation can be found in Appendix A in Eqs. (A.1) - (A.6).
Further, for a given τ_0, ν_0 and ϕ, the optimal g^{dl}, i.e. the one that maximizes Eq. (4.7), is found by

$$\frac{\partial}{\partial \mathrm{Re}\{g^{\mathrm{dl}}\}}\mathrm{Re}\left\{2g^{\mathrm{dl}}\mathbf{c}_{(i)}^{\mathsf{H}}(\tau_0,\nu_0)\mathbf{b}(\phi) - \left|g^{\mathrm{dl}}\right|^2\mathbf{b}^{\mathsf{H}}(\phi)\mathbf{V}_{(i)}\mathbf{b}(\phi)\right\} = 0 \tag{4.8a}$$

$$\frac{\partial}{\partial \mathrm{Im}\{g^{\mathrm{dl}}\}}\mathrm{Re}\left\{2g^{\mathrm{dl}}\mathbf{c}_{(i)}^{\mathsf{H}}(\tau_0,\nu_0)\mathbf{b}(\phi) - \left|g^{\mathrm{dl}}\right|^2\mathbf{b}^{\mathsf{H}}(\phi)\mathbf{V}_{(i)}\mathbf{b}(\phi)\right\} = 0 \tag{4.8b}$$

which results in

$$g_{\mathrm{opt}}^{\mathrm{dl}} = \frac{\mathbf{b}^{\mathsf{H}}(\phi)\mathbf{c}_{(i)}(\tau_0,\nu_0)}{\mathbf{b}^{\mathsf{H}}(\phi)\mathbf{V}_{(i)}\mathbf{b}(\phi)}, \tag{4.9}$$

as derived in Appendix A in Eqs. (A.7) - (A.9).
Substituting expression (4.9) into Eq. (4.7) yields the ML estimate at the UE in the i-th slot as

$$\begin{aligned}(\hat{\tau}_i, \hat{\nu}_i, \hat{\phi}_i) &= \underset{\tau_0,\nu_0,\phi}{\arg\max}\ \mathrm{Re}\left\{2\,\frac{\left|\mathbf{b}^{\mathsf{H}}(\phi)\mathbf{c}_{(i)}(\tau_0,\nu_0)\right|^2}{\mathbf{b}^{\mathsf{H}}(\phi)\mathbf{V}_{(i)}\mathbf{b}(\phi)} - \frac{\left|\mathbf{b}^{\mathsf{H}}(\phi)\mathbf{c}_{(i)}(\tau_0,\nu_0)\right|^2}{\mathbf{b}^{\mathsf{H}}(\phi)\mathbf{V}_{(i)}\mathbf{b}(\phi)}\right\} \\ &= \underset{\tau_0,\nu_0,\phi}{\arg\max}\ \frac{\left|\mathbf{b}^{\mathsf{H}}(\phi)\mathbf{c}_{(i)}(\tau_0,\nu_0)\right|^2}{\mathbf{b}^{\mathsf{H}}(\phi)\mathbf{V}_{(i)}\mathbf{b}(\phi)}\,.\end{aligned} \tag{4.10}$$

Note that for the derived ML estimate the information about past observations is contained within $\mathbf{c}_{(i)}(\tau_0,\nu_0)$ and $\mathbf{V}_{(i)}$. As in every slot i, these two quantities can be computed using only $\mathbf{Y}_i$, $\boldsymbol{x}_i$ and $\mathbf{V}_i$ as well as $\mathbf{c}_{(i-1)}(\tau_0,\nu_0)$ and $\mathbf{V}_{(i-1)}$, the ML estimate in Eq. (4.10) can be implemented to have the same computational complexity in each slot. Further, although for the present thesis only the AoA estimate is of interest, the delay and Doppler estimate are obtained from the derived estimation method without further expense. These two estimates could, for instance, be relevant to beam tracking or beam refinement techniques that might be used after successful BA.

4.1.2. ML estimation at BS

Note that Eq. (2.27) is of the same form as Eq. (2.24) with the minor difference that the complex channel coefficient depends on the slot index in the expression for the received signal at the BS. Therefore, the results derived for ML estimation at the UE can be

reused up to the point where the slot dependent channel coefficient has to be taken into account. By defining

$$\begin{aligned}
\boldsymbol{r}_i &\coloneqq [\boldsymbol{r}_i^{\mathsf{T}}[0,0], \boldsymbol{r}_i^{\mathsf{T}}[0,1], \dots, \boldsymbol{r}_i^{\mathsf{T}}[N-1,M-1]]^{\mathsf{T}} &&\in \mathbb{C}^{NMN_{\mathrm{rf}}\times 1},\\
\boldsymbol{x}_i &\coloneqq [x_i[0,0], x_i[0,1], \dots, x_i[N-1,M-1]]^{\mathsf{T}} &&\in \mathbb{C}^{NM\times 1},\\
\boldsymbol{n}_i &\coloneqq [\boldsymbol{n}_i^{\mathsf{T}}[0,0], \boldsymbol{n}_i^{\mathsf{T}}[0,1], \dots, \boldsymbol{n}_i^{\mathsf{T}}[N-1,M-1]]^{\mathsf{T}} &&\in \mathbb{C}^{NMN_{\mathrm{rf}}\times 1},\\
\tilde{t}_{n,m}(\tau_0,\nu_0) &\coloneqq e^{j2\pi nT_{\mathrm{o}}\nu_0} e^{-j2\pi m\Delta f\tau_0} &&\in \mathbb{C},\\
\tilde{\mathbf{T}}(\tau_0,\nu_0) &\coloneqq \mathrm{diag}(\tilde{t}_{0,0}(\tau_0,\nu_0), \dots, \tilde{t}_{N-1,M-1}(\tau_0,\nu_0)) &&\in \mathbb{C}^{NM\times NM},
\end{aligned}$$

the overall received signal at the BS over all M subcarriers and N OFDM symbols in the i-th slot is denoted by

$$\boldsymbol{r}_i = \left(\tilde{\mathbf{T}}(\tau_0,\nu_0) \otimes g_i^{\mathrm{ul}} \mathbf{U}_{\mathrm{BS},i}^{\mathsf{H}} \mathbf{a}(\theta)\right) \boldsymbol{x}_i + \boldsymbol{n}_i. \tag{4.11}$$

The expression for the ML estimate of the unknown parameters is given the cost function found in Appendix A in Eq. (A.4) as up to this step the results are the same for the constant and the varying complex channel coefficient. Formally, the ML estimate reads

$$\begin{aligned}
(\{\hat{g}^{\mathrm{ul}}\}_{s=1}^{i}, \hat{\tau}_i, \hat{\nu}_i, \hat{\theta}_i) = \underset{\{g^{\mathrm{ul}}\}_{s=1}^{i},\tau_0,\nu_0,\theta}{\arg\min} \mathrm{Re}\Bigg\{ &\sum_{s=1}^{i} \left|g_s^{\mathrm{ul}}\right|^2 \|\boldsymbol{x}_s\|_2^2\, \mathbf{a}^{\mathsf{H}}(\theta) \mathbf{U}_{\mathrm{BS},s} \mathbf{U}_{\mathrm{BS},s}^{\mathsf{H}} \mathbf{a}(\theta)\\
&- 2 g_s^{\mathrm{ul}} \boldsymbol{x}_s^{\mathsf{T}} \tilde{\mathbf{T}}(\tau_0,\nu_0) \mathbf{R}_s^{\mathsf{H}} \mathbf{U}_{\mathrm{BS},s}^{\mathsf{H}} \mathbf{a}(\theta) \Bigg\},
\end{aligned} \tag{4.12}$$

where $\mathbf{R}_s = [\boldsymbol{r}_s[0,0], \dots, \boldsymbol{r}_s[N-1,M-1]] \in \mathbb{C}^{N_{\mathrm{rf}}\times NM}$ is the matrix containing all observations of the BS in the s-th slot as its columns and $\{g^{\mathrm{ul}}\}_{s=1}^{i}$ is the set of all complex channel coefficients up to the i-th slot.

Now, assume that the configuration of the IRS did not change during the AoA estimation at the BS, i.e. $\boldsymbol{\Phi}_s$ is fixed to $\boldsymbol{\Phi}$. Then, the complex UL channel coefficient $g_s^{\mathrm{ul}} = h(\boldsymbol{\Phi}_s)\mathbf{a}^{\mathsf{T}}(\theta)\mathbf{f}$ simplifies to $g^{\mathrm{ul}} = h(\boldsymbol{\Phi})\mathbf{a}^{\mathsf{T}}(\theta)\mathbf{f}$, i.e. becomes independent of the slot index. For this case, g^{ul} is a constant complex channel coefficient, and thus Eq. (4.12) has the exact same form as the expression derived for the estimation at the UE such that the ML estimate in Eq. (4.12) can be simplified to an expression similar to Eq. (4.10).

However, for the general case that g_s^{ul} depends on the slot index s, a different solution must be derived. Therefore, by defining

$$\begin{aligned}
\tilde{\mathbf{U}}_s &\coloneqq \|\boldsymbol{x}_s\|_2^2\, \mathbf{U}_{\mathrm{BS},s} \mathbf{U}_{\mathrm{BS},s}^{\mathsf{H}},\\
\tilde{\mathbf{c}}_s(\tau_0,\nu_0) &\coloneqq \left[\boldsymbol{x}_s^{\mathsf{T}} \tilde{\mathbf{T}}(\tau_0,\nu_0) \mathbf{R}_s^{\mathsf{H}} \mathbf{U}_{\mathrm{BS},s}^{\mathsf{H}}\right]^{\mathsf{H}},
\end{aligned} \tag{4.13}$$

Eq. (4.12) can be rewritten as

$$\begin{aligned}(\{\hat{g}^{\mathrm{ul}}\}_{s=1}^{i}, \hat{\tau}_i, \hat{\nu}_i, \hat{\theta}_i) &= \underset{\{g^{\mathrm{ul}}\}_{s=1}^{i}, \tau_0, \nu_0, \theta}{\arg\min} \ \mathrm{Re}\left\{ \sum_{s=1}^{i} \left|g_s^{\mathrm{ul}}\right|^2 \mathbf{a}^{\mathsf{H}}(\theta)\tilde{\mathbf{U}}_s\, \mathbf{a}(\theta) - 2g_s^{\mathrm{ul}}\, \tilde{\mathbf{c}}_s^{\mathsf{H}}(\tau_0, \nu_0)\mathbf{a}(\theta) \right\} \\ &= \underset{\{g^{\mathrm{ul}}\}_{s=1}^{i}, \tau_0, \nu_0, \theta}{\arg\max} \ \mathrm{Re}\left\{ \sum_{s=1}^{i} 2g_s^{\mathrm{ul}}\, \tilde{\mathbf{c}}_s^{\mathsf{H}}(\tau_0, \nu_0)\mathbf{a}(\theta) - \left|g_s^{\mathrm{ul}}\right|^2 \mathbf{a}^{\mathsf{H}}(\theta)\tilde{\mathbf{U}}_s\mathbf{a}(\theta) \right\} . \end{aligned} \tag{4.14}$$

Then, for a given τ_0, ν_0, θ and $\{g^{\mathrm{ul}}\}_{s=1}^{i-1}$, the g_i^{ul} that maximizes Eq. (4.14) is found by

$$\begin{aligned} \frac{\partial}{\partial \mathrm{Re}\{g_i^{\mathrm{ul}}\}} \mathrm{Re}\left\{ \sum_{s=1}^{i} 2g_s^{\mathrm{ul}}\, \tilde{\mathbf{c}}_s^{\mathsf{H}}(\tau_0, \nu_0)\mathbf{a}(\theta) - \left|g_s^{\mathrm{ul}}\right|^2 \mathbf{a}^{\mathsf{H}}(\theta)\tilde{\mathbf{U}}_s\, \mathbf{a}(\theta) \right\} = 0 \\ \frac{\partial}{\partial \mathrm{Im}\{g_i^{\mathrm{ul}}\}} \mathrm{Re}\left\{ \sum_{s=1}^{i} 2g_s^{\mathrm{ul}}\, \tilde{\mathbf{c}}_s^{\mathsf{H}}(\tau_0, \nu_0)\mathbf{a}(\theta) - \left|g_s^{\mathrm{ul}}\right|^2 \mathbf{a}^{\mathsf{H}}(\theta)\tilde{\mathbf{U}}_s\, \mathbf{a}(\theta) \right\} = 0 \end{aligned}$$

which have the same form as Eqs. (4.8a) and (4.8b), and thus results in

$$g_{i,\mathrm{opt}}^{\mathrm{ul}} = \frac{\mathbf{a}^{\mathsf{H}}(\theta)\tilde{\mathbf{c}}_i(\tau_0, \nu_0)}{\mathbf{a}^{\mathsf{H}}(\theta)\tilde{\mathbf{U}}_i\, \mathbf{a}(\theta)} . \tag{4.15}$$

Furthermore, substituting expression (4.15) into Eq. (4.14), the optimal g_{i-1}^{ul} can then be found for a given τ_0, ν_0, θ and $\{g^{\mathrm{ul}}\}_{s=1}^{i-2}$. Repeating this procedure for every complex UL channel coefficient, the optimal g_s^{ul}, for $s = 1, \ldots, i$, is given by

$$g_{s,\mathrm{opt}}^{\mathrm{ul}} = \frac{\mathbf{a}^{\mathsf{H}}(\theta)\tilde{\mathbf{c}}_s(\tau_0, \nu_0)}{\mathbf{a}^{\mathsf{H}}(\theta)\tilde{\mathbf{U}}_s\, \mathbf{a}(\theta)} . \tag{4.16}$$

Replacing every g_s^{ul} in Eq. (4.14) by the expression found in Eq. (4.16), the ML estimate at the BS in the i-th slot is given by

$$\begin{aligned}(\hat{\tau}_i, \hat{\nu}_i, \hat{\theta}_i) &= \underset{\tau_0, \nu_0, \theta}{\arg\max} \ \mathrm{Re}\left\{ \sum_{s=1}^{i} 2\, \frac{\left|\mathbf{a}^{\mathsf{H}}(\theta)\tilde{\mathbf{c}}_s(\tau_0, \nu_0)\right|^2}{\mathbf{a}^{\mathsf{H}}(\theta)\tilde{\mathbf{U}}_s\mathbf{a}(\theta)} - \frac{\left|\mathbf{a}^{\mathsf{H}}(\theta)\tilde{\mathbf{c}}_s(\tau_0, \nu_0)\right|^2}{\mathbf{a}^{\mathsf{H}}(\theta)\tilde{\mathbf{U}}_s\mathbf{a}(\theta)} \right\} \\ &= \underset{\tau_0, \nu_0, \theta}{\arg\max} \ \sum_{s=1}^{i} \frac{\left|\mathbf{a}^{\mathsf{H}}(\theta)\tilde{\mathbf{c}}_s(\tau_0, \nu_0)\right|^2}{\mathbf{a}^{\mathsf{H}}(\theta)\tilde{\mathbf{U}}_s\mathbf{a}(\theta)}. \end{aligned} \tag{4.17}$$

Note that similar to the ML estimate at the UE, see Eq. (4.10), the ML estimate at the BS can also be implemented to have the same computational complexity in each slot. Also, only the AoA estimate of Eq. (4.17) is of interest for the proposed BA scheme. Yet,

the delay and Doppler estimate are obtained without further expense and could be used potentially for beam tracking or beam refinement techniques that might be applied after successful BA.

4.2. Design Strategy for Combining Matrices

Recall from Sec. 2.3 that both the BS and the UE apply a combining matrix to the signal received at their ULA due to their implemented hybrid BF architecture. Since these combining matrices are chosen in every slot of BA, as discussed in Sec. 3.1, a strategy must be found to design the sequence of combining matrices across all N_{slot} slots of BA for both the BS and the UE. Since in every slot of BA the derived multi-slot ML estimation methods, see Sec. 4.1, consider all received signals up to the current slot, the idea for the design strategy for the combining matrices is to probe different narrow angular ranges of the beam space across different slots. There are two reasons for this idea. On the one hand, by always probing a narrow range at a time a larger BF gain can be leveraged within this angular range, and hence a signal that is less corrupted by noise is obtained in that slot. On the other hand, by also changing the probed direction in every slot, the AoA estimate of the multi-slot ML method should converge to the true AoA after the whole beam space has been explored. To find such design strategy the method that has been used for the design of the transmit BF vector $\mathbf{f}$ in Sec. 2.3 is recalled and extended to prioritize certain directions of the beam space, as introduced in [23]. In the following, the used strategy is only described for the design of the combining matrices at the UE, yet, the same strategy is implemented at the BS as well.
First, the whole FoV $\Omega = [-\frac{\pi}{2}, \frac{\pi}{2}]$ is divided into G equidistant angles $\tilde{\phi}_i$ and the matrix $\mathbf{B} = [\mathbf{b}(\tilde{\phi}_1), \dots, \mathbf{b}(\tilde{\phi}_G)] \in \mathbb{C}^{L_{\text{a}} \times G}$ is defined, where $\mathbf{b}(\cdot)$ is the ULA response vector at the UE defined in Eq. (2.5). Further, the desired radiation pattern is defined by $\bar{\mathbf{b}} = [\bar{b}_1, \dots, \bar{b}_G]^{\intercal} \in \mathbb{R}^G$, where $\bar{b}_i$ corresponds to the magnitude of the desired radiation pattern at angle $\tilde{\phi}_i$. Next, the FoV Ω is divided into a central section Ω_m covering G_m discrete directions each with power φ_m and a peripheral section Ω_p covering G_p discrete directions each with power φ_p. This partitioning of Ω enables prioritizing certain sections of the FoV by choosing the section to prioritize as the central section and increasing its assigned power φ_m, while decreasing the power φ_p of the resulting peripheral section. By allowing only small ripples within the main beam, the result of this procedure is a flat beam in the direction of the central section. In other words, the desired beam pattern $\bar{\mathbf{b}}$ yields an increased total power of $G_m\varphi_m$ over the central section and a reduced total power $G_p\varphi_p = 1 - G_m\varphi_m$ over the peripheral section. A corresponding BF vector $\mathbf{u}$ of

unit norm is then given as the solution of the magnitude least-squares problem

$$\begin{aligned} \min_{\mathbf{u}} \quad & \left\| \mathbf{B}^{\mathsf{H}}\mathbf{u} - \bar{\mathbf{b}} \right\|_2^2 \\ \text{s.t.} \quad & \|\mathbf{u}\|_2 = 1 \end{aligned}, \tag{4.18}$$

where the desired beam pattern $\bar{\mathbf{b}}$ can be designed such that certain sections of the FoV are prioritized. Considering Eq. (4.18), the following design strategy is used for designing the sequence of combining matrices at the UE during BA.
At first, the FoV $\Omega = [-\frac{\pi}{2}, \frac{\pi}{2}]$ is discretized into K equidistant angles and for each angle α_k, for $k = 1, \ldots, K$, a corresponding BF vector $\mathbf{u}_k$ is computed that yields a gain towards its respective angle α_k as well as a small region $\Delta\alpha$ around it and almost no gain over the remaining angular range. This can be achieved by designing the desired beam pattern $\bar{\mathbf{b}}$ in Eq. (4.18) for a given α_k such that the central section, i.e. the region to prioritize, is given by $\Omega_{m,k} = [\alpha_k - \Delta\alpha/2, \alpha_k + \Delta\alpha/2]$. The so obtained BF vectors are then used to construct the UE's BF codebook defined by

$$\mathcal{U}_{\mathrm{UE}} = \{\mathbf{u}_1, \ldots, \mathbf{u}_K\}. \tag{4.19}$$

Note that the process of generating $\mathcal{U}_{\mathrm{UE}}$ is done once before the start of BA, and hence does not introduce any additional overhead to the protocol. The final design strategy for the sequence of combining matrices can then be described as follows. In every slot i of BA, the UE randomly samples L_{rf} BF vectors $\bar{\mathbf{u}}_1, \ldots, \bar{\mathbf{u}}_{L_{\mathrm{rf}}}$ from the set $\mathcal{U}_{\mathrm{UE}}$ and finds its combining matrix as $\mathbf{U}_{\mathrm{UE},i} = \frac{1}{\sqrt{L_{\mathrm{rf}}}}[\bar{\mathbf{u}}_1, \ldots, \bar{\mathbf{u}}_{L_{\mathrm{rf}}}]$. Then, after a certain number of slots have passed, the whole FoV is explored by the UE with narrow and directive beams such that the employed multi-slot ML estimate, which accumulates the observations across different slots, should yield a precise estimate of the AoA. Note that by designing the combining matrices in each slot as described, the assumption used in Sec. 2.3 that the combining matrix of every slot is chosen as a semi-unitary matrix holds in good approximation, and hence the AWGN assumption is valid. Further, observe that although a codebook-based approach is used in this thesis for designing the sequence of combining matrices, the accuracy of the AoA estimation is only partially limited by the accuracy of the codebook. The reason for this is that a separate estimation method is employed that is not based on the BF codebook. However, if very few low-directional beams were used in the codebook, i.e. if K is chosen small and $\Delta\alpha$ large, the estimation accuracy deteriorates since the received signals are more corrupted with noise. Finally, recall that to design the sequence of combining matrices at the BS, the same design strategy is adopted as the one described for the UE.

4.3. Design Strategy for IRS Parameters

As discussed in Ch. 3, once the UE's AoA estimate is reliable, i.e. once the fluctuation of the estimate is less than a predefined value for a predefined number of slots, the UE activates the IRS by configuring the phase shifts $\boldsymbol{\psi}$ and the reflection coefficient β for reflection towards its estimated AoA. Although this procedure determines the framework for the IRS configuration, it remains to define the parameters to when exactly activate the IRS and how to then tune the IRS parameters.
First, to find a heuristic for the activation of the IRS, consider the definition of the half power beam width (HPBW) Θ_h of a ULA with L elements and half wavelength spacing from [29, Ch. 6] as

$$\Theta_h = 2\left[\frac{\pi}{2} - \arccos\left(\frac{2 \cdot 1.391}{\pi L}\right)\right]. \tag{4.20}$$

Further, to capture the fluctuation of the AoA estimates in the i-th slot of BA, the standard deviation of the last N_e AoA estimates at the UE, where $i \geq N_\mathrm{e}$, can be computed by

$$\sigma_{\phi,i} = \sqrt{\frac{1}{N_\mathrm{e}-1}\sum_{j=0}^{N_\mathrm{e}-1}\left(\hat{\phi}_{i-j} - \mu_{\phi,i}\right)^2}, \tag{4.21}$$

where $\hat{\phi}_j$ denotes the estimated AoA at the UE in the j-th slot and $\mu_{\phi,i} = \frac{1}{N_\mathrm{e}}\sum_{j=0}^{N_\mathrm{e}}\hat{\phi}_{i-j}$ is the mean of the last N_e estimates. Note that Eq. (4.21) defines a moving standard deviation, similar to a moving average, that is computed by using a sliding window of the last N_e AoA estimates. Considering the expressions in Eqs. (4.20) and (4.21), it is assumed that the AoA estimation at the UE is successful in the i-th slot if

$$\sigma_{\phi,i} \leq \Theta_h\ . \tag{4.22}$$

To understand the reason for this critera, first note that the HPBW approximates the best possible angular resolution of a ULA for signals coming from boresight, i.e. from the axis of maximum gain, as shown in [26, Ch. 1]. Hence, activating the IRS after the criteria in Eq. (4.22) is fulfilled means that the AoA estimation at the UE varies between so similar angles that the IRS can not distinguish them anyway due to its limited angular resolution. For this reason, using Eq. (4.22) as IRS activation criteria is justified. Once this criteria is fulfilled, the UE activates the IRS by setting $\beta > 0$ and applying the phase shifts $\boldsymbol{\psi}$ to the reflected signal. To understand how the phase shifts $\boldsymbol{\psi}$ should be chosen, recall the definition of the IRS gain from Eq. (2.10) as

$$G_\mathrm{irs}(\boldsymbol{\Phi}_i) \coloneqq \left|\mathbf{b}^\mathsf{T}(\phi)\boldsymbol{\Phi}_i^\mathsf{H}\mathbf{b}(\phi)\right|.$$

	On-Off scheme	Linear scheme	Confidence scheme
$\boldsymbol{\psi}$	$[\boldsymbol{\psi}]_l = \psi_l = 2\pi(l-1)\sin(\hat{\phi}) \quad \forall\, l$		
β	$\beta_j = 1$	$\beta_j = \min(1, \beta_{j-1} + 0.2)$	$\beta_j = \max(\beta_{j-1}, 1 - \sigma_{\phi,j}/\Theta_h)$

Table 4.1.: Overview of considered IRS design strategies. Note that the chosen values for β are given starting from the j-th slot, where j denotes the index of the first slot in which the IRS is activated.

Then, for any given β, the phase shifts at the IRS should be chosen as

$$[\boldsymbol{\psi}_{\text{opt}}]_l = \psi_{\text{opt},l} = 2\pi(l-1)\sin(\phi) \quad \forall\, l, \tag{4.23}$$

since then

$$\begin{aligned} G_{\text{irs}}(\boldsymbol{\Phi}_{\text{opt}}) &= \left|\mathbf{b}^{\mathsf{T}}(\phi)\boldsymbol{\Phi}_{\text{opt}}^{\mathsf{H}}\mathbf{b}(\phi)\right| \\ &= \sum_{l=1}^{L_{\text{a}}} \left|[\mathbf{b}(\phi)]_l \; [\boldsymbol{\Phi}_{\text{opt}}^{\mathsf{H}}]_{l,l} \; [\mathbf{b}(\phi)]_l\right| \\ &= \beta \sum_{l=1}^{L_{\text{a}}} \left|[\mathbf{b}(\phi)]_l \; e^{-j\psi_{\text{opt},l}} \; [\mathbf{b}(\phi)]_l\right| \\ &= \beta \sum_{l=1}^{L_{\text{a}}} \left|e^{j\pi(l-1)\sin(\phi)} e^{-j2\pi(l-1)\sin(\phi)} e^{j\pi(l-1)\sin(\phi)}\right| \\ &= \beta \sum_{l=1}^{L_{\text{a}}} 1 = \beta L_{\text{a}}, \end{aligned} \tag{4.24}$$

i.e. the IRS gain is maximized. Since the phase shifts used in Eq. (4.23) can, however, not be configured as the true AoA ϕ is unknown, the phase shifts are instead set to

$$[\boldsymbol{\psi}]_l = \psi_l = 2\pi(l-1)\sin(\hat{\phi}) \quad \forall\, l\,. \tag{4.25}$$

Note that the phase shifts $\boldsymbol{\psi}$ are not configured before the criteria in Eq. (4.22) is fulfilled, that is before the AoA estimation at the UE is assumed to be successful. Hence, using the setting shown in Eq. (4.25) should yield a good approximation of the optimal setting in Eq. (4.23).

Contrary to the configuration of the phase shifts $\boldsymbol{\psi}$, there is no universal solution to the configuration of β that leads to the best overall system performance for any scenario. For this reason, different strategies are proposed in the following and compared later on in Ch. 5 to find the best performing one. For the first considered strategy, referred to

as On-Off scheme, $\beta = 1$ is set as soon as the UE activates the IRS, i.e. as soon as the criteria in Eq. (4.22) is fulfilled. The idea behind setting β directly to one is that then the SNR at the BS before BF, see Eq. (2.29), is maximized during the whole period in which the BS estimates its AoA. Also, note that for this strategy, the applied phase shifts $\boldsymbol{\psi}$ and the magnitude of the reflection coefficient β are constant over all slots of BA, and consequently the reflection matrix $\boldsymbol{\Phi}$ is constant across all remaining slots of BA. Hence, the overall complex UL channel coefficient g_i^{ul} is constant across all remaining slots and the BS can implement a multi-slot ML estimation method that assumes a constant channel coefficient similar to the UE. The second considered strategy, referred to as linear scheme, starts by setting $\beta = 0.2$ once the UE activates the IRS and afterwards, linearly increases β by 0.2 in every subsequent slot until $\beta = 1$ is reached. This strategy is considered since within the time where $\beta \in (0, 1)$ the BS can start estimating its AoA while the UE can refine its estimate to obtain a more accurate result and further increase the IRS gain. For the same reason, the third design strategy, called confidence scheme, is considered which chooses β in each slot as $\beta = 1 - \sigma_{\phi,i}/\Theta_h$, where Θ_h and $\sigma_{\phi,i}$ are defined in Eqs. (4.20) and (4.21), respectively. The idea for this is that as the UE further refines its estimate the fluctuation of the estimate continuously decreases such that β increases over time. To also ensure that β does not decrease at any point during BA, β is only updated in the confidence scheme if its value increased compared to the previous slot. An overview of the considered design strategies is shown in Tab. 4.3.
Recall from Ch. 3 that after both the BS and the UE have estimated their AoA, the BS sends a predefined request to the UE to terminate the BA protocol. Thus, for the UE to understand this request, the UE must not set $\beta = 1$ as it otherwise reflects all incoming signals and can not process the request of the BS. However, since setting β to a rather high value, e.g., 0.9, would achieve very similar results as setting $\beta = 1$ and still allow the UE to understand the termination request of the BS, this is mentioned here for completeness but not considered further for the simulations in Ch. 5.

4.4. Performance Analysis

After introducing the employed estimation methods as well as the design strategies for the combining matrices and the IRS parameters, the performance of the overall system is investigated on the basis of the Cramér-Rao lower bound (CRLB) of the AoA. The CRLB provides a lower bound on the variance of any estimator of the AoA, and hence shows how accurate the AoA can be estimated at best in every slot of BA. The CRLB is only derived for the AoA at the UE, however, since the expressions for the received signal at the UE and BS, see Eq. (2.24) and Eq. (2.27), respectively, are of similar form,

the conclusions found are assumed to be valid for both sides. Also, note that although only the CRLB of the AoA is of interest, the respective bounds for the delay, the Doppler shift as well as the complex channel coefficient are obtained during the derivation without additional expense.

4.4.1. Exact CRLB

To derive the exact CRLB for the AoA at the UE, consider the following definition of the CRLB for unbiased estimators [28, 30].

Definition 1 (CRLB for unbiased estimators)**.** *Let $\boldsymbol{\xi} = [\xi_1, \dots, \xi_n]$ be the parameter vector containing all deterministic but unknown parameters of a system. The CRLB of any unbiased estimator of the individual parameters in $\boldsymbol{\xi}$ is then given by the diagonal elements of $\mathbf{I}(\boldsymbol{\xi})^{-1}$, where $\mathbf{I}(\boldsymbol{\xi})$ denotes the Fisher information matrix (FIM).*

Therefore, to first compute the FIM, Eq. (2.24) is rewritten as

$$\begin{aligned}\boldsymbol{y}_i[n,m;\boldsymbol{\xi}] &= g^{\mathrm{dl}}\mathbf{V}_i^{\mathsf{H}}\mathbf{b}(\phi)x_i[n,m]e^{-j2\pi m\Delta f(\frac{\tau_0}{2}+\gamma)}e^{j\pi\nu_0 nT_o} + \boldsymbol{w}_i[n,m] \\ &= \underbrace{ge^{j\psi_g}\mathbf{V}_i^{\mathsf{H}}\mathbf{b}(\phi)x_i[n,m]e^{-j2\pi m\Delta f\tau_0'}e^{j\pi\nu_0 nT_o}}_{\mathbf{s}_i[n,m;\boldsymbol{\xi}]} + \boldsymbol{w}_i[n,m] \\ &= \mathbf{s}_i[n,m;\boldsymbol{\xi}] + \boldsymbol{w}_i[n,m], \end{aligned} \tag{4.26}$$

where $\boldsymbol{\xi} = [g, \psi_g, \phi, \tau_0', \nu_0]$ is the parameter vector containing all unknown but deterministic parameters, $\tau_0' = \frac{\tau_0}{2} + \gamma$ and the complex DL channel coefficient g^{dl} is represented in its polar form as $g^{\mathrm{dl}} = ge^{j\psi_g}$. Then, by considering all observations up to the i-th slot, as with the estimation methods, and using the fact that Eq. (4.26) describes a multivariate normal distribution with mean vector $\mathbf{s}_i[n,m;\boldsymbol{\xi}]$ and covariance matrix $\mathbf{I}_{L_{\mathrm{rf}}}$, the FIM is computed according to [31] by

$$\begin{aligned}[\mathbf{I}(\boldsymbol{\xi},\mathbf{X})]_{k,l} &= 2\sum_{s=1}^{i}\sum_{n,m}\mathrm{Re}\left\{\frac{\partial\mathbf{s}_s^{\mathsf{H}}[n,m;\boldsymbol{\xi}]}{\partial\xi_k}\sigma^{-2}\mathbf{I}_{L_{\mathrm{rf}}}^{-1}\frac{\partial\mathbf{s}_s[n,m;\boldsymbol{\xi}]}{\partial\xi_l}\right\} + iNM\left[\mathbf{I}_{L_{\mathrm{rf}}}^{-1}\frac{\partial\mathbf{I}_{L_{\mathrm{rf}}}}{\xi_k}\mathbf{I}_{L_{\mathrm{rf}}}^{-1}\frac{\partial\mathbf{I}_{L_{\mathrm{rf}}}}{\xi_l}\right] \\ &= \frac{2}{\sigma^2}\sum_{s=1}^{i}\sum_{n,m}\mathrm{Re}\left\{\frac{\partial\mathbf{s}_s^{\mathsf{H}}[n,m;\boldsymbol{\xi}]}{\partial\xi_k}\frac{\partial\mathbf{s}_s[n,m;\boldsymbol{\xi}]}{\partial\xi_l}\right\}, \end{aligned} \tag{4.27}$$

where $\mathbf{X} = \{\mathbf{X}_1, \dots, \mathbf{X}_i\}$ denotes the set of all pilot symbols sent up to the i-th slot, $\mathbf{X}_s = \{x_s[n,m]\}\ \forall\ n,m$ the set of all pilot symbols sent in the s-th slot and $\sum_{n,m} = \sum_{n=0}^{N-1}\sum_{m=0}^{M-1}$ is used here and in the following to shorten the notation. Using the result in Eq. (4.27) as well as the fact that the the FIM is symmetric, i.e. $[\mathbf{I}(\boldsymbol{\xi},\mathbf{X})]_{k,l} = [\mathbf{I}(\boldsymbol{\xi},\mathbf{X})]_{l,k}$,

the individual elements of the FIM are defined by

$$\mathbf{I}(\boldsymbol{\xi}, \mathbf{X}) = \frac{1}{\sigma^2} \begin{bmatrix} I_{gg} & I_{g\psi_g} & I_{g\phi} & I_{g\tau_0'} & I_{g\nu_0} \\ I_{g\psi_g} & I_{\psi_g\psi_g} & I_{\psi_g\phi} & I_{\psi_g\tau_0'} & I_{\psi_g\nu_0} \\ I_{g\phi} & I_{\psi_g\phi} & I_{\phi\phi} & I_{\phi\tau_0'} & I_{\phi\nu_0} \\ I_{g\tau_0'} & I_{\psi_g\tau_0'} & I_{\phi\tau_0'} & I_{\tau_0'\tau_0'} & I_{\tau_0'\nu_0} \\ I_{g\nu_0} & I_{\psi_g\nu_0} & I_{\phi\nu_0} & I_{\tau_0'\nu_0} & I_{\nu_0\nu_0} \end{bmatrix}. \tag{4.28}$$

Further, since all elements of $\boldsymbol{\xi}$ are real-valued,

$$\frac{\partial \mathbf{s}_s^{\mathsf{H}}[n, m; \boldsymbol{\xi}]}{\partial \xi_k} = \left[\frac{\partial \mathbf{s}_s[n, m; \boldsymbol{\xi}]}{\partial \xi_k}\right]^{\mathsf{H}}$$

holds, and thus only the derivatives of $\mathbf{s}_s[n, m; \boldsymbol{\xi}]$ with respect to the individual elements in $\boldsymbol{\xi}$ are required to compute Eq. (4.27). From Eq. (4.26), these derivatives are computed as

$$\frac{\partial \mathbf{s}_s[n, m; \boldsymbol{\xi}]}{\partial g} = \frac{1}{g}\mathbf{s}_s[n, m; \boldsymbol{\xi}], \tag{4.29a}$$

$$\frac{\partial \mathbf{s}_s[n, m; \boldsymbol{\xi}]}{\partial \psi_g} = j\mathbf{s}_s[n, m; \boldsymbol{\xi}], \tag{4.29b}$$

$$\frac{\partial \mathbf{s}_s[n, m; \boldsymbol{\xi}]}{\partial \phi} = j\pi\cos(\phi) g e^{j\psi_g} \mathbf{V}_s^{\mathsf{H}} \tilde{\mathbf{b}}(\phi) x_s[n, m] e^{-j2\pi m \Delta f \tau_0'} e^{j\pi\nu_0 n T_\mathrm{o}}, \tag{4.29c}$$

$$\frac{\partial \mathbf{s}_s[n, m; \boldsymbol{\xi}]}{\partial \tau_0'} = -2jm\pi\Delta f \mathbf{s}_s[n, m; \boldsymbol{\xi}], \tag{4.29d}$$

$$\frac{\partial \mathbf{s}_s[n, m; \boldsymbol{\xi}]}{\partial \nu_0} = jn\pi T_\mathrm{o} \mathbf{s}_s[n, m; \boldsymbol{\xi}], \tag{4.29e}$$

where $\tilde{\mathbf{b}}(\phi)$ in Eq. (4.29c) is defined as $\tilde{\mathbf{b}}(\phi) \coloneqq \mathrm{diag}(0, \ldots, L_\mathrm{a} - 1)\, \mathbf{b}(\phi)$.
Considering the derivatives found in Eqs. (4.29a) - (4.29e), the individual elements of the FIM can be computed using Eq. (4.27) such that the expression for the FIM in Eq. (4.28) simplifies to

$$\mathbf{I}(\boldsymbol{\xi}, \mathbf{X}) = \frac{1}{\sigma^2} \begin{bmatrix} I_{gg} & 0 & I_{g\phi} & 0 & 0 \\ 0 & I_{\psi_g\psi_g} & I_{\psi_g\phi} & I_{\psi_g\tau_0'} & I_{\psi_g\nu_0} \\ I_{g\phi} & I_{\psi_g\phi} & I_{\phi\phi} & I_{\phi\tau_0'} & I_{\phi\nu_0} \\ 0 & I_{\psi_g\tau_0'} & I_{\phi\tau_0'} & I_{\tau_0'\tau_0'} & I_{\tau_0'\nu_0} \\ 0 & I_{\psi_g\nu_0} & I_{\phi\nu_0} & I_{\tau_0'\nu_0} & I_{\nu_0\nu_0} \end{bmatrix}, \tag{4.30}$$

where the computation of the individual elements of the FIM can be found in Appendix B in Eqs. (B.1) - (B.16). The CRLB of the AoA ϕ is then found in the i-th slot of BA from

the expression in Eq. (4.30) as

$$\mathrm{Var}\{\hat{\phi}\}_i \geq [\mathbf{I}(\boldsymbol{\xi}, \mathbf{X})^{-1}]_{3,3} = \frac{n_\phi(\mathbf{X})}{\det(\mathbf{I}(\boldsymbol{\xi}, \mathbf{X}))} \tag{4.31}$$

where $\hat{\phi}$ refers to any unbiased estimator of ϕ,

$$n_\phi(\mathbf{X}) = -I_{gg}\Big(I_{\nu_0\nu_0} I^2_{\psi_g\tau_0'} - 2I_{\psi_g\tau_0'} I_{\psi_g\nu_0} I_{\tau_0'\nu_0} + I_{\tau_0'\tau_0'} I^2_{\psi_g\nu_0} + I_{\psi_g\psi_g} I^2_{\tau_0'\nu_0} - I_{\psi_g\psi_g} I_{\tau_0'\tau_0'} I_{\nu_0\nu_0}\Big)$$

is the numerator in Eq. (4.31) and

$$\begin{aligned}
\det(\mathbf{I}(\boldsymbol{\xi}, \mathbf{X})) = \frac{1}{\sigma^2}\Big(& I_{\nu_0\nu_0}\, I^2_{g\phi}\, I^2_{\psi_g\tau_0'} - 2\, I^2_{g\phi}\, I_{\psi_g\tau_0'}\, I_{\psi_g\nu_0}\, I_{\tau_0'\nu_0'} + I_{\tau_0'\tau_0'}\, I^2_{g\phi}\, I^2_{\psi_g\nu_0} \\
& - I_{\psi_g\psi_g}\, I_{\tau_0'\tau_0'}\, I_{\nu_0\nu_0}\, I^2_{g\phi} + I_{gg}\, I^2_{\psi_g\phi}\, I^2_{\tau_0'\nu_0'} - I_{gg}\, I_{\tau_0'\tau_0'}\, I_{\nu_0\nu_0}\, I^2_{\psi_g\phi} + I_{\psi_g\psi_g}\, I^2_{g\phi}\, I^2_{\tau_0'\nu_0'} \\
& + 2\, I_{gg}\, I_{\nu_0\nu_0}\, I_{\psi_g\phi}\, I_{\psi_g\tau_0'}\, I_{\phi\tau_0'} - 2\, I_{gg}\, I_{\psi_g\phi}\, I_{\psi_g\tau_0'}\, I_{\phi\nu_0'}\, I_{\tau_0'\nu_0'} + I_{gg}\, I^2_{\phi\tau_0'}\, I^2_{\psi_g\nu_0} \\
& + 2\, I_{gg}\, I_{\tau_0'\tau_0'}\, I_{\psi_g\phi}\, I_{\psi_g\nu_0}\, I_{\phi\nu_0'} + I_{gg}\, I^2_{\psi_g\tau_0'}\, I^2_{\phi\nu_0'} - 2\, I_{gg}\, I_{\psi_g\phi}\, I_{\phi\tau_0'}\, I_{\psi_g\nu_0}\, I_{\tau_0'\nu_0'} \\
& - 2\, I_{gg}\, I_{\psi_g\tau_0'}\, I_{\phi\tau_0'}\, I_{\psi_g\nu_0}\, I_{\phi\nu_0'} + 2\, I_{gg}\, I_{\phi\phi}\, I_{\psi_g\tau_0'}\, I_{\psi_g\nu_0}\, I_{\tau_0'\nu_0'} - I_{gg}\, I_{\phi\phi}\, I_{\nu_0\nu_0}\, I^2_{\psi_g\tau_0'} \\
& - I_{gg}\, I_{\psi_g\psi_g}\, I_{\nu_0\nu_0}\, I^2_{\phi\tau_0'} + 2\, I_{gg}\, I_{\psi_g\psi_g}\, I_{\phi\tau_0'}\, I_{\phi\nu_0'}\, I_{\tau_0'\nu_0'} - I_{gg}\, I_{\phi\phi}\, I_{\tau_0'\tau_0'}\, I^2_{\psi_g\nu_0} \\
& - I_{gg}\, I_{\psi_g\psi_g}\, I_{\tau_0'\tau_0'}\, I^2_{\phi\nu_0'} - I_{gg}\, I_{\psi_g\psi_g}\, I_{\phi\phi}\, I^2_{\tau_0'\nu_0'} + I_{gg}\, I_{\psi_g\psi_g}\, I_{\phi\phi}\, I_{\tau_0'\tau_0'}\, I_{\nu_0\nu_0}\Big)
\end{aligned}$$

is the determinant of $\mathbf{I}(\boldsymbol{\xi}, \mathbf{X})$.
Since the expression for the exact CRLB of the AoA ϕ in Eq. (4.31) is very complex and further depends on the sent pilot signals $\mathbf{X}$, the CRLB is approximated in the following by assuming that both the number of subcarriers M and the number of OFDM symbols per slot N become large.

4.4.2. Approximated CRLB

To derive an approximation for the exact CRLB of ϕ that does not depend on the sent pilot symbols $\mathbf{X}$, the fact that these symbols only occur in summations over m and n, see Eqs. (B.2) - (B.16), is utilized, as shown in [32]. For this purpose, the identities

$$\begin{aligned}
\sum_{k=0}^{n-1} k &= \frac{n(n-1)}{2}, \\
\sum_{k=0}^{n-1} k^2 &= \frac{n(n-1)(2n-1)}{6},
\end{aligned} \tag{4.32}$$

are considered and the average power constraint defined in Eq. (2.16) is recalled. Then, by assuming M and N to be large, the summations over n and m in Eqs. (B.2) - (B.16) can be approximated, and hence the individual elements of the FIM as well as the numerator and denominator of the CRLB in Eq. (4.31) can be approximated. The detailed derivation of this approximation can be found in Appendix B in Eqs. (B.17) - (B.25).
Using the derived approximations, the approximated CRLB can be stated as

$$\mathrm{Var}\{\hat{\phi}\}_i \geq \frac{n_\phi(\mathbf{X})}{\det(\mathbf{I}(\boldsymbol{\xi}, \mathbf{X}))} \approx \frac{n_{\phi,\mathrm{approx}}}{d_{\phi,\mathrm{approx}}}, \tag{4.33}$$

where

$$n_{\phi,\mathrm{approx}} = -C_\phi^{(i)} M$$

and

$$d_{\phi,\mathrm{approx}} = \frac{2M^2 N P_\mathrm{t} g^2 \pi^2 \cos^2(\phi)}{\sigma^2} \cdot \left(\left(\mathrm{Re}\left\{ \tilde{C}_\phi^{(i)} \right\} \right)^2 \left[3\left(1 - \cos(\phi)\right)^2 + 1 \right] + \left(\mathrm{Im}\left\{ \tilde{C}_\phi^{(i)} \right\} \right)^2 - C_\phi^{(i)} \tilde{\tilde{C}}_\phi^{(i)} \right)$$

are the numerator and denominator of the approximated CRLB, respectively, and the identities

$$\begin{aligned} C_\phi^{(i)} &\coloneqq \sum_{s=1}^{i} \left\| \mathbf{V}_s^\mathsf{H} \mathbf{b}(\phi) \right\|_2^2, \\ \tilde{C}_\phi^{(i)} &\coloneqq \sum_{s=1}^{i} \tilde{\mathbf{b}}^\mathsf{H}(\phi) \mathbf{V}_s \mathbf{V}_s^\mathsf{H} \mathbf{b}(\phi), \\ \tilde{\tilde{C}}_\phi^{(i)} &\coloneqq \sum_{s=1}^{i} \left\| \mathbf{V}_s^\mathsf{H} \tilde{\mathbf{b}}(\phi) \right\|_2^2, \end{aligned} \tag{4.34}$$

are defined to shorten the notation, where $\tilde{\mathbf{b}}(\phi) = \mathrm{diag}(0, \ldots, L_\mathrm{a} - 1)\, \mathbf{b}(\phi)$. The obtained expression in Eq. (4.33) can be further simplified to yield the approximated CRLB in the

i-th slot of BA as

$$
\begin{aligned}
&\mathrm{Var}\{\hat{\phi}\}_i \\
&\geq \frac{-C_\phi^{(i)} M\sigma^2}{2M^2NP_\mathrm{t}g^2\pi^2\cos^2(\phi)\left(\left(\mathrm{Re}\left\{\tilde{C}_\phi^{(i)}\right\}\right)^2\left[3\left(1-\cos(\phi)\right)^2+1\right]+\left(\mathrm{Im}\left\{\tilde{C}_\phi^{(i)}\right\}\right)^2-C_\phi^{(i)}\tilde{\tilde{C}}_\phi^{(i)}\right)} \\
&= \frac{-C_\phi^{(i)} \sigma^2}{2MNP_\mathrm{t}g^2\pi^2\cos^2(\phi)\left(\left(\mathrm{Re}\left\{\tilde{C}_\phi^{(i)}\right\}\right)^2\left[3\left(1-\cos(\phi)\right)^2+1\right]+\left(\mathrm{Im}\left\{\tilde{C}_\phi^{(i)}\right\}\right)^2-C_\phi^{(i)}\tilde{\tilde{C}}_\phi^{(i)}\right)} \\
&= \frac{C_\phi^{(i)} \sigma^2}{2MNP_\mathrm{t}g^2\pi^2\cos^2(\phi)\left(C_\phi^{(i)}\tilde{\tilde{C}}_\phi^{(i)}-\left(\mathrm{Re}\left\{\tilde{C}_\phi^{(i)}\right\}\right)^2\left[3\left(1-\cos(\phi)\right)^2+1\right]-\left(\mathrm{Im}\left\{\tilde{C}_\phi^{(i)}\right\}\right)^2\right)}.
\end{aligned}
\tag{4.35}
$$

After deriving the approximated CRLB, it is investigated which quantities have the most impact on the estimation accuracy of the proposed scheme. First, by recalling the fact that $g = |g^{\mathrm{dl}}|$ as well as the expression for g^{dl} from Eq. (2.24) as $g^{\mathrm{dl}} = \tilde{h}^{\mathrm{dl}}\mathbf{a}^\mathsf{T}(\theta)\mathbf{f}$, observe that the term $P_\mathrm{t}g^2/\sigma^2$ in Eq. (4.35) is of very similar form as the SNR at the UE before BF defined in Eq. (2.28). More precisely, the only difference between the two expressions is that the term $P_\mathrm{t}g^2/\sigma^2$ includes the transmit BF gain $\mathbf{a}^\mathsf{T}(\theta)\mathbf{f}$ of the BS. Since during the whole BA protocol the BS is assumed to transmit a fixed wide beam, see Sec. 2.3, there is almost no transmit BF gain, i.e. $\mathbf{a}^\mathsf{T}(\theta)\mathbf{f} \approx 1$, and hence $\mathrm{SNR}_{\mathrm{UE,BBF}} \approx P_\mathrm{t}g^2/\sigma^2$ holds in good approximation. As a consequence, the CRLB is found to be proportional to $1/\mathrm{SNR}_{\mathrm{UE,BBF}}$ which illustrates that the higher the initial SNR before BF, the lower the CRLB, or in other words, the achievable estimation accuracy increases with increasing SNR before BF. Further, the CRLB also decreases with an increasing number of pilot symbols per slot due to the term MN in the denominator of Eq. (4.35).

Next, the dependency on the AoA ϕ is considered. Looking at the denominator in Eq. (4.35), observe that the CRLB is proportional to $1/\cos^2(\phi)$, which is a consequence of assuming a ULA at the UE that is configured as a broadside array, i.e. the main beam is perpendicular to the axis of the antenna array. This illustrates that the estimation accuracy varies for different signals that arrive from different AoAs. More precisely, the CRLB attains its minimum value for signals coming from boresight, i.e. $\phi = 0$, and monotonically increases when moving away towards the end-fire directions, i.e. $\phi = \pm\pi/2$. The reason for this is that the ULA at the UE, see Eq. (2.5), yields the largest gain, and thus the highest sensitivity towards $\phi = 0$ and almost no gain towards $\phi = \pm\pi/2$. In general, this also shows that the CRLB of the AoA in general depends on the used array geometry,

and thus using an array geometry different to a ULA will either improve or degrade the overall system performance. Note that there is also a second dependency of the CRLB on the AoA due to the term $(1-\cos(\phi))^2$ which, however, only controls the influence of the term $(\mathrm{Re}\{\tilde{C}_\phi^{(i)}\})^2$ on the overall CRLB, and thus can be neglected compared to the term $1/\cos^2(\phi)$.
Last, the influence of the quantities $C_\phi^{(i)}, \tilde{C}_\phi^{(i)}$ and $\tilde{\tilde{C}}_\phi^{(i)}$ is investigated. Looking at Eq. (4.35), observe that the CRLB decreases most noticeable with increasing $\tilde{\tilde{C}}_\phi^{(i)}$ and slightly with increasing $C_\phi^{(i)}$, while it increases quadratically with the real and imaginary part of $\tilde{C}_\phi^{(i)}$. Further, recall from the respective definitions in Eq. (4.34) that these three quantities depend on the sequence of overall combining matrices $\mathbf{V}_s$, for $s = 1, \ldots, i$. Since $\mathbf{V}_s = \mathbf{D}_s\mathbf{U}_{\mathrm{UE},s}$ and $\mathbf{D}_s$ is a scaled identity matrix, see Eq. (2.4), the influence of the quantities $C_\phi^{(i)}, \tilde{C}_\phi^{(i)}$ and $\tilde{\tilde{C}}_\phi^{(i)}$ can equivalently be seen as the influence of the sequence of combining matrices $\mathbf{U}_{\mathrm{UE},s}$, for $s = 1, \ldots, i$. Hence, to minimize the CRLB, the combining matrix $\mathbf{U}_{\mathrm{UE},s}$ should be chosen in each slot s such that $C_\phi^{(i)}$ and $\tilde{\tilde{C}}_\phi^{(i)}$ are maximized, while the overall magnitude of $\tilde{C}_\phi^{(i)}$ should be minimized. Also, when the combining matrices are designed appropriately, the CRLB decreases with an increasing number of slots.

4.5. Resulting Algorithm

After discussing the estimation methods and design strategies in Secs. 4.1 - 4.3 in detail, the proposed BA scheme is summarized in Algorithm 1. To be consistent with the notation introduced in Sec. 3.2, $\mathcal{E}_{\mathrm{UE}}(\cdot,\cdot)$ and $\mathcal{E}_{\mathrm{BS}}(\cdot,\cdot)$, respectively denote the estimation method of the UE and the BS, i.e. the respective employed multi-slot ML estimation. For the same reason, the IRS design strategy is denoted by $\mathcal{G}_i(\cdot)$. The notation $\mathbf{U}_{\mathrm{UE},i} \overset{L_{\mathrm{rf}}}{\leftarrow} \mathcal{U}_{\mathrm{UE}}$ indicates that the UE obtains its combining matrix in the i-th slot by randomly choosing L_{rf} vectors from its codebook $\mathcal{U}_{\mathrm{UE}}$. The same applies to the notation used for the BS. The input parameters to the proposed BA scheme are made explicit for description of the algorithm. Also, note that the lines 16-21 in Algorithm 1 are added to illustrate how the algorithm could be extended to allow the BS to terminate the BA scheme before reaching the maximum number of slots. This could be particularly useful if the time required for BA should be minimized, as the BS could save time resources in exchange for the accuracy of the estimation. However, this part is not implemented in the final scheme used for the simulations in Ch. 5 since the main objective in this thesis is the maximization of the SNR after BF.

Algorithm 1: Proposed BA scheme

Input: Grid size for multi-slot ML estimation (Γ), codebook parameters ($K, \Delta\alpha$), number of estimates for IRS activation (N_e)

Output: $\hat{\phi}_{N_\mathrm{slot}}, \hat{\theta}_{N_\mathrm{slot}}$

Initialize: $\beta_1 = 0$, $\boldsymbol{\psi}_1 = \mathbf{0}$, $\mathcal{U}_\mathrm{UE}(K, \Delta\alpha)$, $\mathcal{U}_\mathrm{BS}(K, \Delta\alpha)$

for $i = 1$ **to** N_slot **do**
- `// If portion of signal is sensed, UE estimates its AoA`
- **if** $\beta_i < 1$ **then**
  - $\mathbf{U}_{\mathrm{UE},i} \overset{L_\mathrm{rf}}{\leftarrow} \mathcal{U}_\mathrm{UE}$
  - UE receives $\boldsymbol{y}_i$
  - $\hat{\phi}_i \leftarrow \mathcal{E}_\mathrm{UE}\left(\boldsymbol{y}^{(i)}, \left(\mathbf{U}_\mathrm{UE}^{(i)}, \beta^{(i)}, \Gamma\right)\right)$
- **end**
- `// If portion of signal is reflected, BS estimates its AoA`
- $\mathbf{U}_{\mathrm{BS},i} \overset{N_\mathrm{rf}}{\leftarrow} \mathcal{U}_\mathrm{BS}$ `// BS always assumes to receive signal`
- **if** $\beta_i > 0$ **then**
  - BS receives $\boldsymbol{r}_i$
  - $\hat{\theta}_i \leftarrow \mathcal{E}_\mathrm{BS}\left(\boldsymbol{r}^{(i)}, \left(\mathbf{U}_\mathrm{BS}^{(i)}, \beta^{(i)}, \boldsymbol{\psi}^{(i)}, \Gamma\right)\right)$
- **end**
- **if** $i \in \{N_\mathrm{e}, \ldots, N_\mathrm{slot} - 1\}$ **then**
  - `// UE checks if IRS should be activated`
  - **if** $\sigma_{\phi,i}(N_\mathrm{e}) \leq \Theta_h$ **or** $\beta_i > 0$ **then**
    - $(\beta_{i+1}, \boldsymbol{\psi}_{i+1}) \leftarrow \mathcal{G}_i\left(\hat{\phi}^{(i)}\right)$
  - **end**
  - `// BS checks if estimate is reliable (not implemented)`
  - **if** $\sigma_{\theta,i}(N_\mathrm{e}) \leq \Theta_h$ **then**
    - $\hat{\phi}_{N_\mathrm{slot}} \leftarrow \hat{\phi}_i$
    - $\hat{\theta}_{N_\mathrm{slot}} \leftarrow \hat{\theta}_i$
    - BS informs UE about completion of BA
    - break
  - **end**
- **end**

end

5. Simulation Results

After introducing the proposed scheme to approach the general BA problem in Ch. 4, its performance is evaluated in this chapter via numerical simulations. For this reason, Sec. 5.1 discusses the implementation details of the simulations by first introducing the chosen system parameters as well as the considered performance measures, followed by a brief description of the overall simulation procedure. Afterwards, Sec. 5.2 presents the simulation results for different scenarios and in comparison to another approach established in the literature.

5.1. Implementation Details

To assess the performance of the proposed scheme for BA in the considered communications system, various parameters have to be set for the simulations. Besides the parameters of the overall system, see Ch. 2, other design parameters, e.g., for the design strategy of the combining matrices and IRS parameters, have to be decided on as well.

5.1.1. System Paramters

A system operating at carrier frequency $f_\mathrm{c} = 60\,\mathrm{GHz}$ over a bandwidth of $B = 1\,\mathrm{GHz}$ is considered. In compliance with the latest standard defined by 3GPP [33], the subcarrier spacing is chosen to be $\Delta f = 480\,\mathrm{kHz}$, and thus the number of subcarriers is set to $M = 2048$ to utilize the full bandwidth. Again, in compliance with 3GPP, the number of OFDM symbols per slot is set to $N = 14$ and the CP duration to $T_\mathrm{cp}\Delta f = 0.07$, i.e. to 7 % of the OFDM symbol duration. The BS is assumed to be equipped with $N_\mathrm{a} = 64$ antennas and $N_\mathrm{rf} = 4$ RF chains, while the UE is equipped with $L_\mathrm{a} = 64$ antennas, given by the number of IRS elements, and $L_\mathrm{rf} = 4$ RF chains. Further, in each slot of BA, the BS transmits its pilot signals with a transmit power of $P_\mathrm{t} = 1\,\mathrm{mW} \triangleq 0\,\mathrm{dBm}$. Based on the considered bandwidth of $B = 1\,\mathrm{GHz}$, the resulting noise power is given by $\sigma^2 = N_0 B = 4 \times 10^{-12}\,\mathrm{W} \triangleq -84\,\mathrm{dBm}$, where $N_0 = 4 \times 10^{-21}\,\mathrm{W/Hz} \approx -174\,\mathrm{dBm/Hz}$ is the noise power density at 300 K. For the transmitted pilot signals, the channel state information reference signal (CSI-RS) from 3GPP's latest 5G standard [33] is taken into account and the pilot signals are designed as complex valued signal that are obtained

Parameter	Value
Operating frequency	$f_\mathrm{c} = 60\,\mathrm{GHz} \Leftrightarrow \lambda_\mathrm{c} = 5\,\mathrm{mm}$
Bandwidth	$B \approx 1\,\mathrm{GHz}$
Subcarriers	$M = 2048$
Subcarrier-spacing	$\Delta f = 480\,\mathrm{kHz}$
OFDM symbols per slot	$N = 14$
CP duration	$T_\mathrm{cp} = 0.07/\Delta f$
BS antennas	$N_\mathrm{a} = 64$
IRS antennas/elements	$L_\mathrm{a} = 64$
RF chains BS/UE	$N_\mathrm{rf} = L_\mathrm{rf} = 4$
Transmit power	$P_t = 0\,\mathrm{dBm} \triangleq 1\,\mathrm{mW}$
Noise power	$\sigma^2 = -84\,\mathrm{dBm} \approx 4 \times 10^{-12}\,\mathrm{W}$
Pilot signals	similar to CSI-RS from [33]
Radar cross-section model of IRS	$\sigma_{\mathrm{rcs},i} = \sigma_{\mathrm{rcs,bbf}} \cdot \cos(\phi) \cdot G_\mathrm{irs}(\mathbf{\Phi}_i)$
ML grid size (angle, delay, Doppler)	$400 \times 20 \times 20$
Codebook parameters	$K = 30$, $\Delta\alpha = 6.6°$
Number of estimates for IRS activation	$N_\mathrm{e} = 5$

Table 5.1.: Overview of used system parameters.

from a random number sequence. In every slot i of BA, the RCS of the IRS is computed by $\sigma_{\mathrm{rcs},i} = \sigma_{\mathrm{rcs,bbf}} \cdot \cos(\phi) \cdot G_\mathrm{irs}(\mathbf{\Phi}_i)$, where $\sigma_{\mathrm{rcs,bbf}} \coloneqq 10^{-\frac{5}{10}}\mathrm{m}^2 \triangleq -5\,\mathrm{dBsm}$ is defined. A detailed derivation of this RCS model is provided in Sec. 5.1.2. For the multi-slot ML estimation methods, the angular range $\left[-\frac{\pi}{2}, \frac{\pi}{2}\right]$ is discretized into 400 equally spaced angles, while the range for the delay and the Doppler is only discretized into 20 values each in order to reduce the computational complexity. Hence, the ML estimation is always performed over a grid of $400 \times 20 \times 20$. The BF codebooks of the BS and the UE both contain $K = 30$ BF vectors, where each of these BF vectors is designed to cover a range of roughly $\Delta\alpha = 6.6°$. Finally, the number of AoA estimates that are considered to decide when the IRS is activated is set to $N_\mathrm{e} = 5$. Note that the values used for the parameters $K, \Delta\alpha$ and N_e, i.e. for the codebook and IRS parameter design, are from initial preliminary simulations that have been conducted prior the simulations presented later in this chapter. An overview of all used system parameters is provided in Tab. 5.1.

5.1.2. Radar cross-section of IRS

The monstatic RCS of the IRS is fundamental for modeling the two-way channel between the BS and the UE. To see the reason for this, recall the SNR at the BS before BF in

Eq. (2.29) as

$$\mathrm{SNR}_{\mathrm{BS,BBF}} = \frac{\lambda^2 \sigma_{\mathrm{rcs,bbf}}}{(4\pi)^3 d^4} \frac{P_{\mathrm{t}}}{\sigma^2},$$

where $\sigma_{\mathrm{rcs,bbf}}$ denotes the radar cross-section (RCS) of the IRS before BF. Also, note that once the IRS is configured for reflection towards a certain direction, its RCS should increase towards this direction by the available IRS gain, while it should decrease for other directions. Hence, the SNR after IRS configuration is also depending on the RCS of the IRS. This illustrates that in order to find the SNR at the BS at any point during the simulations, the RCS of the IRS must be known. However, as there are neither measurements nor simulations available that yield numerical results for this RCS, a model for the RCS of the considered IRS is derived in the following. To this end, various measurements of the RCS of different similar sized objects at mmWave frequencies that have been presented in the literature are examined. For the following derivation, the IRS is considered to be approximately of a size that could fit on the back of conventional current mobile phones.

First, measurements of the back of a human hand [34] at 60 GHz - 90 GHz or other small sized objects such as a can or a small wooden board at 79 GHz [35] yield an average RCS between -20 dBsm and -15 dBsm. However, as all of these objects are more curved and made of a less radar reflective material than an IRS, it is concluded that the monostatic RCS of the IRS should be higher than these values before any BF, i.e. $\sigma_{\mathrm{rcs,bbf}} > -15$ dBsm.

Next, the results found in [36] at 40 GHz show that illuminating an area of size 128 mm $\times$ 53 mm of a trapezoidal cuboid that is made from aluminum yields a monostatic RCS of up to 10 dBsm. The same result of 10 dBsm is also found at 40 GHz when using the approximation $\sigma_{\mathrm{rcs,mp}}(\lambda) = \frac{4\pi A^2}{\lambda^2}$, see [37], for the RCS of a flat metallic plate with the same area A as the cuboid. Since the considered carrier frequency is $f_{\mathrm{c}} = 60$ GHz, see Sec. 5.1.1, the RCS of the same flat metallic plate can be approximated at this frequency by $\sigma_{\mathrm{rcs,mp}}(\lambda_{\mathrm{c}}) = 13$ dBsm, where λ_{c} corresponds to the wavelength at frequency f_{c}. Then, recall that an IRS that is configured for reflection towards a certain direction acts as a directional beamformer towards this direction, similar to a perfectly conducting plate of the same size, as shown in [12] and discussed in Sec. 2.1. Therefore, by assuming the IRS to roughly have an area of $A = 128\,\mathrm{mm} \times 53\,\mathrm{mm}$, its RCS after perfect BF, denoted by $\sigma_{\mathrm{rcs,abf}}$, should always be upper bounded by the RCS of a flat metallic plate with area A, i.e. $\sigma_{\mathrm{rcs,abf}} \leq \sigma_{\mathrm{rcs,mp}}(\lambda_{\mathrm{c}}) = 13$ dBsm.

To summarize, the RCS of the IRS before BF should be larger than -15 dBsm, while the RCS of the IRS after BF should be upper bounded by 13 dBsm. To then find a modeling which allows the monostatic RCS of the IRS to attain its upper bound for the case of

perfectly reflecting towards its AoA, the following model is proposed. In each slot i of BA, the RCS of the IRS is computed by

$$\sigma_{\mathrm{rcs},i} = \sigma_{\mathrm{rcs,bbf}} \cdot \cos(\phi) \cdot G_{\mathrm{irs}}(\mathbf{\Phi}_i), \tag{5.1}$$

where $\sigma_{\mathrm{rcs,bbf}} \coloneqq 10^{-\frac{5}{10}}\,\mathrm{m}^2 \triangleq -5\,\mathrm{dBsm}$ is defined as the RCS of the IRS before BF, the term $\cos(\phi)$ is included to account for the projected area of the IRS at a certain angle ϕ and $G_{\mathrm{irs}}(\mathbf{\Phi}_i) = |\mathbf{b}^{\mathsf{T}}(\phi)\mathbf{\Phi}_i^{\mathsf{H}}\mathbf{b}(\phi)|$ is the resulting IRS gain when applying the reflection matrix $\mathbf{\Phi}_i$, as defined in Eq. (2.10). Note that $-5\,\mathrm{dBsm}$ is chosen for $\sigma_{\mathrm{rcs,bbf}}$ since the IRS gain is upper bounded by

$$G_{\mathrm{irs}}(\mathbf{\Phi}_i) = |\mathbf{b}^{\mathsf{T}}(\phi)\mathbf{\Phi}_i^{\mathsf{H}}\mathbf{b}(\phi)| \leq L_{\mathrm{a}} = 64 \triangleq 18\,\mathrm{dB},$$

and thus the RCS of the IRS $\sigma_{\mathrm{rcs},i}$ can attain its upper bound of $13\,\mathrm{dBsm}$ for $\phi = 0$ and the case of perfect reflection. Also, when the phase shifts at the IRS are mistuned, the IRS gain can yield values significantly less than $0\,\mathrm{dB}$ such that the RCS of the IRS becomes very small, which is reasonable as the monostatic RCS of the IRS should decrease significantly if the IRS reflects the signal towards a completely different direction.

5.1.3. Performance Measure and Simulation Procedure

Two different performance measures are considered for the evaluation of the simulation results. At first, the root-mean-square error (RMSE) between the true and the estimated AoA is used to demonstrate the estimation accuracy at the UE. Denoting the set of true AoAs by ϕ_t and the set of estimated AoAs by $\hat{\phi}_t$, for $t = 1, \ldots, T$, the RMSE is defined by

$$\mathrm{RMSE}\left(\phi^{(T)}, \hat{\phi}^{(T)}\right) = \sqrt{\frac{1}{T}\sum_{t=1}^{T}(\phi_t - \hat{\phi}_t)^2}, \tag{5.2}$$

where the superscript (T) is used to denote $(T) = \{1, \ldots, T\}$.
As second performance measure, the spectral efficiency is considered to infer the performance of the proposed scheme for various scenarios and in comparison to other approaches. Recalling the definition of the SNR after BF from Eq. (2.33), the spectral efficiency is computed by

$$\eta\left(\theta, \phi, N_{\mathrm{slot}}, \mathrm{SNR}_{\mathrm{BBF}}\right) = \log_2\left(1 + \mathrm{SNR}_{\mathrm{ABF}}\left(\hat{\theta}, \hat{\phi}, N_{\mathrm{slot}}, \mathrm{SNR}_{\mathrm{BBF}}\right)\right), \tag{5.3}$$

where the dependency on various parameters is made explicit and $\mathrm{SNR}_{\mathrm{BBF}}$ refers to the SNR at the UE before BF, i.e. the SNR after the one-way channel, defined in

Eq. (2.28). Note that Eq. (5.3) yields the spectral efficiency for a fixed pair of angles as well as for a fixed number of slots and a fixed SNR before BF. To obtain more general results, the considered angular range $\left[-\frac{\pi}{2}, \frac{\pi}{2}\right]$ is divided into 180 equidistant angles $\mathcal{A} = \{\alpha_1, \ldots, \alpha_{180}\}$ and for both the BS and the UE a set is created that contains a randomly shuffled version of $\mathcal{A}$. This array is denoted by $\Theta = \{\theta_1, \ldots, \theta_{180}\}$ for the BS and by $\Phi = \{\phi_1, \ldots, \phi_{180}\}$ for the UE. Note that the angles $\pm\frac{\pi}{2}$ are excluded from this range since the discussion of the CRLB has shown that the estimation fails for these AoAs. Then, for a given number of slots N_{slot} and a given SNR before BF SNR_{BBF}, 180 simulations are performed, where in each simulation s, the AoA at the BS and UE are respectively set to θ_{s} and ϕ_{s}. Using this procedure, the whole angular range is probed both at the BS and at the UE. The performance of the proposed system can then be evaluated in a meaningful way by computing the average spectral efficiency as

$$\bar{\eta}\left(N_{\text{slot}}, \text{SNR}_{\text{BBF}}\right) = \frac{1}{|\mathcal{A}|} \sum_{s=1}^{|\mathcal{A}|} \eta\left(\hat{\theta}_s, \hat{\phi}_s, N_{\text{slot}}, \text{SNR}_{\text{BBF}}\right), \tag{5.4}$$

where $|\mathcal{A}| = 180$ is the cardinality of $\mathcal{A}$. To obtain an upper bound on the achievable spectral efficiency, the optimum beamformer is defined for which the estimated AoAs in Eq. (5.4) are replaced by the true AoAs. The same sets Φ and Θ are also used in Sec. 5.2.1 to compute the RMSE of the AoA estimation at the UE.

5.2. Numerical Results

After describing the implementation details of the simulations in the previous section, the obtained numerical results are presented in the following. First, the estimation accuracy is investigated for the UE to understand in which SNR regimes a reliable AoA estimation is possible. Afterwards, the different IRS design strategies introduced in Sec. 4.3 are evaluated before a final one is chosen and the performance of the proposed scheme is demonstrated. Finally, a performance comparison between the proposed BA scheme and the non-adaptive random code based BA approach from [1] is provided.

5.2.1. Estimation Performance

First, the AoA estimation accuracy at the UE is evaluated to demonstrate the performance of the proposed estimation method and the proposed combining matrix design strategy. For this reason, Fig. 5.1 shows the RMSE of the AoA estimation at the UE as well as of the CRLB as a function of $\text{SNR}_{\text{UE,BBF}}$ using the simulation procedure described in Sec. 5.1.3. Note that since the RMSE is shown in Fig. 5.1, the shown CRLB actually

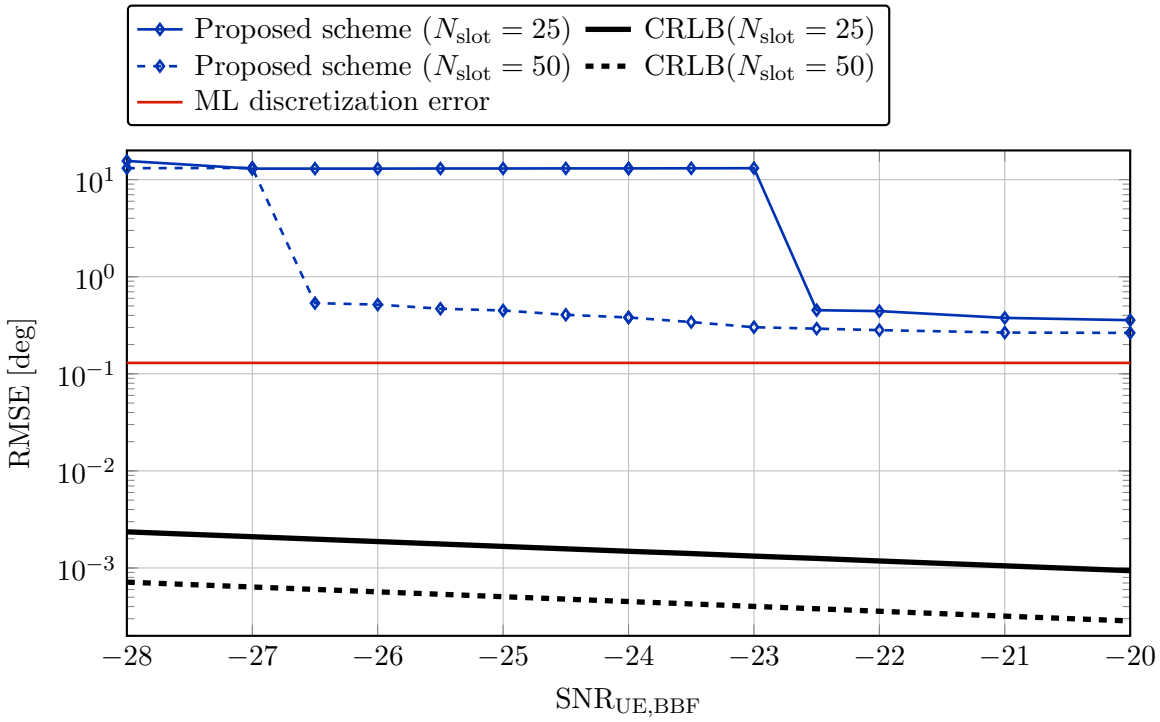

Figure 5.1.: Comparison of the RMSE and the CRLB for the AoA estimation at the UE shown as a function of $\text{SNR}_{\text{UE,BBF}}$ for two different numbers of slots.

refers to the square root of the CRLB to provide a fair comparison. Yet, it is simply denoted and referred to as CRLB for the sake of clarity. The results are presented for two different number of slots $N_{\text{slot}} = \{25, 50\}$. Additionally, the discretization error of the ML estimation, i.e. the lowest achievable RMSE due to the discretized grid of the ML estimation, is shown to evaluate the general quality of the multi-slot ML estimation method of the UE. Note that for the results in Fig. 5.1, the probed angular range is adjusted to $[-87°, 87°]$ as probing even larger angles produced large outliers that distorted the results.

The results show that for SNRs less than $-27\,\text{dB}$ the AoA estimation is inaccurate for both considered scenarios as the RMSE is about 13°. Yet, for a slightly higher SNR of $-26.5\,\text{dB}$, the AoA estimation becomes accurate when 50 slots are used for the estimation which can be seen by the low RMSE of roughly 0.5°. Contrary to that, when the number of slots is fixed to 25, an accurate and reliable AoA estimation is only possible if the SNR is larger than $-22.5\,\text{dB}$. This observation demonstrates that the proposed scheme benefits significantly from using a larger number of slots for BA. On the one hand, this is because the multi-slot ML estimation can base its estimation on a larger

set of received signals. On the other hand, by using a larger number of slots, the used combining matrix design strategy probes each direction more often but every time under slightly different noise conditions such that the influence of noise is mitigated over time and the estimation accuracy improves. The fact that a higher estimation accuracy can be achieved for a larger number of slots can also be seen by comparing the respective CRLBs, since the RMSE achieved by the CRLB for a given $\mathrm{SNR}_{\mathrm{UE,BBF}}$ decreases when the number of slots is increased. Although this does not necessarily mean that the estimation accuracy improves when using a larger number of slots, it indicates that a higher estimation accuracy is possible since the CRLB yields a lower bound on the achievable estimation accuracy. Further, comparing the CRLBs with the discretization error of the multi-slot ML estimation shows the quality of the employed estimation method. Since the ML discretization error does not attain the RMSE the CRLBs, the AoA estimation accuracy of the proposed scheme is limited by the finite discretized grid of the ML estimation. However, as the employed estimation method still enables an RMSE of only 0.13°, the achievable estimation accuracy is more than sufficient for BA.
In summary, the AoA estimation accuracy at the UE is found to improve with an increasing number of slots. This is shown by the RMSE achieved by the proposed scheme as well as by the evolution of the CRLB for different numbers of slots. The results illustrate that the proposed scheme works as initially expected when introducing the individual components of it in Ch. 4. In order to evaluate the performance of the proposed scheme also at the BS and consequently overall, different IRS design strategies are examined in Sec. 5.2.2 to find the best performing one, and hence determine the final BA scheme.

5.2.2. Comparison of IRS design strategies

To find the best IRS design strategy in terms of achieved spectral efficiency, the strategies introduced in Sec. 4.3 are evaluated as a function of $\mathrm{SNR}_{\mathrm{UE,BBF}}$ for a fixed number of slots N_{slot} and as a function of N_{slot} for a fixed $\mathrm{SNR}_{\mathrm{UE,BBF}}$. For the comparison of the IRS design strategies, note that the On-Off design scheme is always shown for two different configurations. Once for the case that the BS employs the ML estimation with varying channel coefficient and once for the case that the BS employs the ML estimation with constant channel coefficient. Recall from Sec. 4.3 that this can be done only for the On-Off design scheme since for this scheme the overall complex UL channel coefficient is constant across all slots of BA after IRS activation.
Figure 5.2 depicts the results as a function of $\mathrm{SNR}_{\mathrm{UE,BBF}}$ and a fixed value of $N_{\mathrm{slot}} = 32$. Note that this value is chosen for the number of slots as then the overall BA procedure takes about 1 ms which is a typical value for the coherence time in mmWave channels.

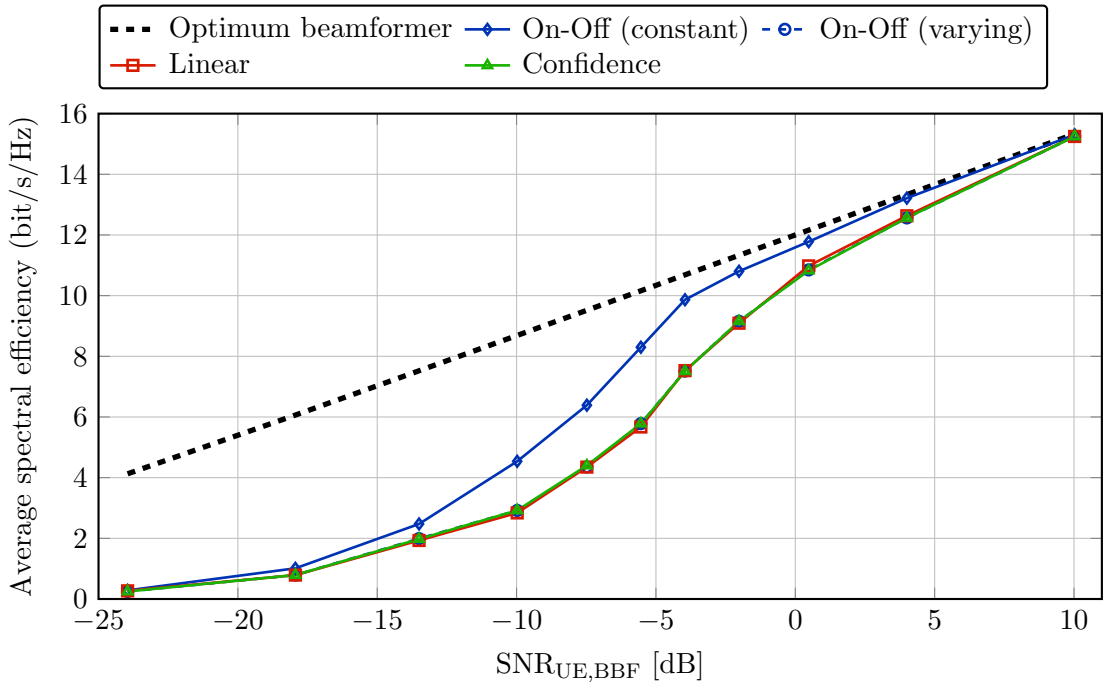

Figure 5.2.: Comparison of the average spectral efficiency using different IRS design strategies for varying SNRs at the UE and a fixed number of slots $N_{\mathrm{slot}} = 32$. Note that the On-Off scheme is tested in two different scenarios, namely when the BS assumes a constant and when it assumes a varying channel coefficient for the ML estimation.

Looking at the results, it can be seen that all design schemes in which the BS employs the ML estimation with varying channel coefficient perform almost identical over the whole SNR range. Contrary to that, using the On-Off scheme together with the constant channel coefficient assumption at the BS significantly outperforms the other design schemes over the whole SNR range. This can be seen by the fact that the On-Off scheme with the constant channel coefficient assumption achieves a certain spectral efficiency, such as 4 bit/s/Hz, at a considerably lower SNR level than the other design schemes. Similarly, for a given SNR, a significantly higher spectral efficiency is obtained with the On-Off scheme and the constant channel coefficient assumption than for any other considered design scheme. This can, for example, be seen by comparing the achieved spectral efficiency of the individual schemes at -10 dB. The discussed results suggest that the difference in the employed estimation method is much more significant than the difference in the chosen IRS design strategy. Also, since the only difference in the IRS design strategies is the design of the reflection coefficient β, see Sec. 4.3, the results indicate that the design of β does not have a great impact on the performance of the proposed scheme in the

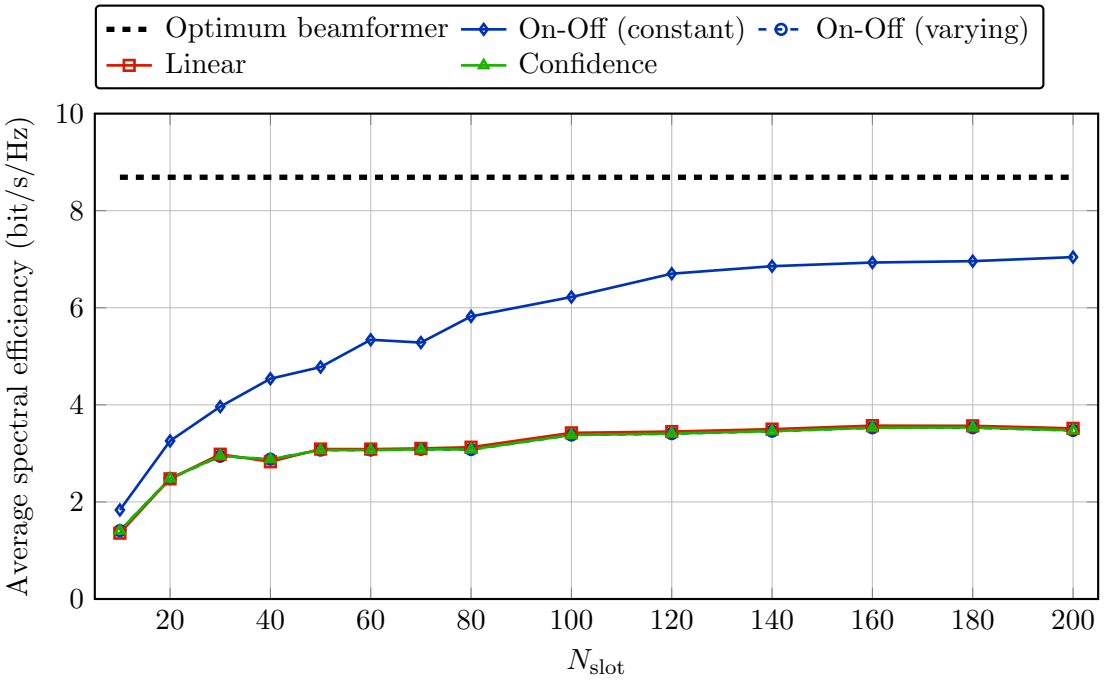

Figure 5.3.: Comparison of the achieved average spectral efficiency using different IRS design strategies for a varying number of slots and a fixed SNR at the UE $\text{SNR}_{\text{UE,BBF}} = -10\,\text{dB}$.

considered communications scenario.

Next, to verify that the found results are valid for other settings as well, Fig. 5.3 evaluates the spectral efficiency at $\text{SNR}_{\text{UE,BBF}} = -10\,\text{dB}$ as a function of N_{slot}. It can again be observed that there is a large performance difference between the On-Off scheme in which the BS assumes a constant channel coefficient for its estimation and all other design schemes. The results also illustrate that their is no difference between the individual IRS design strategies when the BS assumes a varying channel coefficient for its estimation method. Looking at the results in Fig. 5.3, observe that the On-Off scheme with the constant channel coefficient assumption achieves a higher spectral efficiency after 30 slots of BA than the other three design schemes after 200 slots. Further, by using the the On-Off scheme together with the constant channel coefficient assumption, almost twice the spectral efficiency can be attained after 200 slots as compared to the other design schemes. Again, the shown results indicate that the employed estimation method influences the overall performance significantly more than the chosen IRS design strategy.

To summarize, the On-Off scheme in which the BS assumes a constant channel coefficient for its AoA estimation is found to yield the largest spectral efficiency and significantly better results than all other tested design schemes. The reason for this is, however,

not that the On-Off scheme generally achieves better results than the other two design strategies, but rather the fact that using the On-Off scheme allows the BS to implement the ML estimation with constant channel coefficient. The results show that implementing this estimation method at the BS leads to a much greater improvement in terms of spectral efficiency than changing to a different IRS design strategy. The reason for this can be seen as follows. Since the IRS only reflects the incoming signal but does not amplify it, the SNR at the BS is proportional to $1/d^4$, with d denoting the distance, as found in Eq. (2.29). Hence, the path loss of the two-way channel is significantly larger than the path loss of the one-way channel, even if the IRS gain and the receive BF gain of the BS are taken into account. This leads to the fact that in order to obtain an SNR level at the BS at which correct AoA estimation is possible, e.g. $-30\,\mathrm{dB}$, the SNR at the UE has to be considerably higher, e.g. $-10\,\mathrm{dB}$. However, at such high SNR level, the UE is able to estimate its AoA accurately, and hence no period in which the UE refines its estimate is required. For this reason, all IRS design strategies lead to very similar results, whereas changing the estimation method of the BS does still influence the achieved performance. Due to these results, the On-Off scheme in which the BS assumes a constant channel coefficient for its multi-slot ML estimation is used for all subsequent simulations.

5.2.3. Performance of Proposed Scheme

After deciding on the IRS design strategy in Sec. 5.2.2, the final performance of the proposed scheme is demonstrated in the following. To highlight the benefit of the IRS in the considered communications setup, the performance is evaluated for two different scenarios. On the one hand, for the case that the IRS is utilized and configured as described in Sec. 4.3, i.e. the proposed scheme, and on the other hand, for the case that the reflection capability of the IRS is replaced by a single reflector that does not apply any BF to its reflected signal. In the following, the former scenario is referred to as the proposed scheme with IRS and the latter as the proposed scheme without IRS. To obtain a fair comparison, the matrix $\mathbf{\Phi}_{\mathrm{sr}} = \mathrm{diag}\left(\sqrt{L_{\mathrm{a}}}, 0, \ldots, 0\right)$ is used for the reflection matrix of the single reflector such that the Frobenius norm of $\mathbf{\Phi}_{\mathrm{sr}}$ is equal to the Frobenius norm of the reflection matrix $\mathbf{\Phi}$ of the IRS. Using these two scenarios, the influence of the IRS can be determined as otherwise the same estimation methods and combining matrix design strategies are used.

Figure 5.4 depicts the achieved spectral efficiency as a function of $\mathrm{SNR}_{\mathrm{UE,BBF}}$ for a fixed number of slots of $N_{\mathrm{slot}} = 32$. As in Sec. 5.2.2, this number of slots is chosen to ensure the overall BA protocol does not last more than 1 ms, and hence ends with high probability before the coherence time of the mmWave channels is exceeded. Comparing the results in

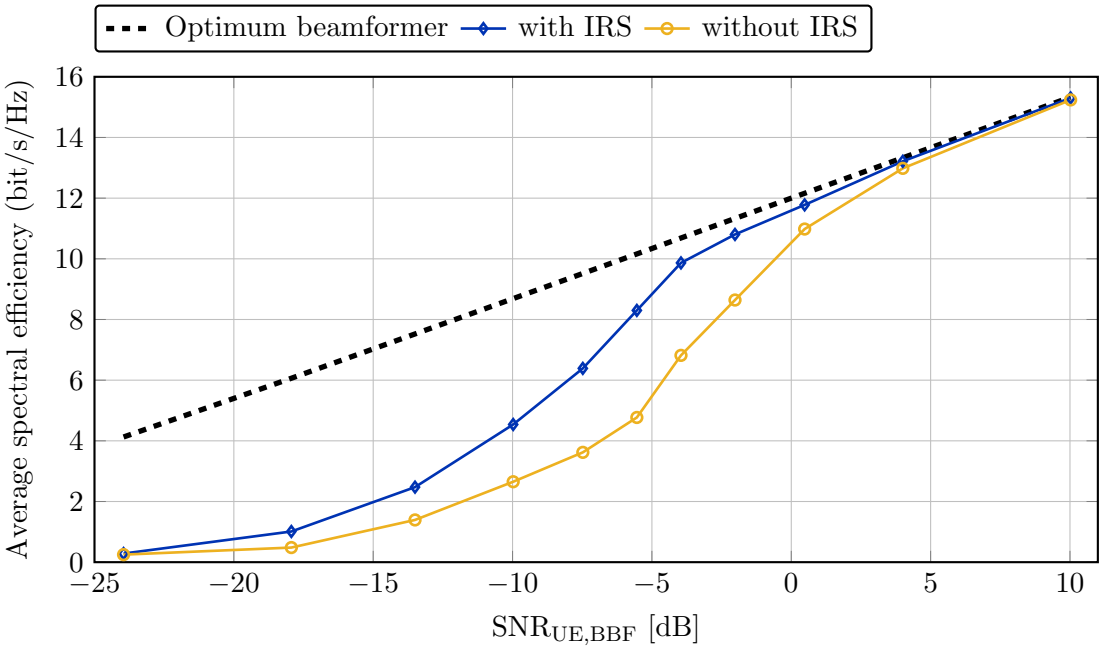

Figure 5.4.: Comparison of the average spectral efficiency using the proposed scheme with and without IRS for varying SNRs at the UE and a fixed number of slots $N_{\text{slot}} = 32$.

Fig. 5.4 illustrates the benefit of the IRS, in particular the benefit of being able to apply and configure directional BF at the IRS. For instance, by using the IRS, an increase in spectral efficiency can be observed at a noticeably lower SNR than compared to the case where the IRS is not used. This can be seen by comparing the achieved spectral efficiency of the two scenarios at $-18\,\text{dB}$. Further, a in practice often desired spectral efficiency of 1–2 bit/s/Hz is reached between $-18\,\text{dB}$ and $-15\,\text{dB}$ when the IRS is used and between $-15\,\text{dB}$ and $-12\,\text{dB}$ when the IRS is not used. Besides these benefits, using the IRS also leads to significant improvements of approximately 2–3 bit/s/Hz between $-10\,\text{dB}$ to $0\,\text{dB}$. Note that these observations are particularly important since BA in mmWave systems is typically performed in low ($-10\,\text{dB}$ to $0\,\text{dB}$) or very low ($< -10\,\text{dB}$) SNR regimes.
Figure 5.5 illustrates the benefits of using the IRS as a function of N_{slot} at two different SNRs. By first comparing the results at $-14\,\text{dB}$, it can be seen that again better results can be achieved over the whole range when the IRS is used. On the one hand, almost twice the spectral efficiency can be reached when all 200 slots are used for BA. On the other hand, the time to achieve a certain target spectral efficiency is significantly reduced when using the IRS. For instance, at $-14\,\text{dB}$, the proposed scheme with IRS reaches a similar spectral efficiency after 20 slots as the proposed scheme without IRS after using all 200 slots. However, neither configuration is able to approach the results achieved

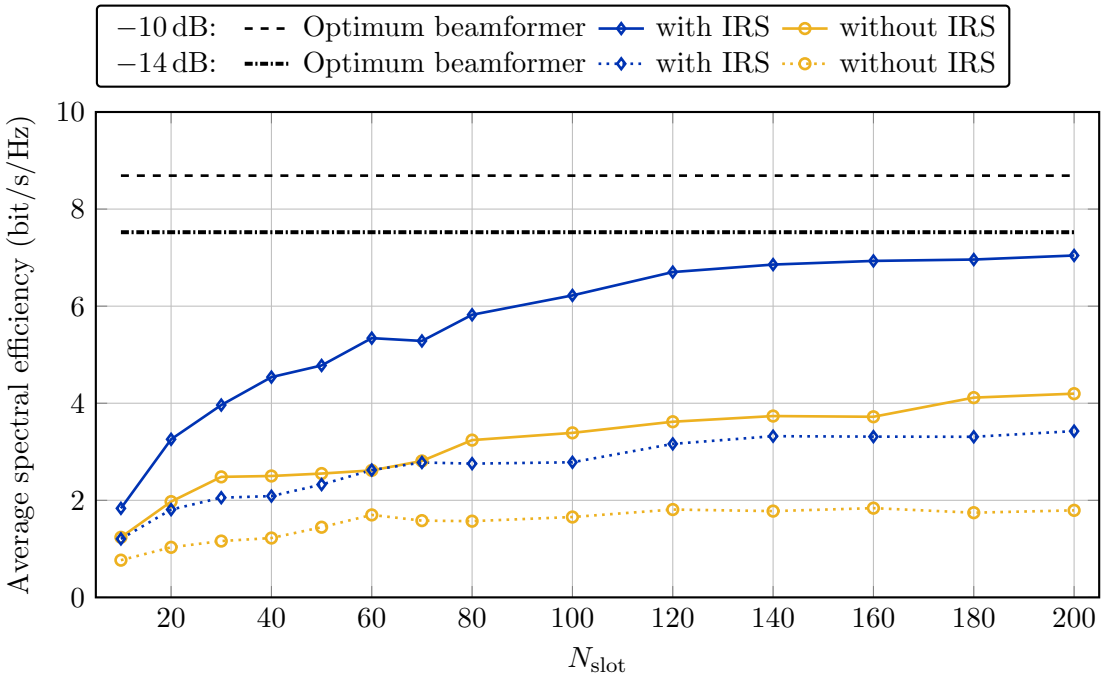

Figure 5.5.: Comparison of the average spectral efficiency using the proposed scheme with and without IRS for a varying number of slots and two fixed SNRs at the UE $\text{SNR}_{\text{UE, BBF}} = \{-10\,\text{dB}, -14\,\text{dB}\}$.

by an optimum beamformer. This implies that although using the IRS improves the performance noticeably, even a high number of slots is not sufficient to allow the BS to estimate its AoA very accurately. The contrary can be observed at $-10\,\text{dB}$ when the IRS is used, where an increasing number of slots results in a continuously increasing spectral efficiency. In particular, using a high number of slots results in a large spectral efficiency between 6–7 bit/s/Hz which implies that the AoA estimation at the BS is estimated much more accurately than at $-14\,\text{dB}$. This also demonstrates that the employed estimation methods improve with an increasing number of observations and why a multi-slot ML estimation scheme has been proposed in Sec. 4.1 in the first place. Contrary to the results with IRS, an accurate AoA estimation can not be found at the BS at $-10\,\text{dB}$ when the IRS is not used. This can be seen by the fact that the spectral efficiency achieved without IRS does increase only slightly over the whole range and in general attains significantly lower values than with IRS. Also, observe that there is a much larger performance difference between the results with and without IRS at $-10\,\text{dB}$ than at $-14\,\text{dB}$. This indicates that highly accurate BA is possible at $-10\,\text{dB}$ only by using the IRS, while it is not possible or at least unreliable for both configurations at $-14\,\text{dB}$.

In summary, the benefits of the IRS in the proposed scheme are shown for two different

cases. On the one hand, it is found that by using the IRS a target spectral efficiency can be reached at a significantly lower SNR or in other words, a higher spectral efficiency can be reached for a given SNR. On the other hand, using the IRS can yield a higher gain for the reflected signal towards the BS due to the BF capability of the IRS, and thus allows to utilize the improvements of the employed estimation method for a larger number of slots at a lower SNR.

5.2.4. Comparison with non-adaptive Random Codes

To infer the performance achieved by the proposed scheme compared to other approaches that are established in the literature, the found results are compared to the non-adaptive random code based BA approach introduced in [1]. A high-level overview of this approach is given in the following, however, for a more detailed description, refer to the provided reference. Since a non-adaptive design strategy is chosen for the combining matrices in this thesis, non-adaptive codebooks are also used for the comparison scheme. In the non-adaptive random code based scheme, the BS periodically probes the channel by transmitting pseudo-random spreading codes via a predefined BF codebook to the UE. To obtain measurements of the channel, the UE applies its own BF codebook to receive a different signal in every slot of BA. Once the UE has gathered a sufficient number of these measurements, the average received power of each pseudo-random beam pair is estimated. Then, by applying non-negative least squares, the resulting under-determined system of equations is solved. Note that for this approach it is assumed that the UE knows the BF codebook of the BS, and thus the probed BF directions of the BS, at any point during BA. From the found solution, the UE determines the AoA at the UE as well as at the BS that leads to the maximum energy transfer. Afterwards, the UE informs the BS about the chosen beam pair during the UL feedback.
Compared to the scheme introduced in this thesis, the non-adaptive random codes yield the advantage of only requiring one-way channels. Hence, the bottleneck of the proposed scheme, i.e. the very low SNR at the BS after the two-way channel, is not present in the comparison scheme. To see if the gain provided by the IRS and the more sophisticated estimation method are sufficient to overcome this drawback, the two schemes are compared in the following. However, note that the proposed scheme also offers some advantages over the non-adaptive random code based scheme. On the one hand, the proposed scheme does not require any additional information, such as the directions probed by the BS in the current slot, at the UE. On the other hand, during the beam reporting phase, the non-adaptive random code based scheme can only utilize a one-sided BF gain, whereas the proposed scheme can utilize a two-sided BF gain in its equivalent BA completion

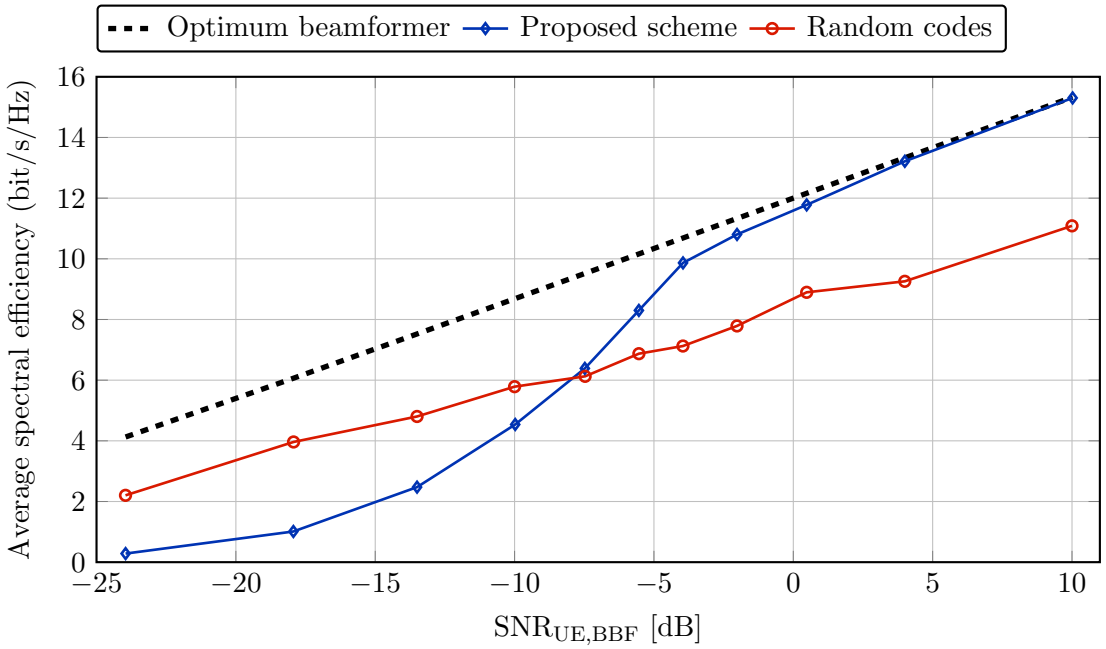

Figure 5.6.: Comparison of the average spectral efficiency of the proposed scheme to the random code based approach from [1] for a varying SNR at the UE and a fixed number of slots $N_{\text{slot}} = 32$.

phase, see Sec. 3.1, since the BS and the UE estimate their respective AoA separately. The use of this two-sided BF gain in the final phase of the BA protocol could lead to significant speed up of the overall protocol, however, this is not examined in the present thesis. In the following comparison, the non-adaptive random code based scheme is referred to as random code based scheme for the sake of simplicity.

Figure 5.6 compares the performance of the two schemes as a function of $\text{SNR}_{\text{UE,BBF}}$ for a fixed number of slots $N_{\text{slot}} = 32$. The results indicate that the random code based scheme performs relatively similar over the whole SNR range. This becomes evident when comparing its achieved results to the optimum beamformer. While the spectral efficiency achieved by the random code based scheme is rather high for very low SNRs and increases over the whole SNR range, there is always a noticeable gap of at least 2 bit/s/Hz to the optimum beamformer. Hence, the random code based scheme is able to estimate the AoAs with a certain accuracy already for very low SNR, however, this accuracy does not increase much with increasing SNR. The exact opposite can be observed for the proposed scheme. While it is not able to estimate the AoAs accurately for very low SNRs, its accuracy improves significantly with increasing SNR. For instance, the proposed scheme attains a spectral efficiency of less than 1 bit/s/Hz at −20 dB and almost reaches the performance of the optimum beamformer at roughly −4 dB. This is because, due to the

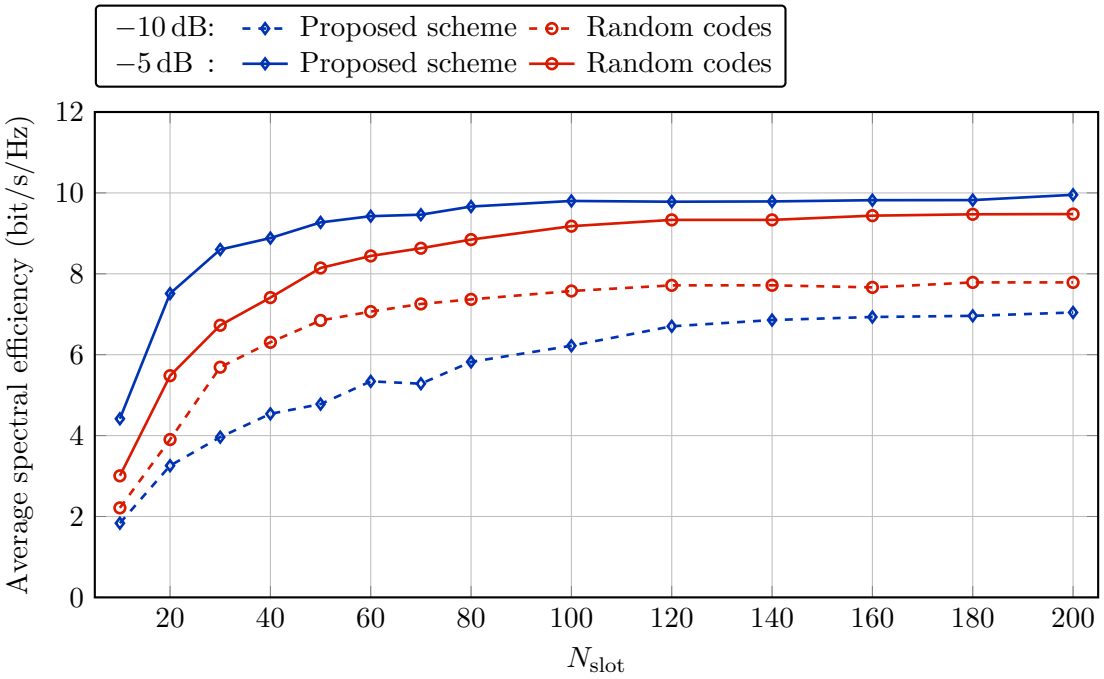

Figure 5.7.: Comparison of the average spectral efficiency of the proposed scheme to the random code based approach for a varying number of slots and two fixed SNRs at the UE $\text{SNR}_{\text{UE,BBF}} = \{-10\,\text{dB}, -5\,\text{dB}\}$.

very high path loss of the two-way channel, an SNR at the UE of less than −15 dB corresponds to an even much lower SNR at the BS such that no accurate AoA estimation is possible at the BS. However, once this threshold SNR of roughly −15 dB is exceeded, the AoA estimation accuracy at the BS, and hence the spectral efficiency, increases significantly. This sudden increase in estimation accuracy of the proposed scheme can be seen in Fig. 5.6 from −15 dB to −5 dB. At approximately −8 dB, the performance of the proposed scheme even surpasses the performance of the random code based scheme. However, since BA in mmWave systems is typically performed in low or very low SNR regimes, the random code based scheme yields better results overall due to the higher spectral efficiency in the very low SNR regime, i.e. below −10 dB. Nevertheless, it should be kept in mind that the proposed scheme performs better in the low SNR regime, i.e. between −10 dB and 0 dB, even without any additional information at the UE. Also, since the proposed scheme yields better results in low SNR regime, it is examined next if time resources can be saved in this SNR range when the proposed scheme is used.

Figure 5.7 depicts the spectral efficiency as a function of N_{slot} for two different SNRs at the UE. On the one hand, for an SNR at which the the random code based scheme has been found to achieve better results according to Fig. 5.6, i.e. $\text{SNR}_{\text{UE,BBF}} = -10\,\text{dB}$,

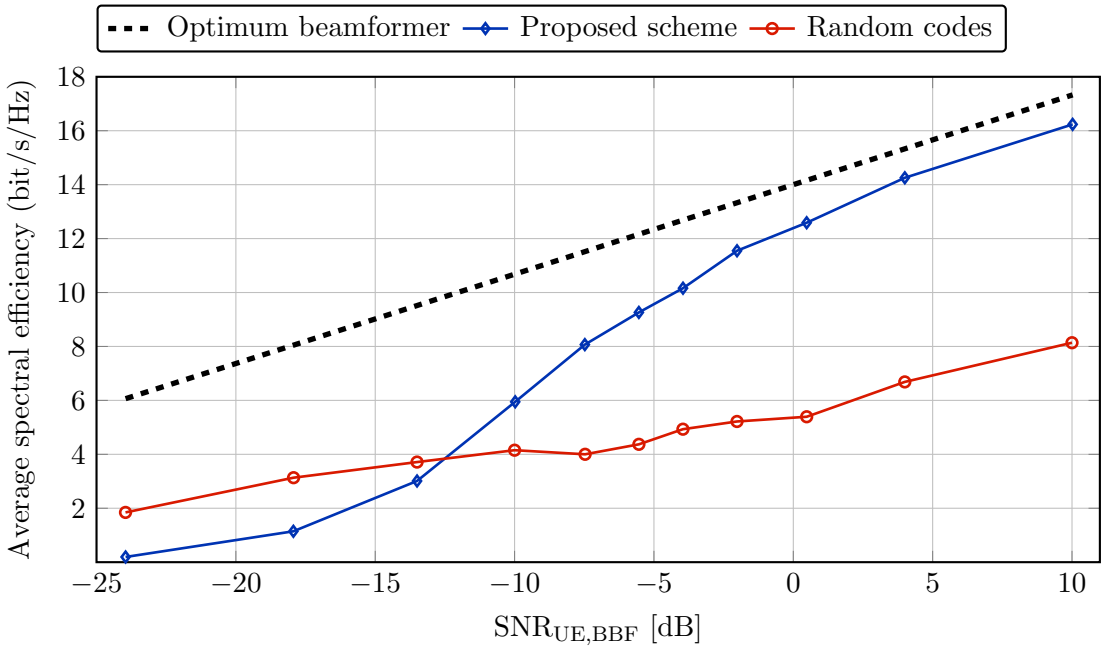

Figure 5.8.: Comparison of the average spectral efficiency of the proposed scheme to the random code based approach. The results are shown for a varying SNR at the UE and a fixed number of slots $N_{\text{slot}} = 32$, when both the BS and the UE are equipped with 128 antennas, i.e. $N_{\text{a}} = L_{\text{a}} = 128$.

and on the other hand, for an SNR at which the proposed scheme achieves better results, i.e. $\text{SNR}_{\text{UE,BBF}} = -5\,\text{dB}$. Note that the performance of the optimum beamformer is not shown in Fig. 5.7 for the sake of clarity. By first looking at the results for an SNR at the UE of $-10\,\text{dB}$, it can be seen that the spectral efficiency achieved by the random code based scheme increases and converges faster compared to the one obtained by the proposed scheme. However, if the SNR at the UE is increased to $-5\,\text{dB}$, the proposed scheme yields a very high spectral efficiency significantly faster than the random code based scheme, while both schemes converge approximately after the same number of slots to their respective maximum. For instance, the proposed scheme reaches the same spectral efficiency after 30 slots as the random code based scheme after more than twice as many slots. These results indicate that above a certain threshold SNR of approximately $-8\,\text{dB}$ the estimation accuracy increases faster with respect to the number of slots for the proposed scheme than for the random code based scheme, and vice versa below said SNR threshold. Hence, time resources can be saved by using the proposed scheme in the low SNR regime, i.e. between $-10\,\text{dB}$ and $0\,\text{dB}$.

Finally, since the main approach to combat the high path loss in mmWave systems is to utilize the BF gain of electrically large antenna arrays, Fig. 5.8 evaluates the perfor-

mance of the two schemes when the number of antennas is increased to 128 at both the BS and the UE. The results are presented as a function of $\mathrm{SNR}_{\mathrm{UE,BBF}}$ for a fixed number of slots $N_{\mathrm{slot}} = 32$. Note that the RCS model of the IRS is adjusted appropriately for the increased number of IRS elements. Compared to the results shown in Fig. 5.6, i.e. to the results when 64 antennas are used, the proposed scheme improves noticeably in performance while the random code based scheme deteriorates significantly. Since for 128 antennas higher BF gains are available at both the BS and the UE, the results show that only the proposed scheme can capitalize on these gains. This indicates that the employed estimation methods and the combining matrix design strategy perform similarly for an increased number of antennas such that due to the larger available BF gains an increase in spectral efficiency is achieved. Hence, the proposed scheme scales well with an increasing number of antennas. Note that this observation is particularly important in mmWave systems where an even larger number of antennas could be used. Nevertheless, for very low SNRs of less than $-12.5\,\mathrm{dB}$, the random code based scheme is still achieving a higher spectral efficiency. This makes the random code based scheme still superior to the proposed scheme in the very low SNR regime, however, the proposed scheme performs better overall for the considered configuration. Also, extrapolating the found results suggests that the proposed scheme surpasses the random code based scheme even for very low SNRs if the number of antennas is further increased. However, due to the limited size of a UE, the number of antennas can most likely only be further increased at the BS.
To summarize, the random code based scheme performs better in very low SNR regimes, i.e. below $-10\,\mathrm{dB}$, while the proposed scheme is better in low SNR regimes, i.e. between $-10\,\mathrm{dB}$ and $0\,\mathrm{dB}$. Yet, as the random code based scheme also achieves good results in the low SNR regime, it leads to better results overall. Nevertheless, time resources can be saved in the low SNR regime by using the proposed scheme. Note that the proposed BA scheme is, however, achieving these results without any additional information at the UE, contrary to the random code based approach which relies on the UE knowing the probed BF directions of the BS. Furthermore, by increasing the number of antennas both at the BS and the UE to 128, the proposed scheme is found to scale significantly better in performance than the random code based scheme. This is a particularly important observation for mmWave systems, where even larger numbers of antennas are possible. To further increase the performance of the proposed scheme in the very low SNR regime, a different transmit BF should be considered. For instance, instead of always transmitting a fixed BF vector at the BS, narrow slot-varying BF vectors could be used. Although this would require both the BS and the UE to use the ML estimation with varying channel coefficient, it could improve the estimation accuracy at the BS for very low SNRs noticeably.

6. Conclusion and Outlook

The aim of this thesis was to develop a complete BA scheme for a communications scenario that involves a single BS and a single UE, where the UE is equipped with a hybrid IRS. In the proposed BA scheme, the AoA at the BS and at the UE are each estimated by a multi-slot ML estimation method, which determines the respective AoA in a certain slot by considering all signals received so far. To complement this estimation method, both the BS and the UE choose their combining matrices such that a random subset of the angular range is probed in each slot of BA with high gain and the entire angular range is explored after as few slots as possible. The UE additionally implements a strategy that based on its AoA estimates decides when to activate and how to configure the IRS. Comparing different IRS design strategies has shown no difference in the final performance. Yet, it has been found that by using an IRS design strategy that keeps the reflection matrix of the IRS constant after activation, the BS can employ a simplified estimation method, resulting in considerable performance improvements.
Overall, simulation results show that the ultimately chosen BA scheme is suitable for BA if the SNR at the UE is higher than $-15\,\mathrm{dB}$. Otherwise, AoA estimation at the BS becomes infeasible due to the very high path loss of the two-way channel. For SNRs at the UE even higher than $-15\,\mathrm{dB}$, significant improvements in the performance of the proposed BA scheme are found for an increasing SNR as well as for an increasing number of slots used for BA. To also compare the performance achieved by the proposed scheme to another approach established in the literature, the non-adaptive random code based BA scheme from [1] was considered. The results show that the proposed scheme achieves better results in the low SNR regime, i.e. from $-10\,\mathrm{dB}$ to $0\,\mathrm{dB}$, while the random code based scheme performs better in the very low SNR regime, i.e. below $-10\,\mathrm{dB}$. Overall, the random code based scheme is found to lead to better results, however, note that to achieve this performance this scheme requires side information at the UE, contrary to the proposed scheme. Further, when increasing the number of antennas at both the BS and the UE, the proposed scheme is found to surpass the random code based scheme in performance. This implies that the proposed scheme is preferable for larger numbers of antennas, which is a particularly important observation for mmWave systems, where antenna arrays with a very high number of elements can be utilized.

To further increase the performance achieved by the proposed scheme, future work should address the following challenges. At first, measurements of the monostatic RCS of an IRS before and after BF should be conducted. This is particularly important as all results shown in this thesis are related to the RCS model formulated in Sec. 5.1.2, for which no information on the RCS of an IRS was available. Next, to obtain a model that is more meaningful in practice, future work should consider a less idealized IRS model. Such a model should, for instance, contain the coupling between the individual parameters of an IRS element, the coupling between individual elements as well as the frequency dependency of reflection coefficients and phase shifts [16, 17]. Besides the used IRS model, the channel model could be adapted likewise to increase the practical relevance. Possible changes are to add complexity to the used model in the form of multipath propagation and phase noise or to use a different type of communications channel such as a fading channel. To improve the estimation accuracy at the BS for very low SNRs, it should be investigated if using a directive transmit BF vector at the BS that is changed in each slot yields better results as the currently used fixed wide beam. Although this would require both the BS and the UE to employ the multi-slot ML estimation method with varying channel coefficient, the estimation accuracy at the BS might improve. Another topic to be investigated in the future are the multi-slot ML estimation methods. On the one hand, it should be examined if the computational complexity can be further reduced by reformulation of the optimization problem or by specific implementations. On the other hand, the delay and Doppler estimates that are provided by the estimation methods could be used to extend the functionality of the overall scheme to enable beam tracking techniques after successful BA. Further, future work should compare the proposed scheme to other approaches with respect to the time required for BA. Since the proposed scheme is able to utilize a two-sided BF gain during its beam reporting phase, contrary to the one-sided BF gain of some other approaches, it could lead to noticeable improvements in terms of required time resources. Finally, since only a single UE is considered in this work, the proposed scheme should be extended to a multi-user scenario in the future.

A. Derivation of ML estimate

To simplify Eq. (4.5), the identities

$$\begin{aligned}
\mathbf{G}_s^{\mathsf{H}}\mathbf{G}_s &= \mathbf{G}_s^{\mathsf{H}}(\tau_0,\nu_0,\phi)\mathbf{G}_s(\tau_0,\nu_0,\phi) \\
&= \left(\mathbf{T}(\tau_0,\nu_0)\otimes\mathbf{V}_s^{\mathsf{H}}\mathbf{b}(\phi)\right)^{\mathsf{H}}\left(\mathbf{T}(\tau_0,\nu_0)\otimes\mathbf{V}_s^{\mathsf{H}}\mathbf{b}(\phi)\right) \\
&= \left(\mathbf{T}^{\mathsf{H}}(\tau_0,\nu_0)\otimes\mathbf{b}^{\mathsf{H}}(\phi)\mathbf{V}_s\right)\left(\mathbf{T}(\tau_0,\nu_0)\otimes\mathbf{V}_s^{\mathsf{H}}\mathbf{b}(\phi)\right) \\
&\overset{(a)}{=} \left(\mathbf{T}^{\mathsf{H}}(\tau_0,\nu_0)\mathbf{T}(\tau_0,\nu_0)\otimes\mathbf{b}^{\mathsf{H}}(\phi)\mathbf{V}_s\mathbf{V}_s^{\mathsf{H}}\mathbf{b}(\phi)\right) \\
&= \left(\mathbf{I}_{NM}\otimes\mathbf{b}^{\mathsf{H}}(\phi)\mathbf{V}_s\mathbf{V}_s^{\mathsf{H}}\mathbf{b}(\phi)\right) \\
&= \mathbf{b}^{\mathsf{H}}(\phi)\mathbf{V}_s\mathbf{V}_s^{\mathsf{H}}\mathbf{b}(\phi)\mathbf{I}_{NM}
\end{aligned} \tag{A.1}$$

and

$$\begin{aligned}
\mathbf{G}_s^{\mathsf{H}}\boldsymbol{y}_s &= \left(\mathbf{T}(\tau_0,\nu_0)\otimes\mathbf{V}_s^{\mathsf{H}}\mathbf{b}(\phi)\right)^{\mathsf{H}}\boldsymbol{y}_s \\
&= \left(\mathbf{T}^{\mathsf{H}}(\tau_0,\nu_0)\otimes\mathbf{b}^{\mathsf{H}}(\phi)\mathbf{V}_s\right)\boldsymbol{y}_s \\
&\overset{(b)}{=} \operatorname{vec}\left(\mathbf{b}^{\mathsf{H}}(\phi)\mathbf{V}_s\operatorname{vec}^{-1}(\boldsymbol{y}_s)\mathbf{T}^{\mathsf{H}}(\tau_0,\nu_0)\right) \\
&\overset{(c)}{=} \left(\mathbf{b}^{\mathsf{H}}(\phi)\mathbf{V}_s\mathbf{Y}_s\mathbf{T}^{\mathsf{H}}(\tau_0,\nu_0)\right)^{\mathsf{T}} \\
&= \mathbf{T}^{\mathsf{H}}(\tau_0,\nu_0)\mathbf{Y}_s^{\mathsf{T}}\mathbf{V}_s^{\mathsf{T}}\mathbf{b}^{*}(\phi),
\end{aligned} \tag{A.2}$$

are used, where $\mathbf{Y}_s = [\boldsymbol{y}_s[0,0],\ldots,\boldsymbol{y}_s[N-1,M-1]] \in \mathbb{C}^{L_{\mathrm{rf}}\times NM}$ is a matrix containing all observations of the UE in the s-th slot as its columns, $\operatorname{vec}(\cdot)$ denotes the vectorization operator such that $\operatorname{vec}(\mathbf{Y}_s) = \boldsymbol{y}_s$ and (a), (b) and (c) follow from [38, Ch. 4]

- (a) mixed property of Kronecker product: $(\mathbf{A}\otimes\mathbf{B})(\mathbf{C}\otimes\mathbf{D}) = (\mathbf{AC}\otimes\mathbf{BD})$,
- (b) mixed Kronecker matrix-vector product: $(\mathbf{A}\otimes\mathbf{B})\mathbf{v} = \operatorname{vec}(\mathbf{BVA}^{\mathsf{T}})$, where $\mathbf{V} = \operatorname{vec}^{-1}(\mathbf{v})$,
- (c) $\operatorname{vec}(\cdot)$-operator applied to row-vector is equivalent to transposing.

Considering Eqs. (A.1) and (A.2) and denoting the cost function of the ML estimate in Eq. (4.5) as

$$f = \sum_{s=1}^{i} \left|g^{\mathrm{dl}}\right|^2 \boldsymbol{x}_s^{\mathsf{H}} \mathbf{G}_s^{\mathsf{H}} \mathbf{G}_s \boldsymbol{x}_s - 2\mathrm{Re}\{(g^{\mathrm{dl}})^* \boldsymbol{x}_s^{\mathsf{H}} \mathbf{G}_s^{\mathsf{H}} \boldsymbol{y}_s\}, \tag{A.3}$$

the cost function simplifies to

$$\begin{aligned} f &= \sum_{s=1}^{i} \left|g^{\mathrm{dl}}\right|^2 \boldsymbol{x}_s^{\mathsf{H}} \mathbf{b}^{\mathsf{H}}(\phi) \mathbf{V}_s \mathbf{V}_s^{\mathsf{H}} \mathbf{b}(\phi) \mathbf{I}_{NM} \boldsymbol{x}_s - 2\mathrm{Re}\left\{(g^{\mathrm{dl}})^* \boldsymbol{x}_s^{\mathsf{H}} \mathbf{T}^{\mathsf{H}}(\tau_0, \nu_0) \mathbf{Y}_s^{\mathsf{T}} \mathbf{V}_s^{\mathsf{T}} \mathbf{b}^*(\phi)\right\} \\ &= \sum_{s=1}^{i} \left|g^{\mathrm{dl}}\right|^2 \|\boldsymbol{x}_s\|_2^2 \mathbf{b}^{\mathsf{H}}(\phi) \mathbf{V}_s \mathbf{V}_s^{\mathsf{H}} \mathbf{b}(\phi) - 2\mathrm{Re}\left\{g^{\mathrm{dl}} \boldsymbol{x}_s^{\mathsf{T}} \mathbf{T}(\tau_0, \nu_0) \mathbf{Y}_s^{\mathsf{H}} \mathbf{V}_s^{\mathsf{H}} \mathbf{b}(\phi)\right\} \\ &= \mathrm{Re}\left\{\sum_{s=1}^{i} \left|g^{\mathrm{dl}}\right|^2 \|\boldsymbol{x}_s\|_2^2 \, \mathbf{b}^{\mathsf{H}}(\phi) \mathbf{V}_s \mathbf{V}_s^{\mathsf{H}} \mathbf{b}(\phi) - 2g^{\mathrm{dl}} \boldsymbol{x}_s^{\mathsf{T}} \mathbf{T}(\tau_0, \nu_0) \mathbf{Y}_s^{\mathsf{H}} \mathbf{V}_s^{\mathsf{H}} \mathbf{b}(\phi)\right\} \qquad \text{(A.4)} \\ &= \mathrm{Re}\left\{\left|g^{\mathrm{dl}}\right|^2 \mathbf{b}^{\mathsf{H}}(\phi) \left[\sum_{s=1}^{i} \|\boldsymbol{x}_s\|_2^2 \mathbf{V}_s \mathbf{V}_s^{\mathsf{H}}\right] \mathbf{b}(\phi) - 2g^{\mathrm{dl}} \left[\sum_{s=1}^{i} \boldsymbol{x}_s^{\mathsf{T}} \mathbf{T}(\tau_0, \nu_0) \mathbf{Y}_s^{\mathsf{H}} \mathbf{V}_s^{\mathsf{H}}\right] \mathbf{b}(\phi)\right\} \\ &= \mathrm{Re}\left\{\left|g^{\mathrm{dl}}\right|^2 \mathbf{b}^{\mathsf{H}}(\phi) \mathbf{V}_{(i)} \mathbf{b}(\phi) - 2g^{\mathrm{dl}} \mathbf{c}_{(i)}^{\mathsf{H}}(\tau_0, \nu_0) \mathbf{b}(\phi)\right\}, \qquad \text{(A.5)} \end{aligned}$$

where

$$\begin{aligned} \mathbf{V}_{(i)} &:= \sum_{s=1}^{i} \|\boldsymbol{x}_s\|_2^2 \mathbf{V}_s \mathbf{V}_s^{\mathsf{H}}, \\ \mathbf{c}_{(i)}(\tau_0, \nu_0) &:= \left[\sum_{s=1}^{i} \boldsymbol{x}_s^{\mathsf{T}} \mathbf{T}(\tau_0, \nu_0) \mathbf{Y}_s^{\mathsf{H}} \mathbf{V}_s^{\mathsf{H}}\right]^{\mathsf{H}}. \end{aligned}$$

Hence, the simplified ML estimate reads

$$\begin{aligned} (\hat{g}_i^{\mathrm{dl}}, \hat{\tau}_i, \hat{\nu}_i, \hat{\phi}_i) &= \underset{g^{\mathrm{dl}}, \tau_0, \nu_0, \phi}{\arg\min} \; f \\ &= \underset{g^{\mathrm{dl}}, \tau_0, \nu_0, \phi}{\arg\min} \; \mathrm{Re}\left\{\left|g^{\mathrm{dl}}\right|^2 \mathbf{b}^{\mathsf{H}}(\phi) \mathbf{V}_{(i)} \mathbf{b}(\phi) - 2g^{\mathrm{dl}} \mathbf{c}_{(i)}^{\mathsf{H}}(\tau_0, \nu_0) \mathbf{b}(\phi)\right\} \\ &= \underset{g^{\mathrm{dl}}, \tau_0, \nu_0, \phi}{\arg\max} \; \mathrm{Re}\left\{2g^{\mathrm{dl}} \mathbf{c}_{(i)}^{\mathsf{H}}(\tau_0, \nu_0) \mathbf{b}(\phi) - \left|g^{\mathrm{dl}}\right|^2 \mathbf{b}^{\mathsf{H}}(\phi) \mathbf{V}_{(i)} \mathbf{b}(\phi)\right\} \qquad \text{(A.6)} \end{aligned}$$

Defining $g^{\mathrm{dl}} \coloneqq g_{\mathrm{r}} + jg_{\mathrm{i}}$, Eq. (4.8a) is computed by

$$
\begin{aligned}
& \frac{\partial}{\partial \mathrm{Re}\{g^{\mathrm{dl}}\}} \mathrm{Re}\left\{2g^{\mathrm{dl}}\mathbf{c}_{(i)}^{\mathsf{H}}(\tau_0,\nu_0)\mathbf{b}(\phi) - \left|g^{\mathrm{dl}}\right|^2 \mathbf{b}^{\mathsf{H}}(\phi)\mathbf{V}_{(i)}\mathbf{b}(\phi)\right\} = 0 \\
\Leftrightarrow \quad & \frac{\partial}{\partial g_{\mathrm{r}}} \mathrm{Re}\left\{2(g_{\mathrm{r}} + jg_{\mathrm{i}})\mathbf{c}_{(i)}^{\mathsf{H}}(\tau_0,\nu_0)\mathbf{b}(\phi) - \left(g_{\mathrm{r}}^2 + g_{\mathrm{i}}^2\right)\mathbf{b}^{\mathsf{H}}(\phi)\mathbf{V}_{(i)}\mathbf{b}(\phi)\right\} = 0 \\
\Leftrightarrow \quad & \frac{\partial}{\partial g_{\mathrm{r}}} \mathrm{Re}\left\{2(g_{\mathrm{r}} + jg_{\mathrm{i}})\mathbf{c}_{(i)}^{\mathsf{H}}(\tau_0,\nu_0)\mathbf{b}(\phi)\right\} - \frac{\partial}{\partial g_{\mathrm{r}}} \mathrm{Re}\left\{\left(g_{\mathrm{r}}^2 + g_{\mathrm{i}}^2\right)\mathbf{b}^{\mathsf{H}}(\phi)\mathbf{V}_{(i)}\mathbf{b}(\phi)\right\} = 0 \\
\Leftrightarrow \quad & \frac{\partial}{\partial g_{\mathrm{r}}} g_{\mathrm{r}} \,\mathrm{Re}\left\{2\mathbf{c}_{(i)}^{\mathsf{H}}(\tau_0,\nu_0)\mathbf{b}(\phi)\right\} - \frac{\partial}{\partial g_{\mathrm{r}}} g_{\mathrm{r}}^2\, \mathbf{b}^{\mathsf{H}}(\phi)\mathbf{V}_{(i)}\mathbf{b}(\phi) = 0 \\
\Leftrightarrow \quad & \mathrm{Re}\left\{2\mathbf{c}_{(i)}^{\mathsf{H}}(\tau_0,\nu_0)\mathbf{b}(\phi)\right\} - 2g_{\mathrm{r}}\mathbf{b}^{\mathsf{H}}(\phi)\mathbf{V}_{(i)}\mathbf{b}(\phi) = 0 \\
\Leftrightarrow \quad & g_{\mathrm{r}} = \frac{\mathrm{Re}\left\{\mathbf{c}_{(i)}^{\mathsf{H}}(\tau_0,\nu_0)\mathbf{b}(\phi)\right\}}{\mathbf{b}^{\mathsf{H}}(\phi)\mathbf{V}_{(i)}\mathbf{b}(\phi)}
\end{aligned}
\tag{A.7}
$$

and Eq. (4.8b) by

$$
\begin{aligned}
& \frac{\partial}{\partial \mathrm{Im}\{g^{\mathrm{dl}}\}} \mathrm{Re}\left\{2g^{\mathrm{dl}}\mathbf{c}_{(i)}^{\mathsf{H}}(\tau_0,\nu_0)\mathbf{b}(\phi) - \left|g^{\mathrm{dl}}\right|^2 \mathbf{b}^{\mathsf{H}}(\phi)\mathbf{V}_{(i)}\mathbf{b}(\phi)\right\} = 0 \\
\Leftrightarrow \quad & \frac{\partial}{\partial g_{\mathrm{i}}} \mathrm{Re}\left\{2(g_{\mathrm{r}} + jg_{\mathrm{i}})\mathbf{c}_{(i)}^{\mathsf{H}}(\tau_0,\nu_0)\mathbf{b}(\phi) - \left(g_{\mathrm{r}}^2 + g_{\mathrm{i}}^2\right)\mathbf{b}^{\mathsf{H}}(\phi)\mathbf{V}_{(i)}\mathbf{b}(\phi)\right\} = 0 \\
\Leftrightarrow \quad & \frac{\partial}{\partial g_{\mathrm{i}}} g_{\mathrm{i}} \,\mathrm{Re}\left\{2j\,\mathbf{c}_{(i)}^{\mathsf{H}}(\tau_0,\nu_0)\mathbf{b}(\phi)\right\} - \frac{\partial}{\partial g_{\mathrm{i}}} g_{\mathrm{i}}^2\, \mathbf{b}^{\mathsf{H}}(\phi)\mathbf{V}_{(i)}\mathbf{b}(\phi) = 0 \\
\Leftrightarrow \quad & \underbrace{\mathrm{Re}\left\{2j\,\mathbf{c}_{(i)}^{\mathsf{H}}(\tau_0,\nu_0)\mathbf{b}(\phi)\right\}}_{-\mathrm{Im}\left\{2\mathbf{c}_{(i)}^{\mathsf{H}}(\tau_0,\nu_0)\mathbf{b}(\phi)\right\}} - 2g_{\mathrm{i}}\mathbf{b}^{\mathsf{H}}(\phi)\mathbf{V}_{(i)}\mathbf{b}(\phi) = 0 \\
\Leftrightarrow \quad & g_{\mathrm{i}} = -\frac{\mathrm{Im}\left\{\mathbf{c}_{(i)}^{\mathsf{H}}(\tau_0,\nu_0)\mathbf{b}(\phi)\right\}}{\mathbf{b}^{\mathsf{H}}(\phi)\mathbf{V}_{(i)}\mathbf{b}(\phi)}.
\end{aligned}
\tag{A.8}
$$

The optimal DL coefficient is then given by

$$
g_{\mathrm{opt}}^{\mathrm{dl}} = g_{\mathrm{r}} + jg_{\mathrm{i}} = \frac{\left(\mathbf{c}_{(i)}^{\mathsf{H}}(\tau_0,\nu_0)\mathbf{b}(\phi)\right)^*}{\mathbf{b}^{\mathsf{H}}(\phi)\mathbf{V}_{(i)}\mathbf{b}(\phi)} = \frac{\mathbf{b}^{\mathsf{H}}(\phi)\mathbf{c}_{(i)}(\tau_0,\nu_0)}{\mathbf{b}^{\mathsf{H}}(\phi)\mathbf{V}_{(i)}\mathbf{b}(\phi)},
\tag{A.9}
$$

where the last equality follows from the fact that $\mathbf{c}_{(i)}^{\mathsf{H}}(\tau_0,\nu_0)\mathbf{b}(\phi)$ is a scalar.

B. Derivation of CRLB

Derivation of FIM

For the derivation of the FIM elements, the following identities are defined:

$$\begin{aligned} C_s(\phi) &\coloneqq \mathbf{b}^{\mathsf{H}}(\phi)\mathbf{V}_s\mathbf{V}_s^{\mathsf{H}}\mathbf{b}(\phi) = \|\mathbf{V}_s^{\mathsf{H}}\mathbf{b}(\phi)\|_2^2 \in \mathbb{R} \\ \tilde{\tilde{C}}_s(\phi) &\coloneqq \tilde{\mathbf{b}}^{\mathsf{H}}(\phi)\mathbf{V}_s\mathbf{V}_s^{\mathsf{H}}\tilde{\mathbf{b}}(\phi) = \left\|\mathbf{V}_s^{\mathsf{H}}\tilde{\mathbf{b}}(\phi)\right\|_2^2 \in \mathbb{R} \\ \tilde{C}_s(\phi) &\coloneqq \tilde{\mathbf{b}}^{\mathsf{H}}(\phi)\mathbf{V}_s\mathbf{V}_s^{\mathsf{H}}\mathbf{b}(\phi) \in \mathbb{C} \\ \|\mathbf{s}_s[n,m;\boldsymbol{\xi}]\|_2^2 &= g^2 C_s(\phi)|x_s[n,m]|^2 \\ \frac{\partial \mathbf{s}_s^{\mathsf{H}}[n,m;\boldsymbol{\xi}]}{\partial\phi}\mathbf{s}_s[n,m,\boldsymbol{\xi}] &= -j\pi\cos(\phi)g^2\tilde{C}_s(\phi)|x_s[n,m]|^2 \end{aligned} \tag{B.1}$$

Recalling the derivatives found in Eqs. (4.29a) - (4.29e), the diagonal elements of the FIM, defined in Eq. (4.28), are computed by

$$\begin{aligned} I_{gg} &= 2\sum_{s=1}^{i}\sum_{n,m}\mathrm{Re}\left\{\frac{\partial \mathbf{s}_s^{\mathsf{H}}[n,m;\boldsymbol{\xi}]}{\partial g}\frac{\partial \mathbf{s}_s[n,m;\boldsymbol{\xi}]}{\partial g}\right\} \\ &= 2\sum_{s=1}^{i}\sum_{n,m}\mathrm{Re}\left\{\frac{1}{g^2}\|\mathbf{s}_s[n,m;\boldsymbol{\xi}]\|_2^2\right\} \\ &= 2\sum_{s=1}^{i}C_s(\phi)\sum_{n,m}|x_s[n,m]|^2, \end{aligned} \tag{B.2}$$

$$\begin{aligned} I_{\psi_g\psi_g} &= 2\sum_{s=1}^{i}\sum_{n,m}\mathrm{Re}\left\{\frac{\partial \mathbf{s}_s^{\mathsf{H}}[n,m;\boldsymbol{\xi}]}{\partial \psi_g}\frac{\partial \mathbf{s}_s[n,m;\boldsymbol{\xi}]}{\partial \psi_g}\right\} \\ &= 2\sum_{s=1}^{i}\sum_{n,m}\mathrm{Re}\left\{-j^2\|\mathbf{s}_s[n,m;\boldsymbol{\xi}]\|_2^2\right\} \\ &= 2g^2\sum_{s=1}^{i}C_s(\phi)\sum_{n,m}|x_s[n,m]|^2, \end{aligned} \tag{B.3}$$

$$
\begin{aligned}
I_{\phi\phi} &= 2\sum_{s=1}^{i}\sum_{n,m}\mathrm{Re}\left\{\frac{\partial \mathbf{s}_s^{\mathsf{H}}[n,m;\boldsymbol{\xi}]}{\partial\phi}\frac{\partial \mathbf{s}_s[n,m;\boldsymbol{\xi}]}{\partial\phi}\right\} \\
&= 2\sum_{s=1}^{i}\sum_{n,m}\mathrm{Re}\left\{-j^2\pi^2\cos^2(\phi)g^2\left\|\mathbf{V}_s^{\mathsf{T}}\tilde{\mathbf{b}}(\phi)\right\|_2^2|x_s[n,m]|^2\right\} \\
&= 2\pi^2 g^2\cos^2(\phi)\sum_{s=1}^{i}\tilde{\tilde{C}}_s(\phi)\sum_{n,m}|x_s[n,m]|^2\,, \qquad \text{(B.4)}
\end{aligned}
$$

$$
\begin{aligned}
I_{\tau_0'\tau_0'} &= 2\sum_{s=1}^{i}\sum_{n,m}\mathrm{Re}\left\{\frac{\partial \mathbf{s}_s^{\mathsf{H}}[n,m;\boldsymbol{\xi}]}{\partial\tau_0'}\frac{\partial \mathbf{s}_s[n,m;\boldsymbol{\xi}]}{\partial\tau_0'}\right\} \\
&= 2\sum_{s=1}^{i}\sum_{n,m}\mathrm{Re}\left\{-j^2(2m\pi\Delta f)^2\left\|\mathbf{s}_s[n,m;\boldsymbol{\xi}]\right\|_2^2\right\} \\
&= 8\pi^2 g^2(\Delta f)^2\sum_{s=1}^{i}C_s(\phi)\sum_{n,m}m^2|x_s[n,m]|^2\,, \qquad \text{(B.5)}
\end{aligned}
$$

$$
\begin{aligned}
I_{\nu_0\nu_0} &= 2\sum_{s=1}^{i}\sum_{n,m}\mathrm{Re}\left\{\frac{\partial \mathbf{s}_s^{\mathsf{H}}[n,m;\boldsymbol{\xi}]}{\partial\nu_0}\frac{\partial \mathbf{s}_s[n,m;\boldsymbol{\xi}]}{\partial\nu_0}\right\} \\
&= 2\sum_{s=1}^{i}\sum_{n,m}\mathrm{Re}\left\{-j^2(n\pi T_\mathrm{o})^2\left\|\mathbf{s}_s[n,m;\boldsymbol{\xi}]\right\|_2^2\right\} \\
&= 2\pi^2 g^2 T_\mathrm{o}^2\sum_{s=1}^{i}C_s(\phi)\sum_{n,m}n^2|x_s[n,m]|^2\,. \qquad \text{(B.6)}
\end{aligned}
$$

Further, the off-diagonal elements of the FIM defined in Eq. (4.28) are computed by

$$
\begin{aligned}
I_{g\psi_g} &= 2\sum_{s=1}^{i}\sum_{n,m}\mathrm{Re}\left\{\frac{\partial \mathbf{s}_s^{\mathsf{H}}[n,m;\boldsymbol{\xi}]}{\partial g}\frac{\partial \mathbf{s}_s[n,m;\boldsymbol{\xi}]}{\partial\psi_g}\right\} \\
&= 2\sum_{s=1}^{i}\sum_{n,m}\mathrm{Re}\left\{j\frac{1}{g}\left\|\mathbf{s}_s[n,m;\boldsymbol{\xi}]\right\|_2^2\right\} \\
&= 2\sum_{s=1}^{i}\sum_{n,m}\frac{1}{g}\left\|\mathbf{s}_s[n,m;\boldsymbol{\xi}]\right\|_2^2\mathrm{Re}\left\{j\right\} = 0 \qquad \text{(B.7)}
\end{aligned}
$$

$$
\begin{aligned}
I_{g\phi} &= 2\sum_{s=1}^{i}\sum_{n,m}\mathrm{Re}\left\{\frac{\partial \mathbf{s}_s^{\mathsf{H}}[n,m;\boldsymbol{\xi}]}{\partial g}\frac{\partial \mathbf{s}_s[n,m;\boldsymbol{\xi}]}{\partial \phi}\right\} \\
&= 2\sum_{s=1}^{i}\sum_{n,m}\mathrm{Re}\left\{j\frac{\pi\cos(\phi)g^2}{g}\mathbf{b}^{\mathsf{H}}(\phi)\mathbf{V}_s^{*}\mathbf{V}_s^{\mathsf{T}}\tilde{\mathbf{b}}(\phi)\left|x_s[n,m]\right|^2\right\} \\
&= 2\pi g\cos(\phi)\sum_{s=1}^{i}\sum_{n,m}\left|x_s[n,m]\right|^2\underbrace{\mathrm{Re}\left\{j\tilde{C}_s^{*}(\phi)\right\}}_{\mathrm{Im}\left\{\tilde{C}_s(\phi)\right\}} \\
&= 2\pi g\cos(\phi)\sum_{s=1}^{i}\mathrm{Im}\left\{\tilde{C}_s(\phi)\right\}\sum_{n,m}\left|x_s[n,m]\right|^2
\end{aligned}
\tag{B.8}
$$

$$
\begin{aligned}
I_{g\tau_0'} &= 2\sum_{s=1}^{i}\sum_{n,m}\mathrm{Re}\left\{\frac{\partial \mathbf{s}_s^{\mathsf{H}}[n,m;\boldsymbol{\xi}]}{\partial g}\frac{\partial \mathbf{s}_s[n,m;\boldsymbol{\xi}]}{\partial \tau_0'}\right\} \\
&= 2\sum_{s=1}^{i}\sum_{n,m}\mathrm{Re}\left\{j\frac{-2m\pi\Delta f}{g}\left\|\mathbf{s}_s[n,m;\boldsymbol{\xi}]\right\|_2^2\right\} \\
&= 2\sum_{s=1}^{i}\sum_{n,m}\frac{-2m\pi\Delta f}{g}\left\|\mathbf{s}_s[n,m;\boldsymbol{\xi}]\right\|_2^2\mathrm{Re}\left\{j\right\} = 0
\end{aligned}
\tag{B.9}
$$

$$
\begin{aligned}
I_{g\nu_0} &= 2\sum_{s=1}^{i}\sum_{n,m}\mathrm{Re}\left\{\frac{\partial \mathbf{s}_s^{\mathsf{H}}[n,m;\boldsymbol{\xi}]}{\partial g}\frac{\partial \mathbf{s}_s[n,m;\boldsymbol{\xi}]}{\partial \nu_0}\right\} \\
&= 2\sum_{s=1}^{i}\sum_{n,m}\mathrm{Re}\left\{j\frac{n\pi T_{\mathrm{o}}}{g}\left\|\mathbf{s}_s[n,m;\boldsymbol{\xi}]\right\|_2^2\right\} \\
&= 2\sum_{s=1}^{i}\sum_{n,m}\frac{n\pi T_{\mathrm{o}}}{g}\left\|\mathbf{s}_s[n,m;\boldsymbol{\xi}]\right\|_2^2\mathrm{Re}\left\{j\right\} = 0
\end{aligned}
\tag{B.10}
$$

$$
\begin{aligned}
I_{\psi_g\phi} &= 2\sum_{s=1}^{i}\sum_{n,m}\mathrm{Re}\left\{\frac{\partial \mathbf{s}_s^{\mathsf{H}}[n,m;\boldsymbol{\xi}]}{\partial \psi_g}\frac{\partial \mathbf{s}_s[n,m;\boldsymbol{\xi}]}{\partial \phi}\right\} \\
&= 2\sum_{s=1}^{i}\sum_{n,m}\mathrm{Re}\left\{-j^2\pi\cos(\phi)g^2\mathbf{b}^{\mathsf{H}}(\phi)\mathbf{V}_s^{*}\mathbf{V}_s^{\mathsf{T}}\tilde{\mathbf{b}}(\phi)\left|x_s[n,m]\right|^2\right\} \\
&= 2\pi g^2\cos(\phi)\sum_{s=1}^{i}\sum_{n,m}\left|x_s[n,m]\right|^2\mathrm{Re}\left\{-j^2\tilde{C}_s^{*}(\phi)\right\} \\
&= 2\pi g^2\cos(\phi)\sum_{s=1}^{i}\mathrm{Re}\left\{\tilde{C}_s(\phi)\right\}\sum_{n,m}\left|x_s[n,m]\right|^2
\end{aligned}
\tag{B.11}
$$

$$
\begin{aligned}
I_{\psi_g \tau_0'} &= 2 \sum_{s=1}^{i} \sum_{n,m} \mathrm{Re} \left\{ \frac{\partial \mathbf{s}_s^{\mathsf{H}}[n,m;\boldsymbol{\xi}]}{\partial \psi_g} \frac{\partial \mathbf{s}_s[n,m;\boldsymbol{\xi}]}{\partial \tau_0'} \right\} \\
&= 2 \sum_{s=1}^{i} \sum_{n,m} \mathrm{Re} \left\{ j^2 \, 2m\pi\Delta f \, \|\mathbf{s}_s[n,m;\boldsymbol{\xi}]\|_2^2 \right\} \\
&= -4\pi g^2 \Delta f \sum_{s=1}^{i} C_s(\phi) \sum_{n,m} m \, |x_s[n,m]|^2
\end{aligned} \tag{B.12}
$$

$$
\begin{aligned}
I_{\psi_g \nu_0} &= 2 \sum_{s=1}^{i} \sum_{n,m} \mathrm{Re} \left\{ \frac{\partial \mathbf{s}_s^{\mathsf{H}}[n,m;\boldsymbol{\xi}]}{\partial \psi_g} \frac{\partial \mathbf{s}_s[n,m;\boldsymbol{\xi}]}{\partial \nu_0} \right\} \\
&= 2 \sum_{s=1}^{i} \sum_{n,m} \mathrm{Re} \left\{ -j^2 \, n\pi T_\mathrm{o} \, \|\mathbf{s}_s[n,m;\boldsymbol{\xi}]\|_2^2 \right\} \\
&= 2\pi g^2 T_\mathrm{o} \sum_{s=1}^{i} C_s(\phi) \sum_{n,m} n \, |x_s[n,m]|^2
\end{aligned} \tag{B.13}
$$

$$
\begin{aligned}
I_{\phi \tau_0'} &= 2 \sum_{s=1}^{i} \sum_{n,m} \mathrm{Re} \left\{ \frac{\partial \mathbf{s}_s^{\mathsf{H}}[n,m;\boldsymbol{\xi}]}{\partial \phi} \frac{\partial \mathbf{s}_s[n,m;\boldsymbol{\xi}]}{\partial \tau_0'} \right\} \\
&= 2 \sum_{s=1}^{i} \sum_{n,m} \mathrm{Re} \left\{ j^2 \, 2m\Delta f \pi^2 \cos(\phi) g^2 \tilde{C}_s(\phi) \, |x_s[n,m]|^2 \right\} \\
&= -4\pi^2 g^2 \cos(\phi) \Delta f \sum_{s=1}^{i} \mathrm{Re} \left\{ \tilde{C}_s(\phi) \right\} \sum_{n,m} m \, |x_s[n,m]|^2
\end{aligned} \tag{B.14}
$$

$$
\begin{aligned}
I_{\phi \nu_0} &= 2 \sum_{s=1}^{i} \sum_{n,m} \mathrm{Re} \left\{ \frac{\partial \mathbf{s}_s^{\mathsf{H}}[n,m;\boldsymbol{\xi}]}{\partial \phi} \frac{\partial \mathbf{s}_s[n,m;\boldsymbol{\xi}]}{\partial \nu_0} \right\} \\
&= 2 \sum_{s=1}^{i} \sum_{n,m} \mathrm{Re} \left\{ -j^2 \, nT_\mathrm{o} \pi^2 \cos(\phi) g^2 \tilde{C}_s(\phi) \, |x_s[n,m]|^2 \right\} \\
&= 2\pi^2 g^2 \cos(\phi) T_\mathrm{o} \sum_{s=1}^{i} \mathrm{Re} \left\{ \tilde{C}_s(\phi) \right\} \sum_{n,m} n \, |x_s[n,m]|^2
\end{aligned} \tag{B.15}
$$

$$
\begin{aligned}
I_{\tau_0' \nu_0} &= 2 \sum_{s=1}^{i} \sum_{n,m} \mathrm{Re} \left\{ \frac{\partial \mathbf{s}_s^{\mathsf{H}}[n,m;\boldsymbol{\xi}]}{\partial \tau_0'} \frac{\partial \mathbf{s}_s[n,m;\boldsymbol{\xi}]}{\partial \nu_0} \right\} \\
&= 2 \sum_{s=1}^{i} \sum_{n,m} \mathrm{Re} \left\{ j^2 \, 2\pi mn\Delta f T_\mathrm{o} \, \|\mathbf{s}_s[n,m;\boldsymbol{\xi}]\|_2^2 \right\} \\
&= -4\pi^2 g^2 \Delta f T_\mathrm{o} \sum_{s=1}^{i} C_s(\phi) \sum_{n,m} mn \, |x_s[n,m]|^2
\end{aligned} \tag{B.16}
$$

Approximation of CRLB

To derive an approximated CRLB of the AoA ϕ that does not depend on the sent pilot symbols $\mathbf{X}$, recall the average power constraint in Eq. (2.16). By using the identities in Eq. (4.32) and assuming M and N to be large, the summations over m and n in Eqs. (B.2) - (B.16) can be approximated, according to [32], by

$$\begin{aligned}\sum_{n,m} |x_s[n,m]|^2 &= NM \frac{1}{NM} \sum_{n,m} |x_s[n,m]|^2 \\ &\approx NMP_\mathrm{t}, \end{aligned} \tag{B.17}$$

$$\begin{aligned}\sum_{n,m} m\,|x_s[n,m]|^2 &= \sum_{m=0}^{M-1} m \sum_{n=0}^{N-1} |x_s[n,m]|^2 \\ &\approx \sum_{m=0}^{M-1} mNP_\mathrm{t} \\ &= P_\mathrm{t} N \frac{M(M-1)}{2}, \end{aligned} \tag{B.18}$$

$$\begin{aligned}\sum_{n,m} n\,|x_s[n,m]|^2 &= \sum_{n=0}^{N-1} n \sum_{m=0}^{M-1} |x_s[n,m]|^2 \\ &\approx \sum_{n=0}^{N-1} nMP_\mathrm{t} \\ &= P_\mathrm{t} M \frac{N(N-1)}{2}, \end{aligned} \tag{B.19}$$

$$\begin{aligned}\sum_{n,m} m^2\,|x_s[n,m]|^2 &= \sum_{m=0}^{M-1} m^2 \sum_{n=0}^{N-1} |x_s[n,m]|^2 \\ &\approx \sum_{m=0}^{M-1} m^2 NP_\mathrm{t} \\ &= P_\mathrm{t} N \frac{M(M-1)(2M-1)}{6}, \end{aligned} \tag{B.20}$$

$$\begin{aligned}\sum_{n,m} n^2\,|x_s[n,m]|^2 &= \sum_{n=0}^{N-1} n^2 \sum_{m=0}^{M-1} |x_s[n,m]|^2 \\ &\approx \sum_{n=0}^{N-1} n^2 MP_\mathrm{t} \\ &= P_\mathrm{t} M \frac{N(N-1)(2N-1)}{6}, \end{aligned} \tag{B.21}$$

$$
\begin{aligned}
\sum_{n,m} nm\,|x_s[n,m]|^2 &= \sum_{m=0}^{M-1} m \sum_{n=0}^{N-1} n\,|x_s[n,m]|^2 \\
&= \sum_{m=0}^{M-1} m \left(\sum_{k=0}^{W-1} \sum_{l=0}^{N_W-1} (lW+k)\,|x_s[n,m]|^2 \right), \\
&\qquad n = lW + k,\ N_W = \frac{N}{W}, \\
&\qquad k = 0,\dots,W-1,\ l = 0,\dots,N_W-1 \\
&= \sum_{m=0}^{M-1} m \left(W \sum_{l=0}^{N_W-1} l \sum_{k=0}^{W-1} |x_s[n,m]|^2 + \sum_{k=0}^{W-1} k \sum_{l=0}^{N_W-1} |x_s[n,m]|^2 \right) \\
&\overset{(a)}{\approx} \sum_{m=0}^{M-1} m \left(W \sum_{l=0}^{N_W-1} lWP_\mathrm{t} + \sum_{k=0}^{W-1} kN_W P_\mathrm{t} \right) \\
&= \sum_{m=0}^{M-1} m \left(P_\mathrm{t} W^2 \frac{N_W(N_W-1)}{2} + P_\mathrm{t} N_W \frac{W(W-1)}{2} \right) \\
&= P_\mathrm{t} \sum_{m=0}^{M-1} m \left(\frac{W^2N_W^2 - W^2N_W + N_W W^2 - N_W W}{2} \right) \\
&= P_\mathrm{t} \sum_{m=0}^{M-1} m \left(\frac{W^2N_W^2 - N_W W}{2} \right) \\
&= P_\mathrm{t} \frac{N^2 - N}{2} \sum_{m=0}^{M-1} m \\
&= P_\mathrm{t} \frac{N(N-1)}{2} \frac{M(M-1)}{2},
\end{aligned} \tag{B.22}
$$

where $\sum_{n,m} = \sum_{n=0}^{N-1} \sum_{m=0}^{M-1}$ is used to shorten the notation and (a) follows from assuming that N_W and W are large.

Using the derived identities in Eqs. (B.17) - (B.22) and defining

$$
\begin{aligned}
C_\phi^{(i)} &:= \sum_{s=1}^{i} C_s(\phi), \\
\tilde{C}_\phi^{(i)} &:= \sum_{s=1}^{i} \tilde{C}_s(\phi), \\
\tilde{\tilde{C}}_\phi^{(i)} &:= \sum_{s=1}^{i} \tilde{\tilde{C}}_s(\phi),
\end{aligned}
$$

where $C_s(\phi), \tilde{C}_s(\phi)$ and $\tilde{\tilde{C}}_s(\phi)$ are introduced in Eq. (B.1), the individual elements of the FIM, computed in Eqs. (B.2) - (B.16), are approximated by

$$
\begin{aligned}
I_{gg} &\approx 2C_\phi^{(i)} NMP_\mathrm{t}, \\
I_{\psi_g\psi_g} &\approx 2g^2 C_\phi^{(i)} NMP_\mathrm{t}, \\
I_{\phi\phi} &\approx 2\pi^2 \cos^2(\phi) g^2 \tilde{\tilde{C}}_\phi^{(i)} NMP_\mathrm{t}, \\
I_{\tau_0'\tau_0'} &\approx 8\pi^2 \Delta f^2 g^2 C_\phi^{(i)} P_\mathrm{t} N \frac{M(M-1)(2M-1)}{6}, \\
I_{\nu_0\nu_0} &\approx 2\pi^2 T_o^2 g^2 C_\phi^{(i)} P_\mathrm{t} M \frac{N(N-1)(2N-1)}{6}, \\
I_{g\phi} &\approx 2\pi \cos(\phi) g \ \mathrm{Im}\left\{\tilde{C}_\phi^{(i)}\right\} NMP_\mathrm{t}, \\
I_{\psi_g\phi} &\approx 2\pi \cos(\phi) g^2 \ \mathrm{Re}\left\{\tilde{C}_\phi^{(i)}\right\} NMP_\mathrm{t}, \\
I_{\psi_g\tau_0'} &\approx -4\pi \Delta f g^2 C_\phi^{(i)} P_\mathrm{t} N \frac{M(M-1)}{2}, \\
I_{\psi_g\nu_0} &\approx 2\pi T_o g^2 C_\phi^{(i)} P_\mathrm{t} M \frac{N(N-1)}{2}, \\
I_{\phi\tau_0'} &\approx -4\pi^2 \cos(\phi) \Delta f g^2 \ \mathrm{Re}\left\{\tilde{C}_\phi^{(i)}\right\} P_\mathrm{t} N \frac{M(M-1)}{2}, \\
I_{\phi\nu_0} &\approx 2\pi^2 \cos(\phi) T_o g^2 \ \mathrm{Re}\left\{\tilde{C}_\phi^{(i)}\right\} P_\mathrm{t} M \frac{N(N-1)}{2}, \\
I_{\tau_0'\nu_0} &\approx -4\pi^2 \Delta f T_o g^2 C_\phi^{(i)} P_\mathrm{t} \frac{M(M-1)}{2} \frac{N(N-1)}{2}\ .
\end{aligned}
\tag{B.23}
$$

Substituting these approximations from Eqs. (B.23) into the expression of the exact CRLB, see Eq. (4.31), the numerator and denominator of the CRLB are respectively approximated by

$$
n_\phi(\mathbf{X}) \approx n_{\phi,\mathrm{approx}} = -C_\phi^{(i)}(M+1) \overset{(a)}{\approx} -C_\phi^{(i)} M \tag{B.24}
$$

and

$$
\begin{aligned}
\det(\mathbf{I}(\boldsymbol{\xi}, \mathbf{X})) &\approx d_{\phi,\text{approx}} \\
&= \frac{2MNP_\text{t}g^2\pi^2\cos^2(\phi)}{\sigma^2} \\
&\quad \Bigg(6\left(\text{Re}\left\{\tilde{C}_\phi^{(i)}\right\}\right)^2\cos(\phi) - 3\left(\text{Re}\left\{\tilde{C}_\phi^{(i)}\right\}\right)^2\cos^2(\phi) + M\left(\text{Im}\left\{\tilde{C}_\phi^{(i)}\right\}\right)^2 \\
&\qquad + 4M\left(\text{Re}\left\{\tilde{C}_\phi^{(i)}\right\}\right)^2 - C_\phi^{(i)}\tilde{\tilde{C}}_\phi^{(i)} + \left(\text{Im}\left\{\tilde{C}_\phi^{(i)}\right\}\right)^2 - 2\left(\text{Re}\left\{\tilde{C}_\phi^{(i)}\right\}\right)^2 \\
&\qquad - C_\phi^{(i)}\tilde{\tilde{C}}_\phi^{(i)}M - 6M\left(\text{Re}\left\{\tilde{C}_\phi^{(i)}\right\}\right)^2\cos(\phi) + 3M\left(\text{Re}\left\{\tilde{C}_\phi^{(i)}\right\}\right)^2\cos^2(\phi)\Bigg) \\
&= \frac{2MNP_\text{t}g^2\pi^2\cos^2(\phi)}{\sigma^2} \\
&\quad \Bigg(\left(\text{Re}\left\{\tilde{C}_\phi^{(i)}\right\}\right)^2\left[6\cos(\phi) - 3\cos^2(\phi) + 4M - 2 - 6M\cos(\phi) + 3M\cos^2(\phi)\right] \\
&\qquad \left(+\text{Im}\left\{\tilde{C}_\phi^{(i)}\right\}\right)^2[M+1] - C_\phi^{(i)}\tilde{\tilde{C}}_\phi^{(i)}[M+1]\Bigg) \\
&\overset{(a)}{\approx} \frac{2MNP_\text{t}g^2\pi^2\cos^2(\phi)}{\sigma^2} \\
&\quad \left(\left(\text{Re}\left\{\tilde{C}_\phi^{(i)}\right\}\right)^2 M\left[3\left(1-\cos(\phi)\right)^2+1\right] + \left(\text{Im}\left\{\tilde{C}_\phi^{(i)}\right\}\right)^2 M - C_\phi^{(i)}\tilde{\tilde{C}}_\phi^{(i)}M\right) \\
&= \frac{2M^2NP_\text{t}g^2\pi^2\cos^2(\phi)}{\sigma^2} \\
&\quad \left(\left(\text{Re}\left\{\tilde{C}_\phi^{(i)}\right\}\right)^2\left[3\left(1-\cos(\phi)\right)^2+1\right] + \left(\text{Im}\left\{\tilde{C}_\phi^{(i)}\right\}\right)^2 - C_\phi^{(i)}\tilde{\tilde{C}}_\phi^{(i)}\right),
\end{aligned}
\tag{B.25}
$$

where (a) follows from recalling that M is assumed to be large.

Bibliography

[1] X. Song, S. Haghighatshoar, and G. Caire, "Efficient Beam Alignment for Millimeter Wave Single-Carrier Systems With Hybrid MIMO Transceivers," *IEEE Transactions on Wireless Communications*, vol. 18, no. 3, pp. 1518–1533, 2019.

[2] R. W. Heath, N. González-Prelcic, S. Rangan, W. Roh, and A. M. Sayeed, "An Overview of Signal Processing Techniques for Millimeter Wave MIMO Systems," *IEEE Journal of Selected Topics in Signal Processing*, vol. 10, no. 3, pp. 436–453, 2016.

[3] T. S. Rappaport, Y. Xing, G. R. MacCartney, A. F. Molisch, E. Mellios, and J. Zhang, "Overview of Millimeter Wave Communications for Fifth-Generation (5G) Wireless Networks—With a Focus on Propagation Models," *IEEE Transactions on Antennas and Propagation*, vol. 65, no. 12, pp. 6213–6230, 2017.

[4] X. Song, S. Haghighatshoar, and G. Caire, "A Scalable and Statistically Robust Beam Alignment Technique for Millimeter-Wave Systems," *IEEE Transactions on Wireless Communications*, vol. 17, no. 7, pp. 4792–4805, 2018.

[5] S. Haghighatshoar and G. Caire, "The Beam Alignment Problem in mmWave Wireless Networks," in *2016 50th Asilomar Conference on Signals, Systems and Computers*, pp. 741–745, 2016.

[6] F. Sohrabi, Z. Chen, and W. Yu, "Deep Active Learning Approach to Adaptive Beamforming for mmWave Initial Alignment," in *ICASSP 2021 - 2021 IEEE International Conference on Acoustics, Speech and Signal Processing (ICASSP)*, pp. 4940–4944, 2021.

[7] Ö. Özdogan, E. Björnson, and E. G. Larsson, "Using Intelligent Reflecting Surfaces for Rank Improvement in MIMO Communications," in *ICASSP 2020 - 2020 IEEE International Conference on Acoustics, Speech and Signal Processing (ICASSP)*, pp. 9160–9164, 2020.

[8] G. C. Alexandropoulos, N. Shlezinger, I. Alamzadeh, M. F. Imani, H. Zhang, and Y. C. Eldar, "Hybrid Reconfigurable Intelligent Metasurfaces: Enabling Simultaneous Tunable Reflections and Sensing for 6G Wireless Communications," 2021.

[9] A. Alkhateeb, O. El Ayach, G. Leus, and R. W. Heath, "Channel Estimation and Hybrid Precoding for Millimeter Wave Cellular Systems," *IEEE Journal of Selected Topics in Signal Processing*, vol. 8, no. 5, pp. 831–846, 2014.

[10] S.-E. Chiu, N. Ronquillo, and T. Javidi, "Active Learning and CSI Acquisition for mmWave Initial Alignment," *IEEE Journal on Selected Areas in Communications*, vol. 37, no. 11, pp. 2474–2489, 2019.

[11] F. Pedraza, M. Kobayashi, and C. Giuseppe, "Two-Sided Beam Alignment with Side Information in mmWave Channels."

[12] Ö. Özdogan, E. Björnson, and E. G. Larsson, "Intelligent Reflecting Surfaces: Physics, Propagation, and Pathloss Modeling," *IEEE Wireless Communications Letters*, vol. 9, no. 5, pp. 581–585, 2020.

[13] Q. Wu, S. Zhang, B. Zheng, C. You, and R. Zhang, "Intelligent Reflecting Surface-Aided Wireless Communications: A Tutorial," *IEEE Transactions on Communications*, vol. 69, no. 5, pp. 3313–3351, 2021.

[14] Ö. Özdogan and E. Björnson, "Deep Learning-based Phase Reconfiguration for Intelligent Reflecting Surfaces," in *2020 54th Asilomar Conference on Signals, Systems, and Computers*, pp. 707–711, 2020.

[15] F. Sohrabi, T. Jiang, W. Cui, and W. Yu, "Active Sensing for Communications by Learning," 2022.

[16] W. Cai, H. Li, M. Li, and Q. Liu, "Practical Modeling and Beamforming for Intelligent Reflecting Surface Aided Wideband Systems," 2020.

[17] I. Alamzadeh, G. C. Alexandropoulos, N. Shlezinger, and M. F. Imani, "A reconfigurable intelligent surface with integrated sensing capability," *Scientific Reports*, vol. 11, p. 20737, Oct 2021.

[18] S. Xu, J. Liu, Y. Cao, J. Li, and Y. Zhang, "Intelligent Reflecting Surface Enabled Secure Cooperative Transmission for Satellite-Terrestrial Integrated Networks," *IEEE Transactions on Vehicular Technology*, vol. 70, no. 2, pp. 2007–2011, 2021.

[19] M. Cui, G. Zhang, and R. Zhang, "Secure Wireless Communication via Intelligent Reflecting Surface," *IEEE Wireless Communications Letters*, vol. 8, no. 5, pp. 1410–1414, 2019.

[20] X. Yu, D. Xu, Y. Sun, D. W. K. Ng, and R. Schober, "Robust and Secure Wireless Communications via Intelligent Reflecting Surfaces," *IEEE Journal on Selected Areas in Communications*, vol. 38, no. 11, pp. 2637–2652, 2020.

[21] S. K. Dehkordi, L. Gaudio, M. Kobayashi, G. Caire, and G. Colavolpe, "Beam-Space MIMO Radar with OTFS Modulation for Integrated Sensing and Communications."

[22] B. Matuz, H. Bartz, and M. Sener, "Wireless Communications." Lecture notes, Institute for Communications Engineering, Technical University of Munich, 2021.

[23] S. K. Dehkordi, L. Gaudio, M. Kobayashi, G. Caire, and G. Colavolpe, "Beam-Space MIMO Radar for Joint Communication and Sensing with OTFS Modulation," 2022.

[24] A. Omri, M. Shaqfeh, A. Ali, and H. Alnuweiri, "Synchronization Procedure in 5G NR Systems," *IEEE Access*, vol. 7, pp. 41286–41295, 2019.

[25] J. O. Smith, *Mathematics of the Discrete Fourier Transform (DFT)*. http://ccrma.stanford.edu/∼jos/mdft/, accessed on 30 August 2022. online book, 2007 edition.

[26] M. A. Richards, *Fundamentals of Radar Signal Processing*. McGraw-Hill Education, 2005.

[27] M. Giordani, M. Polese, A. Roy, D. Castor, and M. Zorzi, "A Tutorial on Beam Management for 3GPP NR at mmWave Frequencies," *IEEE Communications Surveys & Tutorials*, vol. 21, no. 1, pp. 173–196, 2019.

[28] L. L. Scharf, *Statistical Signal Processing: Detection, Estimation, and Time Series Analysis*. Boston: Addison-Wesley, 1991.

[29] C. A. Balanis, *Antenna theory: Analysis and Design*. John Wiley & Sons Inc., third ed., 2005.

[30] A. Papoulis and S. U. Pillai, *Probability, Random Variables, and Stochastic Processes*. McGraw Hill, fourth ed., 2002.

[31] O. Besson and Y. I. Abramovich, "On the Fisher Information Matrix for Multivariate Elliptically Contoured Distributions," *IEEE Signal Processing Letters*, vol. 20, no. 11, pp. 1130–1133, 2013.

[32] B. Bissinger, "Waveform Design for Joint Radar and V2X Communication," Master's thesis, Technical University of Munich, 2019.

[33] 3rd Generation Partnership Project, *5G; NR; Physical channels and modulation (3GPP TS 38.211 version 17.2.0 Release 17)*, June 2022.

[34] P. Hügler, M. Geiger, and C. Waldschmidt, "RCS Measurements of a Human Hand for Radar-Based Gesture Recognition at E-band," in *2016 German Microwave Conference (GeMiC)*, pp. 259–262, 2016.

[35] M. Shibao, K. Uchiyama, and A. Kajiwara, "RCS Characteristics of Road Debris at 79GHz Millimeter-wave Radar," in *2019 IEEE Radio and Wireless Symposium (RWS)*, pp. 1–4, 2019.

[36] V. Semkin, J. Haarla, T. Pairon, C. Slezak, S. Rangan, V. Viikari, and C. Oestges, "Analyzing Radar Cross Section Signatures of Diverse Drone Models at mmWave Frequencies," *IEEE Access*, vol. 8, pp. 48958–48969, 2020.

[37] H.-J. Li and Y.-W. Kiang, "10 - Radar and Inverse Scattering," in *The Electrical Engineering Handbook* (W.-K. CHEN, ed.), pp. 671–690, Burlington: Academic Press, 2005.

[38] R. A. Horn and C. R. Johnson, *Topics in Matrix Analysis*. Cambridge University Press, 1991.